

Master Thesis
A Statistical Analysis of Cloud Impacts
on Tropospheric NO₂ Columns
Retrieved from space-based Remote Sensing

Saqr Munassar

saqr.munassar@gmail.com

Institute of Environmental Physics
Bremen University, Germany

February 2017

Supervisor

Prof. John P. Burrows

Supervisor

Prof. Mihalis Vrekoussis



Acknowledgements

Having been affiliated to its academic staff, I acknowledge University of Ibb, Yemen, which sponsored my Master study. I am sincerely thankful to Dr. Andreas Richter for his assistance, his patient encouragement, and his distinctive guidance during his supervision on my Master thesis; Prof. Dr. John P. Burrows and Prof. Mihalis Vrekoussis for their generous acceptance to be the reviewers of my dissertation and for their helpful feedback on the thesis paper; DOAS group's members for their continued support during our weekly meetings and upon need.

While being far away from my family during this research, I gratefully thank from the bottom of my heart my wife, son, daughter, parents, brothers, and sisters for their patience and their inspirational prayers.

Saqr Munassar

University of Bremen

Bremen, Germany

Table of Contents

Abstract.....	1
1 Introduction	1
2 Scientific background.....	3
2.1 Clouds in the atmosphere.....	3
2.1.1 Cloud composition	3
2.1.2 Cloud distribution in the atmosphere.....	4
2.1.3 Cloud determination.....	5
2.2 NO ₂ in the atmosphere	6
2.2.1 Sources and sinks of the tropospheric NO ₂	6
2.2.2 Tropospheric distribution of NO ₂	7
2.2.3 NO ₂ column retrieval by space-based observations.....	8
2.2.4 The effect of clouds on trace gases retrieval.....	9
2.3 Overview about satellite instruments.....	9
2.3.1 The Global Ozone Monitoring Experiment (GOME)	9
2.3.2 The Scanning Imaging Absorption Spectrometer for Atmospheric Chatography (SCIAMACHY)	10
2.3.3 The Ozone Monitoring Instrument (OMI).....	11
3 The aim of the study and its significance.....	11
3.1 Cloud effects on the tropospheric NO ₂ retrieval	11
3.1.1 The observed cloud effects on tropospheric NO ₂ columns	12
3.1.2 Enhancement of tropospheric NO ₂ columns by clouds	13
3.1.3 The NO ₂ column errors due to cloud errors	14
3.2 The cloud algorithms used.....	14
3.2.1 GOME-2A cloud products	15
3.2.2 OMI cloud products	18
4 GOME-2A measurements on clouds and NO ₂	21
4.1 Cloud fraction comparison.....	21
4.2 Cloud pressure comparison	23
4.3 Cloud impacts on tropospheric NO ₂ SC.....	25
4.4 Cloud top height effects on tropospheric NO ₂ SC.....	26

4.5	Cloud impacts on NO ₂ VC.....	27
5	Cloud parameter effects on NO ₂ AMF	29
5.1	An overview of AMF.....	29
5.2	Evaluation of NO ₂ AMFs in satellite data	30
5.2.1	Cloud cover impact on NO ₂ AMF	30
5.2.2	Cloud top height impact on NO ₂ AMF.....	31
5.2.3	Effects of cloud correction on NO ₂ AMF at cloud fraction <20%.....	31
6	Cloud impacts on NO ₂ retrieval observed from the OMI instrument.....	34
6.1	Cloud distributions using the old and the new cloud algorithm.....	34
6.1.1	Cloud distributions over Central Eastern China	35
6.1.2	Cloud distributions over Central Western Europe.....	36
6.1.3	Cloud distributions over Eastern US	37
6.1.4	Cloud distribution over Central Africa	38
6.1.5	Cloud distribution over Yemen	39
6.1.6	Cloud distributions over Northern Pacific Ocean	41
6.2	Cloud impacts on NO ₂ SC from OMI	42
6.3	Impacts of clouds on tropospheric NO ₂ VC.....	46
7	Cloud impacts on NO ₂ columns: The global view	48
7.1	Global cloud distributions	48
7.2	Global cloud impacts on Tropospheric NO ₂ SC in 2007 and 2012	50
7.3	Effects on Tropospheric NO ₂ AMF and VC.....	51
8	Conclusion.....	52
9	Outlook	53
10	References	55
11	Appendix	59

Abstract

Clouds cover roughly 50% of Earth's surface. They are mostly distributed above the tropics and mid-latitudes at altitudes (cloud tops) of up to 15 km, varying strongly in type and properties. As a result of their shielding effect, clouds hide a large fraction of tropospheric trace gas columns from satellites view, leading to uncertainty in the retrievals. On the other hand, clouds can induce an enhancement in tropospheric retrievals due to multiple scattering and extended absorption paths. Nitrogen dioxide (NO_2) is one of the gases that are affected by cloud uncertainties, with a short atmospheric life-time of a few hours. NO_2 is located near the surface and lifted up from its sources.

In this study, the GOME-2A and OMI satellite instruments were used to retrieve cloud and NO_2 datasets. Additionally, the last two versions of GOME-2A and OMI cloud algorithms (FRESCO+ and OMCLDO2, respectively) were compared. A statistical analysis of tropospheric NO_2 and cloud data was performed. The results show that cloud fraction and cloud pressure distributions change according to the region, season, and instrument (regarding its cloud algorithm). The tropospheric slant column density of NO_2 is affected by clouds depending on cloud cover and cloud top height. The shielding effect of high clouds has a major impact on NO_2 retrievals at large cloud fractions while low clouds enhance NO_2 retrievals because of the high cloud albedo and multiple scattering. A layer of aerosol or a thin cloud allow the satellite sensitivity to penetrate into the lower troposphere retrieving NO_2 . Cloud algorithms treat such a layer as a small cloud fraction (up to 30%) of optically thick clouds due to their optical thickness. Although the cloud correction of NO_2 AMF is taken into consideration including small cloud fractions (0-20%) the NO_2 VC appears to be particularly uncertain around very small cloud fractions (underestimation) and very large cloud fractions (overestimation).

1 Introduction

Cloud effects on tropospheric trace gases are related to cloud's role in the atmosphere. In addition to controlling the hydrological cycle in the atmosphere, clouds play a substantial role in balancing Earth's radiation budget by reflecting ultraviolet and visible solar radiation and absorbing a wide spectrum of infrared radiation, including Earthshine. Cloud fraction, cloud pressure, and cloud

optical thickness are the relevant cloud parameters to determine cloud properties and their impacts on NO_2 retrieval. NO_2 and nitrogen oxide NO ($\text{NO}_x = \text{NO}_2 + \text{NO}$) are connected through their formation and removal processes. The main NO_x sources in the troposphere are combustion engines and power production, lightning, soil emissions, and ammonia oxidation (Crutzen, 1979). NO_x in the atmosphere plays a main role in production and destruction of ozone in the troposphere and stratosphere, respectively. Both processes lead to hazards on the atmosphere and life's safety on Earth. Space based observations determine cloud properties and NO_2 columns over large regions compared to ground based observations which are local. In this study, GOME-2A and OMI are the satellite instruments that are used to retrieve clouds from the atmosphere by processing cloud parameters retrieved using different cloud algorithms. The FRESCO+ and OMCLDO2 algorithms used for GOME-2A and OMI, respectively, determine cloud parameters employing the O_2 A-band between 758 nm and 768 nm (Wang et al. 2008) and the O_2 - O_2 band around 477 nm (Accareta et al., 2004) for each algorithm, respectively. DOAS fitting is used between 425 nm and 497 nm to determine NO_2 absorption for both instruments (Burrows et al. 2011). The fraction of NO_2 columns is located under clouds is undetectable for satellite observations as a result of a small retrieved signal below clouds while NO_2 columns above clouds, stratospheric NO_2 and the upper part of the troposphere, are well visible for satellite observations because of the high cloud albedo. Shielding of NO_2 column and enhancement of NO_2 retrievals are therefore twofold cloud impacts on retrieved NO_2 .

The scientific background section in Chapter 2 introduces some important information about clouds and NO_2 columns and their evaluation using satellite instruments, including instrument descriptions. The goals of this study are discussed in Chapter 3 by reviewing relevant studies about cloud effects on tropospheric NO_2 emphasizing that high uncertainty of retrieved tropospheric NO_2 column is caused by clouds. Additionally, a short description about cloud products and their principles is provided for GOME-2A and OMI. Chapter 4 presents some cloud distributions and their impacts on tropospheric NO_2 slant columns and vertical column densities over 6 regions processed using the last two versions of FRESCO+. The NO_2 AMF dependence on clouds is analyzed on global measurements from GOME-2A and OMI in Chapter 5. Regional measurements of clouds and NO_2 columns over the 6 regions from the OMI instrument are present in Chapter 6 to be compared to cloud effects on NO_2 columns, which are observed from GOME-2A. In addition to global cloud statistics, Chapter 7 demonstrates how NO_2 columns are globally

retrieved in the presence of clouds, with taking into account statistical effects. Chapter 8 gives a short summary on the Master thesis and Chapter 9 outlines possible future work as an outlook on this study.

2 Scientific background

2.1 Clouds in the atmosphere

2.1.1 Cloud composition

A cloud can be defined as a visible ensemble of droplets and particles in the atmosphere that may have equal or different sizes, compositions, and forms. Thermodynamical processes of the atmosphere determine the consecutive stages in the formation of clouds by heterogeneous and homogeneous nucleation. Homogeneous nucleation refers to condensation from supersaturated water vapour without the aid of particles in the air by collisions between water molecules to form a droplet of pure water, but this process is not effective in the atmosphere. Heterogeneous nucleation represents an effective process to form cloud droplets in the atmosphere. In this case, atmospheric aerosol (e.g. sodium chloride and ammonium sulfate) plays an important role in the condensation of water droplets that are activated and grow to form cloud droplets at supersaturations achieved in clouds (roughly 0.1-1%). These particles are called Cloud Condensation Nuclei (CCN) (Wallace and Hobbs, 2006). Condensation and coagulation are important processes for describing the growth of cloud droplets until reaching raindrop sizes depending on water vapour content and the atmospheric conditions such as temperature, pressure, and relative humidity. Adiabatic or radiative cooling is also a prerequisite for cloud formation by raising the relative humidity to exceed the saturation point. Moreover, saturation and supersaturation processes over water vapour pressure in the atmosphere are crucial factors to form droplets and ice crystals of clouds. Water vapour is the main constituent, which creates a broad spectrum of size distributions of cloud droplets. Their shapes are mostly approximated as spherical shapes for droplets and hexagonal shapes for ice crystals. In addition to water, cloud droplets also contain small amounts of other species such as chloride, nitrate, sulphate, ammonium, hydronium etc.

There is no doubt clouds play an important role in the atmosphere and climate system whether in influencing the Earth's energy balance due to modification of radiative transfer or in driving the hydrological cycle by evaporation and precipitation. In terms of Earth's energy balance the solar radiation reaching the top of the atmosphere is partially reflected by clouds due to their large albedo, and partially absorbed by clouds due to their water content. Shortwave solar radiation (VIS) is strongly reflected, while long-wave radiation (IR) is strongly absorbed and re-emitted. Besides modification of the temperature field due to the release of latent heat during phase transitions, cloud's water vapour content represents a greenhouse gas. As a result of the cloud feedback loop on climate warming depending on their altitude, a cooling effect takes place by reflection and scattering of UV and VIS radiation while IR radiation absorbed by clouds leads to a warming effect.

2.1.2 Cloud distribution in the atmosphere

According to the International Satellite Cloud Climatology Project (ISCCP) (<http://isccp.giss.nasa.gov/role>), clouds typically cover almost two-thirds of the planet. The sky over oceans is cloudier and the tops of its clouds are more than a kilometer lower. The distribution and properties of clouds widely vary with location, time of day, changing weather and season. Tropics and mid-latitudes are the cloudiest regions, while the subtropics and the Polar Regions have less cloud cover, as we can notice from Figure 2.1. In a vertical perspective, tropical cloud tops are substantially higher than cloud tops in the subtropics, mid-latitudes and the North Pole, extending up to 15 km. Clouds are much higher on average over the South Pole than over the Arctic because the ice sheet surface is so much higher in altitude. The distribution of clouds strongly depends on temperature, humidity, and pressure regions in the atmosphere. Many types of clouds are known based on their vertical and horizontal distribution; five Latin root words (cumulus, stratus, cirrus,

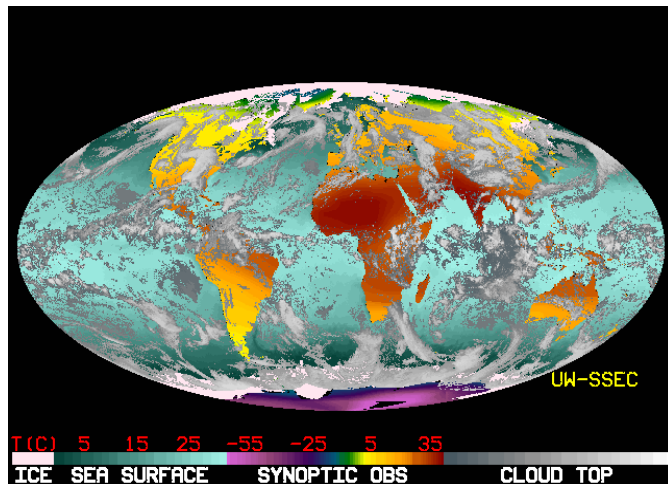


Figure 2.1: Cloud appearance viewed from space. Combined from GMS, GOES-8 and Meteosat imagery on October 15, 2015. http://www.ssec.wisc.edu/data/comp/latest_cmoll.gif

Figure 2.1. In a vertical perspective, tropical cloud tops are substantially higher than cloud tops in the subtropics, mid-latitudes and the North Pole, extending up to 15 km. Clouds are much higher on average over the South Pole than over the Arctic because the ice sheet surface is so much higher in altitude. The distribution of clouds strongly depends on temperature, humidity, and pressure regions in the atmosphere. Many types of clouds are known based on their vertical and horizontal distribution; five Latin root words (cumulus, stratus, cirrus,

nimbus, and altum) are used separately or in combination to describe cloud type, the accepted nomenclature having been composed since 1803 by the London chemist Luke Howar.

2.1.3 Cloud determination

The remote sensing of cloud is a unique method to determine not only clouds but also other atmospheric trace gases. The principle of remote sensing is to exploit the interaction between electromagnetic (EM) radiation and molecules or particles. For solar radiation, ultra-violet radiation (UV) and visible light (VIS) are reflected and scattered from clouds. In general, measurement techniques of the atmosphere use passive (e.g. IR images) or active (e.g. LIDARs) remote sensing. Most remote sensing techniques that are used to determine clouds are passive techniques where the instrument does not have its own source of radiation but rather uses radiation from the sun scattered in the atmosphere or thermal emission of the atmosphere itself. The principle of measurement and radiative transfer has been discussed in Richter, (2010). Satellites can globally sense backscattered radiation from clouds and then the radiative transfer equation can be evaluated to determine cloud parameters using Beer-Lambert's law expressed as

$$I(\lambda) = I_0(\lambda)e^{-\tau(\lambda)} \quad 2.1$$

$$\tau(\lambda) = \ln \frac{I_0(\lambda)}{I(\lambda)} = L[\alpha_A(\lambda) + \alpha_S(\lambda)] \quad 2.2$$

Where $I(\lambda)$ is the measured intensity, $I_0(\lambda)$ the un-attenuated reference intensity, $\tau(\lambda)$ the optical thickness, here for a cloud, α_A and α_S the extinction coefficients by absorption and scattering (Mie and Rayleigh scattering), respectively, and (L) the path length. In terms of infrared (IR) and microwave (MW) radiation energy that is coming by down-welling from the sun or by up-welling from Earthshine, can be absorbed and re-emitted by clouds into space in all directions. Ground-based observations and space-based observations can sense the absorbed and re-emitted spectrum of clouds and then the radiative transfer equation can also be used to determine cloud parameters. Cloud fraction, cloud phase, cloud optical thickness, cloud droplet/crystal effective radius, cloud liquid/ice water path, and cloud top properties are the most important of cloud parameters that have to be evaluated. These parameters and their retrieval techniques from the atmosphere are described in Burrows et al. (2011). Space-based instruments are more effective to monitor clouds as they can cover and observe a wider swath compared to ground-based instruments. In the last decades, numerous satellite instruments have been used for this purpose

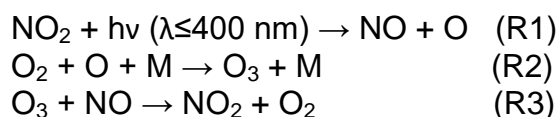
such as the Global Ozone Monitoring Experiments (GOME), the Scanning Imaging Absorption Spectrometer for Atmospheric Chartography (SCIAMACHY) and the Ozone Monitoring Instrument (OMI).

2.2 NO₂ in the atmosphere

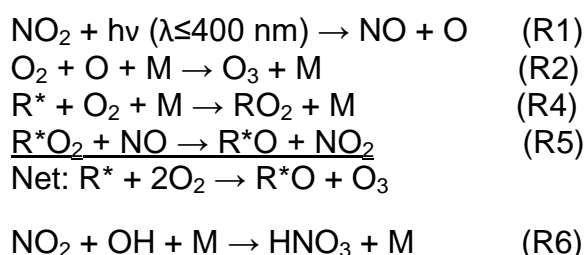
2.2.1 Sources and sinks of the tropospheric NO₂

Nitrogen dioxide (NO₂) is a significant trace gas of nitrogen compounds in the atmosphere. Formation of NO₂ is primarily related to the abundance of nitric oxides (NO), in particular in the troposphere; nitrogen oxides (NO₂+NO) are known as the NO_x group. In the troposphere, NO_x plays a main role in the formation of tropospheric ozone in clean and polluted regions as shown in Equations R1, R2, R3, R4, and R5 below. Radical species (R*) such as H, CH₃, and CH₃C(O) are effective pathways for the conversion of NO to NO₂ in polluted regions which leads to enhanced production of ozone compared to clean regions. Ozone is a pollutant and considered as a greenhouse gas. In addition to that, NO₂ is harmful for human health and ecosystems. The combustion of fossil fuel and biomass (anthropogenic effect), lightning, soil emissions, and ammonia oxidation are the main sources of tropospheric NO_x as shown in Table 2.1 below. The formation of nitric acid in polluted environments during daytime cleans the troposphere by removing NO₂ as shown in Equation R6 below while during night time NO₂ is converted first to NO₃ then to N₂O₅, which is finally removed by wet deposition and to a lesser degree by dry deposition.

Important tropospheric reactions of NO_x for clean regions



Important tropospheric reactions of NO_x for polluted regions



In the stratosphere, NO_x plays a substantial role in destroying the ozone layer by direct reactions with atomic oxygen and the reaction cycles with halogen compounds as shown in Equations R7, R8, and R9 below. Nitrous oxides (N₂O) oxidation, galactic cosmic rays, solar proton events, and nuclear bombs are the main sources of NO_x in the stratosphere as shown in Table 2.1 below. The

mechanism of nitric acid formation in the troposphere is also taking place in removing NO₂ from the stratosphere. In addition to that, chemical reaction of NO_x with Cl_x and H_x groups represents an important mechanism to remove NO_x from the stratosphere as shown in Equations R10 and R11. Reaction 10 also limits ozone destruction by ClO via forming the ClONO₂ reservoir species

Important stratospheric reactions of NO_x

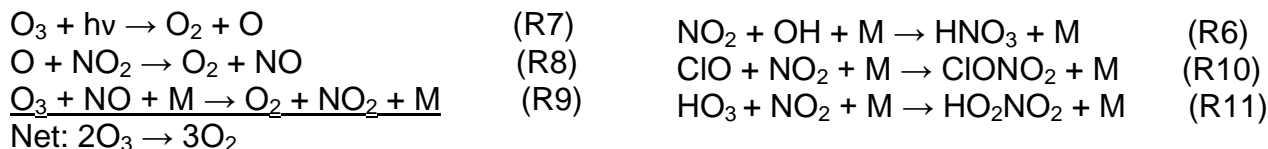


Table 2.1: Sources of atmospheric NO_x (1 Tg = 10¹² g). Collected from (Crutzen, 1979)

<u>Troposphere:</u>		<u>Stratosphere:</u>	
Combustions:	20 Tg N/yr	N ₂ O oxidation:	1 Tg N/yr
Lightning:	8-40 Tg N/yr	Solar proton event:	0.12 Tg N/yr
Soil emissions:	10 Tg N/yr	Galactic cosmic rays:	0.024–0.036 Tg N/yr
Ammonia oxidation:	< 8Tg N/yr	Nuclear bombs:	0.024 Tg N/megaton TNT

2.2.2 Tropospheric distribution of NO₂

Due to its atmospheric lifetime (a few hours to one day), NO₂ is globally concentrated close to the surface, in particular where its main sources are located. The concentrations of NO₂ above urban and industrial areas are higher than in rural environments because of the sources distribution. The NO₂ concentration in the troposphere is rapidly decreasing with altitude above polluted regions. Winds and atmospheric circulation drive NO₂

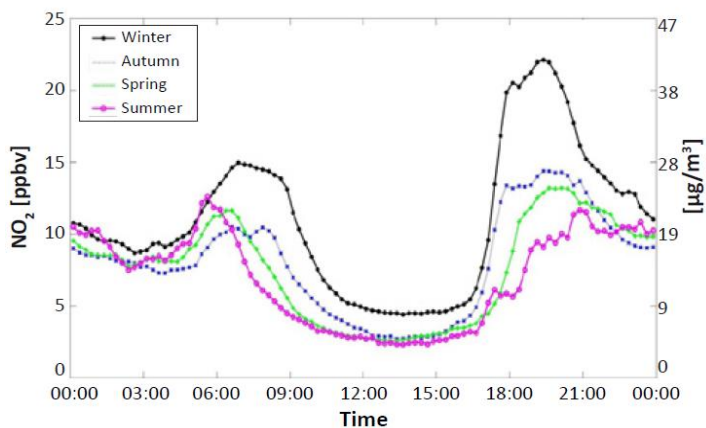


Figure 2.2: Average diurnal seasonal concentration of NO₂. Adapted from (Venter et al. 2012).

throughout the atmosphere, spreading it regionally and globally in vertical and horizontal directions. As a result of its short lifetime, there is a pronounced variation in the distribution of NO₂ concentration during daytime and nighttime (diurnal variation). During daytime the photolysis

reaction of NO_2 (R1) recycles back the hydroperoxy radical HO_2 to OH including the production of ozone to the expense of NO_2 concentration, while during nighttime the concentration of OH is almost zero. During night NO_2 reacts with ozone to generate the nitrate radical (NO_3) (Wayne et al. 1991) by this reaction ($\text{NO}_2 + \text{O}_3 \rightarrow \text{NO}_3 + \text{O}_2$). NO_3 radicals react further with NO_2 until establishing a chemical equilibrium with N_2O_5 , which can be taken up by aerosol particles. Figure 2.2 above shows an example demonstrating the diurnal cycle based on air quality measurements over South Africa for the sampling period from 8 February 2008 to 17 May 2010 by (Venter et al. 2012). In general, the smallest concentration of NO_2 is recorded during daytime, especially around 12 o'clock at noon, while high values are found around sunrise and sunset times because of traffic emissions and household combustion as shown in Figure 2.2 above. In terms of seasonal variation, the concentration raise of NO_2 is more notable in winter compared to summer season in the Northern Hemisphere because of the increase of energy use for room heating and the longer life time of NO_2 during winter.

2.2.3 NO_2 column retrieval by space-based observations

The fundamental base for observing many atmospheric trace gases, including NO_2 , from space is passive remote sensing of scattered and reflected solar radiation as explained in Section 2.1.3 for cloud determination. Each type of atmospheric molecule or particle has a distinctive spectrum in absorbing, scattering or emitting of electromagnetic radiation depending on its optical and electronic properties. Depending on the quantity of interest, various space-based and ground-based instrumentation using different spectral windows can be used. The most important techniques and satellites that are used for this purpose have been explained in Burrows et al. (2011). NO_2 has strong absorption at wavelengths around 400 nm within the visible spectrum. This spectral range is therefore used for NO_2 retrieval in the troposphere and stratosphere by satellite instruments such as GOME, SCIAMACHY and OMI using back-scattered light from Earth's atmosphere. The Differential Optical Absorption Spectroscopy (DOAS) technique is used to identify and quantify the NO_2 abundances with narrow band absorption structure in its wavelength range in the open atmosphere. The basic idea of this technique is to separate the trace gas absorption cross section into two parts, one that varies slowly with wavelength, and a rapidly varying differential cross section; the latter can be thought of as absorption lines or bands (Hoenninger et al. 2004). DOAS uses the Beer-Lambert law (Equation 2.1) with modified source

intensity and absorption cross section σ' to eliminate contributions that vary only slowly with wavelength. Here the differential optical thickness is expressed as $\sigma(\lambda) = \sigma'(\lambda) \times s$, where s the slant column density (SCD), which is defined as the trace gas concentration integrated along the effective light path and usually converted to the vertical column density (VCD) which is defined as the trace gas concentration integrated along the vertical path through the atmosphere (Hoenninger et al. 2004). In order to interpret scattered light measurements, DOAS uses the concept of air mass factor (AMF), which is defined as the ratio between slant column density and vertical column density.

2.2.4 The effect of clouds on trace gases retrieval

Due to cloud's role and their distribution in the atmosphere, wide areas of the Earth's surface are shielded by the presence of clouds (cloud fraction). UV radiation and visible light are reflected and scattered strongly from clouds (albedo effect) while IR radiation is absorbed by water molecules, except narrow windows between 8 and 14 μm where radiation can penetrate to the surface. Cloud albedo leads to enhancement of single and multiple scattering light paths from sun to cloud to satellite in the upper part of the cloud. For low clouds, this leads to enhanced absorption and increasing depth of absorption lines of O_2 and O_4 above the cloud (Stammes et al. 2008). For satellite observations, the part of the atmosphere above the clouds (cloud pressure) is seen and retrieved with good signal but the sensitivity to the atmosphere below the cloud, mostly tropospheric gases, is usually very low.

2.3 Overview about satellite instruments

2.3.1 The Global Ozone Monitoring Experiment (GOME)

The GOME instrument was the first European passive remote sensing spectrometer, considered as a medium resolution nadir-scanning UV/VIS spectrometer. It was launched in April 1995 by the European Space Agency (ESA) aboard the Second European Remote Sensing Satellite (ERS-2), into a near-polar sun-synchronous orbit at a mean altitude of 785 km with a local equator crossing time at 10:30 a.m. (descending node). GOME was designed to measure the Earthshine radiance and the solar irradiance in the UV/VIS spectral range (240-790 nm) at a moderate spectral resolution of (0.2-0.4 nm). GOME could achieve global coverage in three days after 43 orbits and its spatial resolution was $40 \times 320 \text{ km}^2$ (Burrows et al. 1999). The important atmospheric

measurements that can be determined by the GOME spectrometer are radiance measurements (e.g. the solar radiance, nadir spectrum, and lunar spectrum). Within this spectral region, trace gases retrieval (e.g. O₃, NO₂, BrO, H₂O, O₄, O₂, OCIO, SO₂, H₂CO, and ozone vertical profiles), clouds (cloud cover, cloud reflectance, cloud-top height and optical depth), surface properties (albedo and surface spectral reflectance), aerosols, and solar UV irradiance variability can be performed (Burrows et al. 1999). Recently, the second version of GOME, GOME-2/MetOp-A and GOME-2/MetOp-B, have been launched in 2006 and 2012, respectively, on sun-synchronous orbits with a repeat cycle of 29 days and an equator crossing time of 09:30 local time (descending node). In tandem mode since 2013, GOME-2/MetOp-A is now operated on a reduced swath width of 960 km with an increased spatial resolution (approximately 40×40 km²), while GOME-2/MetOp-B operates on a wide swath at 1920 km with spatial resolution of 80×40 km². This enhancement leads to an increase of both the daily coverage (about 1.5 days) and the spatial resolution of GOME-2 measurements (Hao et al. 2014).

2.3.2 The Scanning Imaging Absorption Spectrometer for Atmospheric Chatography (SCIAMACHY)

The SCIAMACHY instrument, an extended version of the GOME instrument was launched by ESA in March 2002 onboard Environmental Satellite (ENVISAT), flying in a polar sun-synchronous orbit with a morning descending node crossing time at 10:00 a.m., where its orbital period is 100.6 min (Gottwald et al. 2006). The SCIAMACHY spectrometer comprises of a mirror system, a telescope, and thermal and electronic subsystem which operate in the UV, VIS, and NIR wavelength regions (240-2380 nm) at moderate spectral resolution (0.2-1.5 nm). According to its field of view (FOI), SCIAMACHY measures the Earthshine radiance in limb and nadir viewing geometries and solar or lunar light observed in occultation (Bovensmann et al. 1999). The spatial resolution is different depending on viewing geometry mode, in nadir approximately 30(along track) × 240(across track) km²; in limb approximately 240(azimuth) × 3 (elevation) km²; and in solar occultation approximately 30 (azimuth) × 2.5(elevation) km². The SCIAMACHY instrument has been designed to determine the amounts and distributions of trace gases (e.g. O₂, O₃, O₄, BrO, OCIO, SO₂, NO₂, NO₃, CO, CO₂, CH₄, H₂O) and aerosols in the troposphere and stratosphere including ozone layer observation; cloud parameters (cloud fraction and cloud-top height); and surface spectral reflectance.

2.3.3 The Ozone Monitoring Instrument (OMI)

OMI is a UV/vis nadir solar backscatter spectrometer, launched in July 2004 on the Earth Observing System Aura satellite in a sun-synchronous orbit (98.2° inclination) at 705 km altitude with a local afternoon equator crossing time at 13:45 (ascending node), providing daily global coverage and 14 orbits a day. The UV/VIS spectral range of OMI is (270-500 nm) with spectral resolution of about 0.5 nm and a very high spatial resolution of 13 km×24 km at nadir. As a result of its high spatial and spectral resolution, small footprint (pixel size) and daily global coverage, the OMI spectrometer is able to detect and determine trace gas columns (e.g. O₃, NO₂, HCHO, BrO, and OCIO), cloud-top height and cloud fraction, and aerosols (Levelt et al. 2006). To measure the solar irradiance and the Earth radiance spectrum, OMI utilizes a 2-D Charge-Coupled Device (CCD) detector; one dimension is used for the spatial information and the additional dimension for the spectral information. In contrast to GOME and SCIAMACHY, OMI does not use scan mirrors to obtain the across track spatial information, but a large field of view (114°), which is focused on the two dimensional detector with an imaging optical design (Levelt et al. 2006). In order to retrieve cloud information, OMI uses the O₄ absorption band at 477 nm instead of the O₂ A-band at 760 nm because it does not cover the spectral range of the O₂ A-band.

Table 2.2. Instruments characteristics summary

Instrument	Date		Spectral range (nm)	Spectral resolution (nm)	Nadir spatial resolution (km ²)	Global coverage
	From	To				
GOME-1	1995	2003	240 - 790	0.2 - 0.4	40 × 320	3 days
SCIAMACHY	2002	2012	240 - 2380	0.2 - 1.5	30 × 60	6 days
OMI	2004	Present	270 - 500	Around 0.5	13 × 24	1 day
GOME-2A	2006	Present	240 - 790	0.2 - 0.4	40×80/40×40	1.5 days
GOME-2B	2012	Present	240 - 790	0.2 - 0.4	40 × 80	1.5 days

3 The aim of the study and its significance

3.1 Cloud effects on the tropospheric NO₂ retrieval

Figure 3.1 illustrates two main scenarios for retrieving NO₂ in the atmosphere using satellite passive remote sensing. As shown from different paths on the scheme, there is not obviously cloud impacts if a satellite instrument retrieves NO₂ in the absence of clouds for cloud free pixels

(first scenario). Two situations for fully cloudy pixels of the instrument are assumed when the retrieval of NO_2 and clouds are synchronized in the atmosphere (second scenario). The NO_2 columns below clouds are expected to be screened from the satellite view. Such NO_2 columns are called ghost columns and determined using a model according to the NO_2 profile. On the other hand NO_2 can be located above clouds or within clouds. In this case, the retrieval of NO_2 is not only possible but NO_2 visibility can be enhanced as a result of high cloud albedo and multiple scattering depending on cloud type and optical thickness. For partly cloudy pixels of the instrument, both scenarios can be occurred relative to cloud fraction. As follows, more information about these effects will be provided and, practically, analyzed using satellite datasets in more details in the result sections as a main goal of this study.

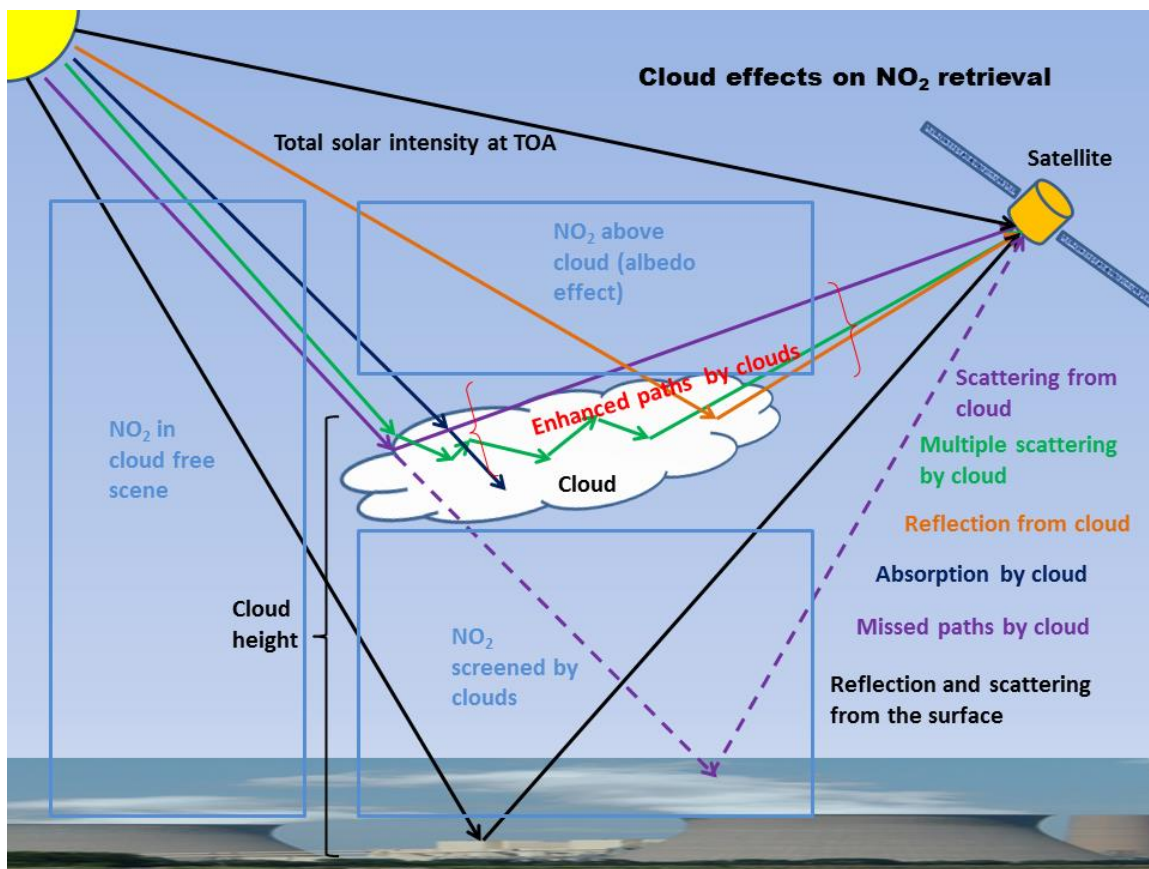


Figure 3.1: Scheme of the relevant effects of cloud on NO_2 column retrievals

3.1.1 The observed cloud effects on tropospheric NO_2 columns

Many studies discussed the most important cloud effects on NO_2 columns retrieved by space borne measurements. If clouds are present, they shield a part of the boundary layer NO_2 from view

of satellite measurements in the UV-visible wavelength range. In this case, the tropospheric column below the cloud is excluded from the measurements. This leads to large uncertainties in the tropospheric NO₂ results, introduced by residual clouds in the ground pixels. For instance, most GOME measurements are contaminated by clouds, as a result of the large ground pixel size. Richter and Burrows (2002) found that the tropospheric NO₂ columns derived from GOME increase with decreasing cloud cover in two polluted sites (above Bremen and Tokyo) and concluded that most NO₂ resides below the clouds and is effectively shielded from being observed if clouds are present. On the other hand they noticed that vertical columns over Bremen were larger even at large cloud fraction compared to the vertical column over Tokyo. They justified this effect by assuming that some NO₂ is also present above the clouds and that this is more important over Europe than over low latitudes because of lower clouds. In this case, clouds can increase the absorption of NO₂ and multiple scattering enhances the light path. In terms of the effect on NO₂ AMF, large cloud fraction and high cloud lead to small AMF as a result of the shielding effect.

3.1.2 Enhancement of tropospheric NO₂ columns by clouds

Some studies of NO₂ measurement demonstrated that NO₂ columns retrieval can be enhanced by clouds. Wang et al. (2005) used an airborne multi-axis DOAS instrument (AMAX-DOAS) in three different wavelength windows (345-380, 410-456 and 472-497 nm) to detect tropospheric NO₂ over Europe under cloudy and cloud free conditions, in nadir and zenith viewing direction, during one flight of the SCIAVALUE campaign on 19th March 2003. They explained that enhancement of NO₂ columns was observed in cloudy situations, in particular when approaching cloud free areas; low clouds increase the column through the effect of increased albedo and multiple scattering. Cloud top height and cloud optical thickness were derived from the O₄ measurements where good consistency was obtained for a low cloud layer between 0.4 and 1.5 km having an optical depth of 25. This study also emphasizes that enhanced NO₂ columns must be above or in the clouds and the bulk of the NO₂ must be located in the boundary layer resulting from local emissions. Albedo and multiple scattering effects lead to large AMF if NO₂ is above or within the upper part of a cloud.

3.1.3 The NO₂ column errors due to cloud errors

The overall magnitude of cloud fraction-related errors was estimated by taking more than 500,000 GOME pixels in March 1997 filtered for cloud radiance fractions <50% (geometric cloud fraction roughly <15%) to ensure a strong signal from the boundary layer over continental regions with high tropospheric NO₂ columns, typically uncertainties up to 30% occur (Boersma et al. 2004). These uncertainties were largest for the polluted pixels near source regions of tropospheric NO₂ columns. The tropospheric AMF uncertainties due to cloud fraction uncertainties are also in the 0 - 30% range, with 20–30% uncertainties for polluted regions with small cloud fractions. In addition to cloud fraction errors, cloud top errors induce retrieval errors, on average less than 10%. Most low clouds occur over the sub-tropical oceans and sometimes over coastal regions, like SCIAMACHY observation, GOME observation indicated that cloud tops are mainly situated between the surface and 800 hPa. The AMF uncertainties due to cloud pressure uncertainties are higher in outflow areas because the cloud tops are lower and nearer to the tropospheric NO₂ outflow plumes. Boersma et al. (2004) also observed that sea pixels in the vicinity of source regions exhibit uncertainties of up to 25% with the expectation of relatively high NO₂ concentrations close to the cloud height. Polluted pixels having low clouds can cause large uncertainties in NO₂ ghost columns compared to the uncertainties that are caused by high clouds, where the absolute uncertainty is actually produced from the NO₂ ghost columns.

3.2 The cloud algorithms used

Due to the fact that the atmosphere below clouds is blocked from satellite observations, cloud algorithms are based on two main reflectors during the determination of cloud parameters. Cloud top surface and the ground are the relevant reflectors and they are both assumed to be Lambertian surfaces with different albedo to retrieve the atmospheric information above these sectors using remote sensing methods as describes in the following sections. The scattering by aerosols is excluded from the calculations in such algorithms because of their variability. In this section, a description of cloud product algorithms of the GOME-2A and OMI instruments is provided to explain the principle of cloud retrievals. To evaluate which of the cloud products is best used for the retrieval of NO₂ slant columns, the last two versions of GOME-2A algorithms are then compared using datasets taken from FRESCO+ version 6 and FRESCO+ version 7 in July and December of 2007 over certain regions.

3.2.1 GOME-2A cloud products

3.2.1.1 FRESCO

The Fast REtrieval Scheme for Clouds from the Oxygen A-band (FRESCO) algorithm is a method to calculate cloud properties from measurements of the O₂ A-band. This method determines cloud fraction and cloud top pressure using three spectral windows of the oxygen A-band absorption, namely, at 758-759 nm (no absorption), at 761-762 nm (strong absorption), and at 765-766 nm (moderate absorption) (Tuinder et al. 2004). The oxygen transmission is calculated using a line-by-line method for a 1-pm wavelength grid using the line parameters from HITRAN 2004 and then convolving the spectrum using the instrument response function at the measurement wavelength grid (Wang et al., 2008). The absorption due to oxygen molecules above clouds and the ground surface are taken into account according to the attenuated spectra along photon paths, which are passed from the Sun to the ground and then to the satellite and from the Sun to the cloud tops and then to the satellite (Koelemeijer et al. 2001) as shown in Figure 3.2.b. The cloud tops and the surface are assumed to be Lambertian reflectors which absorb a part of the incident radiation and illuminate the other part into all directions regardless the reflection angles. From Figure 3.2.a, it can be seen that a deeper absorption of the O₂ A-band is observed over low clouds than over high clouds because of the increment of oxygen optical thickness in the lower atmosphere. This process enables FRESCO+ to evaluate cloud top pressure as shown in Figure 3.2.b. Single Rayleigh scattering is also taken into account.

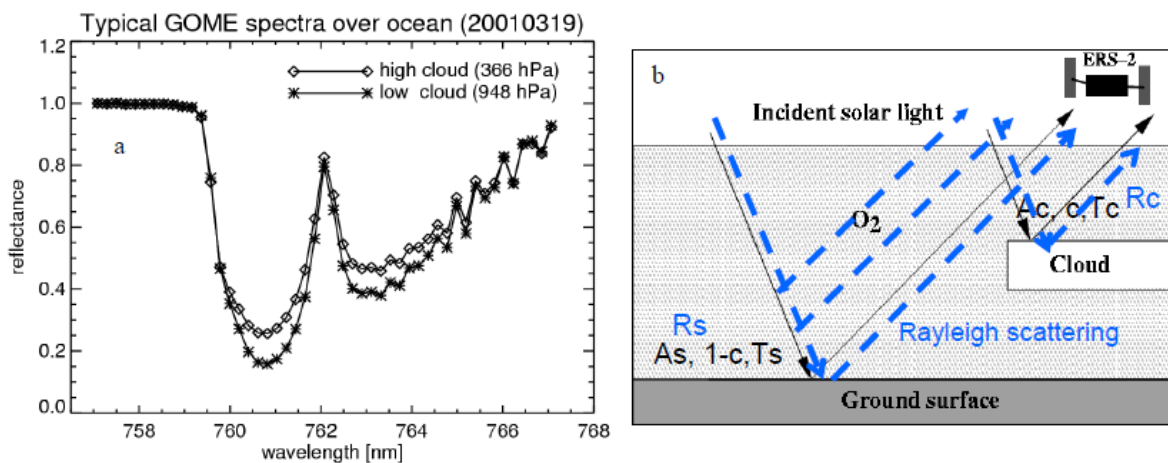


Figure 3.2: a) O₂ A-band spectra measured by GOME, b) an illustration sketch of the retrieved reflectances of FRESCO+ from clouds and the ground surface (black lines) including single Rayleigh scattering (blue dashed lines). Taken from (Wang et al., 2006).

The reflectivity of each cloudy pixel depends on its own optical thickness and is computed based on the Independent Pixel Approximation (IPA) (Marshak et al., 1995). The FRESCO algorithm determines the simulated reflectivity over a cloud free scene and a cloudy scene by

$$R_{sim}(\lambda) = (1-c) A_s T'_s(\lambda, P_s, \theta, \theta_0) + c A_c T'_c(\lambda, P_c, \theta, \theta_0) \quad 3.1$$

Where, A_s and A_c are the surface albedo and cloud albedo respectively. The values of albedo are assumed to be equal to 0.02 for the sea surface, 0.8 for clouds, and varying values for the land surface according to a global minimum reflectivity database (Koelemeijer et al. 2001). The c , p_s , and p_c symbols are cloud fraction, pressure at the surface, and pressure at cloud tops respectively. The solar and viewing zenith angles are θ_0 and θ . T'_s and T'_c represent the transmittances of the atmosphere to the surface and the clouds, respectively, as a function of wavelength, pressure, SZA, and VZA including the absorbed part of the solar irradiance by the surface and clouds, as calculated from the following equation

$$T(\lambda, P_s, \theta, \theta_0) = e^{-\tau_{o_2}(\lambda, P_s, \theta, \theta_0)} \quad 3.2$$

Where, τ_{o_2} is the slant oxygen optical thickness, determined by calculating the oxygen absorption cross section and oxygen density at each altitude, which can be converted from pressure using the hydrostatic equation. In addition to calculating $R_{sim}(\lambda)$, it is important to determine the so-called measured reflectivity $R_{meas}(\lambda)$ from Equation 4.3 in order to derive cloud fraction and cloud pressure by a nonlinear least squares minimization of $R_{meas}(\lambda)$ and $R_{sim}(\lambda)$ and varying cloud fraction and cloud pressure using the $R_{meas}(\lambda) \approx R_{sim}(\lambda)$ assumption (Koelemeijer et al. 2001).

$$R_{meas}(\lambda) = \frac{I(\lambda)}{\cos\theta_0 F_0(\lambda)} \quad 3.3$$

Where $I(\lambda)$ and $F_0(\lambda)$ are the measured Earth's radiance and solar irradiance respectively.

3.2.1.2 FRESCO+

The principle of the FRESCO+ algorithm is similar to the FRESCO principle, as described in the previous section. The FRESCO algorithm has been developed to FRESCO+ by including single Rayleigh scattering as a new term to improve the determination of cloud parameters. The Rayleigh scattering coefficient calculation is therefore added to calculate the total atmospheric optical thickness $\tau(\lambda, p, \theta, \theta_0)$ in such a method, expressed by $\alpha_{sct}(\lambda, z) = n_{air}(z) \sigma_R(\lambda, z)$, where $n_{air}(z)$

denotes the air density and $\sigma_R(\lambda, z)$ is the Rayleigh scattering cross-section which is calculated from the formula $\sigma_R = \left(\frac{32\pi^3}{3N^2\lambda^4} \right) (n_{air} - 1)^2 F_k'(air)$. Here, $(n_{air} - 1)$ is the refractive index, the air number density N , and $F_k'(air)$ the effective King correction factor (Wang et al. 2008). The same fitting between a simulated reflectance and the measured reflectance spectrum in the three windows of the O₂ A-band absorption is used by the FRESCO+ algorithm to retrieve the effective cloud fraction and cloud top pressure (Wang et al. 2008). The simulated reflectance (R_{sim}) at TOA for one pixel is given by

$$R_{sim}(\lambda) = (1-c) [A_s T_s'(\lambda, P_s, \theta, \theta_0) + R_s(\lambda, P_s, \theta, \theta_0)] + c [A_c T_c'(\lambda, P_c, \theta, \theta_0) + R_c(\lambda, P_c, \theta, \theta_0)] \quad 3.4$$

R_s and R_c are the single Rayleigh scattering reflectance of the cloud free and cloudy scenes of the pixel, respectively, pre-calculated and stored as look-up-table (LUT). In this method, Rayleigh scattering extinction and O₂ absorption are taken into account for the transmittance term of clouds and the surface. The contribution of single Rayleigh scattering in this algorithm is small but significant for determining low clouds (high cloud pressure), in particular at small effective cloud fractions (partly and cloud free scenes).

From a comparison between the results obtained from the FRESCO+ and FRESCO algorithms, Wang et al. (2008) found that FRESCO+ yields more accurate cloud pressure in less cloudy scenes. The difference between FRESCO+ and FRESCO cloud pressure is about 50 hPa, FRESCO+ being higher (lower cloud top height), while the FRESCO+ effective cloud fraction is about 0.01 larger in the monthly global average. Overall, an improvement of FRESCO+ in cloud pressure and cloud fraction retrievals is expected because of the insertion of single Rayleigh scattering contribution. FRESCO and FRESCO+ data for GOME, SCIAMACHY, GOME-2A and GOME-2B are available at the www.temis.nl web page.

The FRESCOv7 and FRESCOv6 algorithms are the last and previous versions of FRESCO+ , respectively, used for GOME-2A for determining cloud parameters in this study. The change of climatology of surface albedo from the GOME data base (FRESCOv6) to the GOME-2 data base (FRESCOv7) is the main difference between both algorithms. More details is provided in the results of GOME-2A clouds as follows.

3.2.2 OMI cloud products

3.2.2.1 OMCLDO2

The OMI O₂-O₂ cloud product (OMCLDO2) algorithm is designed to derive cloud pressure and cloud fraction parameters using the oxygen dimer (O₂-O₂) absorption band at 477 nm. This algorithm is used in the OMI instrument because the OMI spectral coverage includes the oxygen dimer absorption band whereas it does not cover the O₂ A-band, which is used in the FRESCO algorithm as discussed above. The oxygen dimer absorption band is induced by collisional interaction between two molecules of oxygen for a short time (Acarreta et al. 2004). Despite the weakness of this band in comparison with the O₂ A-band, it can be retrieved by DOAS. The oxygen dimer spectral absorption cross section multiplied with the equilibrium constant between O₂ and O₄ is around 10⁻⁴⁶ cm⁵ molecule⁻², calculated under standard pressure (1 bar) at temperature of 223 and 283 K and wavelengths of 455 to 670 nm, measured by Newnham and Ballard, (1998). O₄ has a broad band of absorption in the interval 460-490 nm around 477 nm, as shown in Figure 3.3.

The ground pixel reflectance is treated in the independent pixel approximation given by Acarreta et al. (2004)

$$R(\lambda, \theta, \theta_0, \varphi - \varphi_0; c_l, z_l, A_s, z_s) = c R^l(\lambda, \theta, \theta_0, \varphi - \varphi_0; A_l, z_l) + (1-c)R^{\text{clear}}(\lambda, \theta, \theta_0, \varphi - \varphi_0; A_s, z_s) \quad 3.5$$

Where, $\varphi - \varphi_0$ is the relative azimuth angle between the incident sunlight and the emergent scattered light. R^l and R^{clear} , c_l , z_l , and A_l are the reflectance from the cloudy and the clear sub-pixels, effective cloud fraction, cloud height, and cloud albedo (fixed to 0.8), respectively. Cloud surface and ground surface are assumed to be Lambertian reflectors. The surface albedo is calculated via interpolating the ground albedo database of (Koelemeijer et al. 2003).

Figure 3.3 shows that the reflectance of a fully cloudy pixel ($c_l=1$) over high clouds is larger than over low clouds. Hence, the cloud fraction is determined from the reflectance and the cloud pressure is determined from the O₄ slant column. The window 460-490 nm is used to fit the

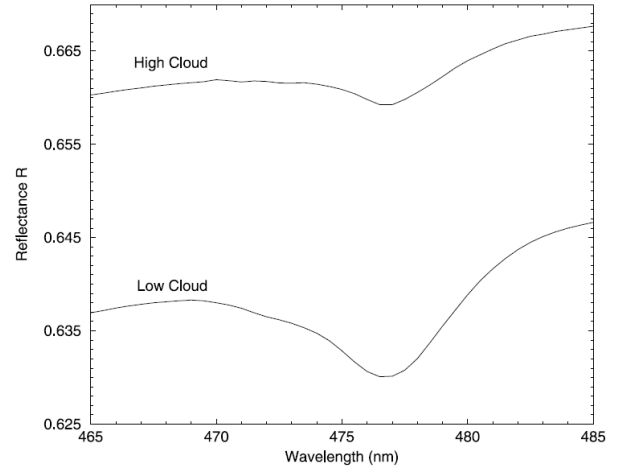


Figure 3.3: A simulated reflectance of the O₂-O₂ band over the ocean from low and high clouds for a fully cloudy scene (Acarreta et al., 2004).

absorption cross-section spectrum of the oxygen dimer $\sigma(\lambda)_{O_2-O_2}$ to the negative logarithm of the measured reflectance spectrum using the DOAS method. Because of the overlap between the oxygen dimer and the O_3 spectrum, the O_3 cross-section spectrum $\sigma(\lambda)_{O_3}$ (Burrows et al. 1999) is included in the spectral fit. The following equation is applied to calculate the simulated spectra, and then to determine the slant column density of the oxygen dimer (N_s) and the continuum reflectance (R_c)

$$-\ln R(\lambda) = \gamma_1 + \gamma_2 \lambda + (N_s \sigma(\lambda))_{O_2-O_2} + (N_s \sigma(\lambda))_{O_3} \quad 3.6$$

Where, $\gamma_1 + \gamma_2 \lambda$ represent the negative logarithm of the continuum reflectance ($R_c = \exp(-(\gamma_1 + \gamma_2 \lambda))$). A look-up-table is used to convert the retrieved quantities N_s and R_c into cloud heights and effective cloud fraction (Acarreta et al. 2004).

A new version of OMCLDO2 (version 2.0) is presented by Veefkind et al. (2016), containing some improvements to improve the cloud fraction and cloud pressure retrievals. A temperature correction is taken into account when deriving the O_2-O_2 slant columns accounting for the temperature variation over latitudes and seasons. The dependency of pressure on temperature due to the equation of state leads to a large effect on cloud top pressures, especially in the lower troposphere, where oxygen is present at higher concentration according to the profile of oxygen mixing ratio in the atmosphere. In this study, this version of the algorithm has been compared to the previous version using datasets obtained from the OMI instrument above different regions in summer and winter as follows.

3.2.2.2 OMCLDRR

The OMCLDRR algorithm retrieves cloud parameters employing Rotational Raman Scattering (RRS) by atmospheric molecules in the UV and VIS spectral regions. If light scattered by a molecule differs in frequency from the incident light, it is called inelastic scattering such as RRS. In the atmosphere, RRS lines contain roughly 4% of the total scattered energy by oxygen and nitrogen molecules, transferred to longer wavelengths (Stokes lines) and shorter wavelengths (anti-Stokes lines) with shifts of up to 2 nm in the UV (Joiner and Vasilkov, 2006). The selection of spectral fitting window of OMCLDRR algorithm differs from version to version. For instance, the first released version (OMCLDRR v1.0.2) employed the (392-398 nm) window while OMCLDRR v1.2.0 uses the (345-354 nm) window as shown in Figure 4.3.

The effective cloud fraction is expressed by

$$f = (I_m - I_g) / (I_c - I_g) \quad 3.7$$

Where, I_m is the measured TOA radiance, I_g and I_c represent sub-pixel radiances of cloud free and cloudy part, respectively, and are measured according to albedo assumptions of the ground and clouds. As RRS causes filling-in of the solar Fraunhofer line cores, the Ring effect (Vountas et al. 1998), this process is measured by the OMCLDRR algorithm to retrieve effective cloud pressure using the Mixed

Lambertian Equivalent Reflectivity (MLER) approximation, which treats a cloud or ground as a horizontally homogenous opaque Lambertian reflecting surface (Vasilkov et al. 2008). A percentage ratio between the inelastic RRS component of the TOA radiance and the elastically scattered component defines the RRS filling-in. The effective cloud pressure is derived from the spectral fit of the observed high-frequency structure of the TOA reflectance using a minimum-variance technique. Figure 3.4 shows the RRS filling-in within the OMCLDRR fitting window to differentiate between two cloud pressures. This algorithm is not practically used in this study to determine cloud parameters.

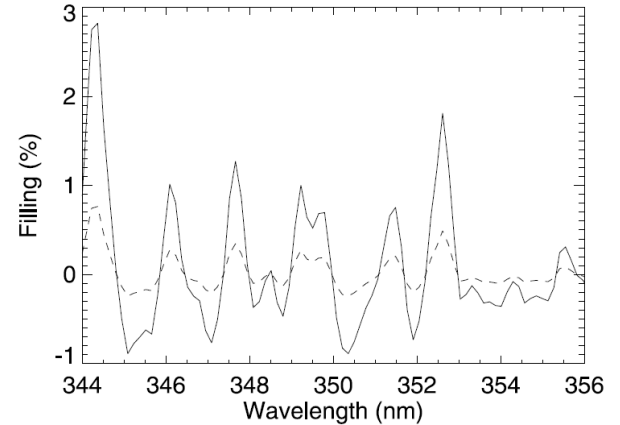


Figure 3.4: A nadir observation of RRS filling-in at 700 hPa (solid line) and at 200 hPa (dashed line) with albedo of 0.6 for a Lambertian surface (Vasilkov et al., 2008).

4 GOME-2A measurements on clouds and NO₂

To compare between clouds of the FRESCO+ version 6 (FRESCOv6) and FRESCO+ version 7 (FRESCOv7) algorithms, the cloud parameters (cloud fraction and cloud pressure) retrieved by both algorithms were determined over 6 different regions (Table 4.1) in July and December of 2007. July and December are chosen to represent summer and winter when the seasonal variation of clouds and NO₂ are quite pronounced. Cloud fraction and cloud pressure were analyzed to study in how far they agree or disagree and what their effects are on the tropospheric NO₂ columns.

Table 4.1: The targeted regions for the seasonal variations of clouds and NO₂

Region	latitude	Longitude
Central Eastern China	30° N-40° N	110° E-120° E
Central Western Europe	45° N-55° N	5° W- 15° E
Eastern US	30° N-45° N	70° W-90° W
Central Africa	5° S-15° S	10° E- 30° E
Yemen	10° N-20° N	40° E-55° E
Northern pacific ocean	30° N-40° N	150° E-165° W

4.1 Cloud fraction comparison

When looking at the differences of cloud fraction distributions above Central Western Europe and the Eastern US (Figure 4.1), it can be seen that more cloud pixels are recorded at small cloud fractions (<0.5) in July (summer) and at large cloud fractions (>0.5) in December (winter). This implies, that is generally cloudier in winter than in summer over the mentioned regions because of the seasonal variation of clouds. The cloud fraction values peak at cloud free scenes (0) and fully cloudy scenes (1) as a result of the cloud fraction determination. Based on the Lambertian assumption for the cloud surface albedo (0.8), the effective cloud fraction will be larger than 1 if the measured reflectance is larger than 0.8. In this case the cloud fraction is clipped to 1. On the other hand, if the effective cloud fraction is smaller than 0, then it is clipped to 0. The change of the surface albedo climatology from the GOME reflectance data base (FRESCOv6) to the GOME-2 LER setting (FRESCOv7) results in a clear difference for the distribution of cloud pixels between the FRESCO6 and FRESCOv7 algorithms, as shown in Figure 4.1. The FRESCOv6 results in

more pixels at very small cloud fractions while the FRESCOv7 pixels show generally larger cloud fractions, regardless region and season. The difference of global cloud distributions between the FRESCOv7 and FRESCOv6 algorithms (Figure 4.2) cannot easily be distinguished whereas it is clear from the histograms (Figure 4.1). Since a large fraction of the pixels of the GOME-2A instrument are affected by clouds, the cloud correction is significant to tackle the trace gas VCs, in particular at small cloud fractions (<0.3).

Cloud fractions do not change much between the FRESCOv7 and FRESCOv6 algorithms but overall there are significantly less cloud free pixels with FRESCOv7.

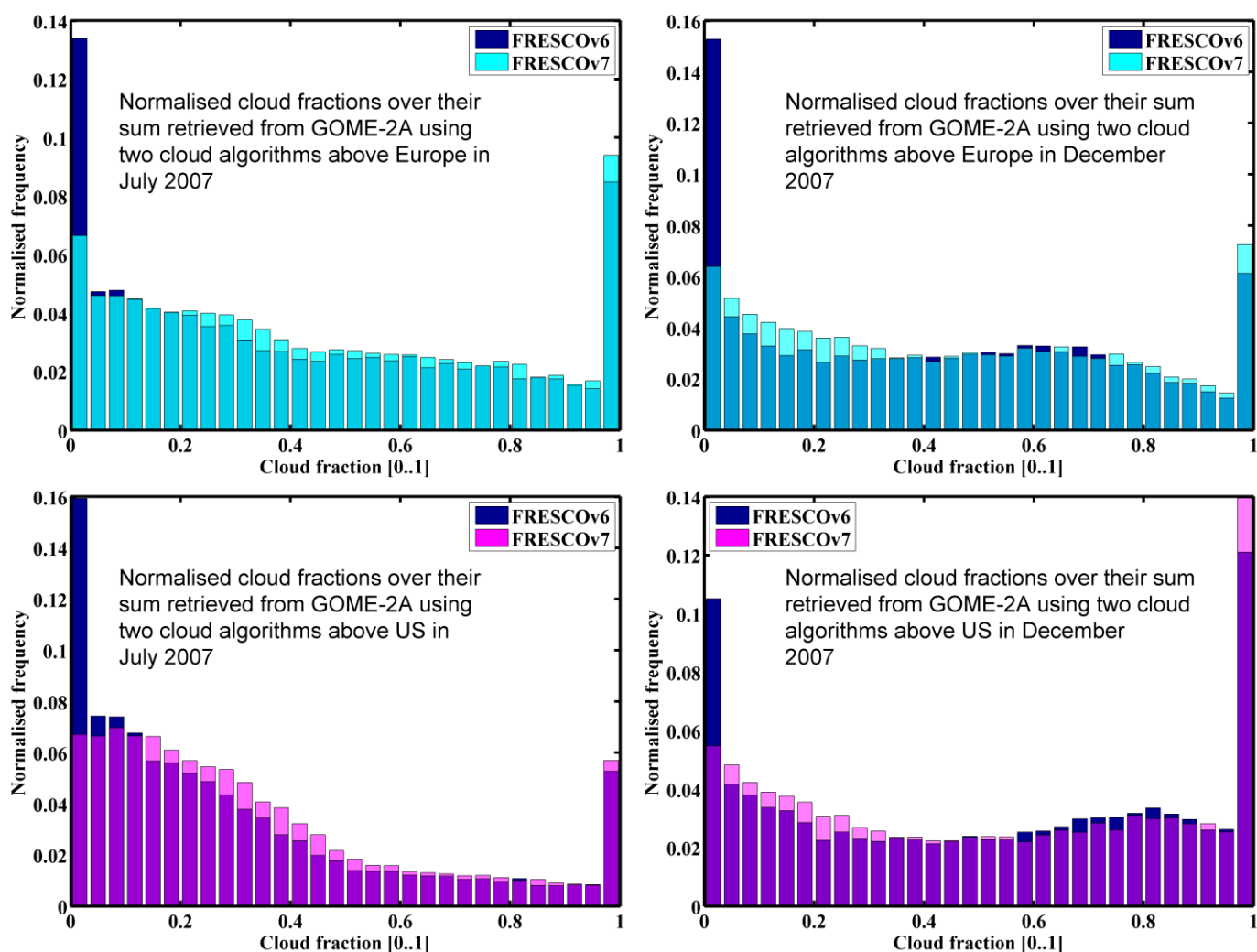


Figure 4.1: Normalised frequencies of cloud fraction from FRESCOv6 and FERSCOv7 algorithms from GOME-2A over Europe and US in July and December 2007.

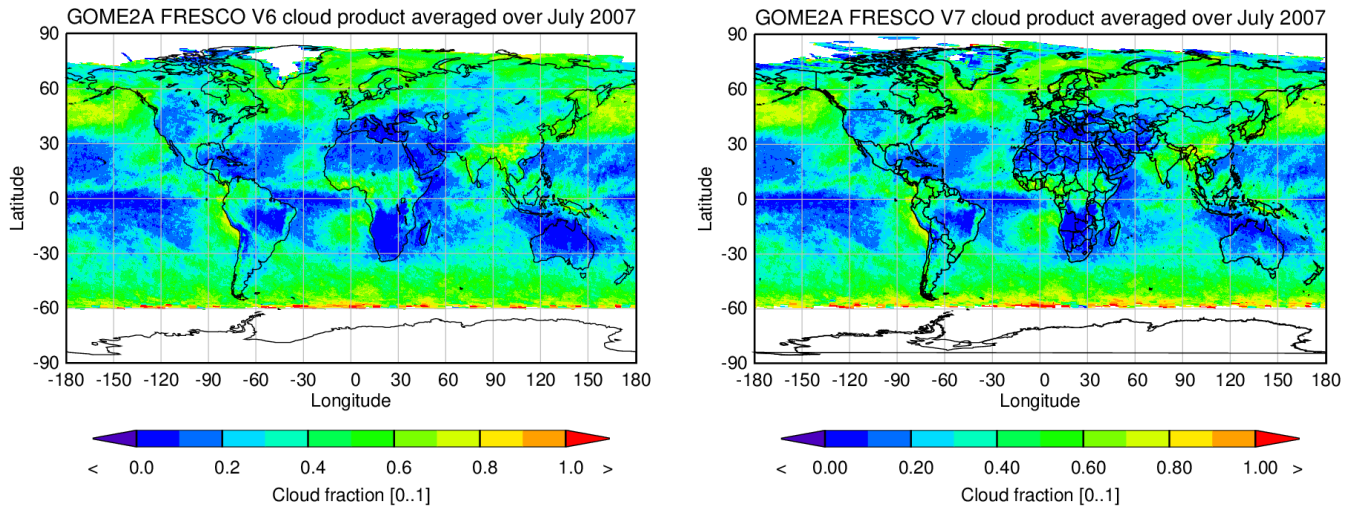


Figure 4.2: Global cloud fraction retrieved by FRESKOv6 and FRESKOv7 algorithms averaged over July, 2007.

4.2 Cloud pressure comparison

Cloud pressure is typically determined from the strong and moderate absorption of the oxygen A-band. Figure 4.3 shows the cloud pressure distributions above Central Western Europe and Eastern US using the FRESKOv6 and FRESKOv7 algorithms. Summer clouds (in July) are higher than winter clouds (in December) because of the seasonal variation of temperature, as well as pressure. The cloud pressure pixels differ in distribution from FRESKOv6 to FRESKOv7, especially, at cloud fractions smaller than 0.3. FRESKOv6 results in more pixels at cloud pressures smaller than 800 mbar while the FRESKOv7 pixels are peaked at cloud pressures larger than 800 mbar over all regions and seasons, this is the result of the impact of the surface albedo climatology change on cloud fractions as mentioned before which also has an impact on cloud pressure. As a result of higher clouds in summer, a larger amount of the tropospheric NO_2 is expected to be screened from the GOME-2A view in the presence of clouds for the same cloud fraction above the northern hemisphere regions than in winter.

Cloud distributions were retrieved above the 6 regions from Table 4.1 demonstrating similar varieties of cloud distributions when using different algorithms with respect to the regional variation. The histograms showing cloud distributions over the other regions are provided in the Appendix. In summary, FRESKOv7 reports lower clouds in all regions and seasons, resulting in less cloud shielding than FRESKOv6.

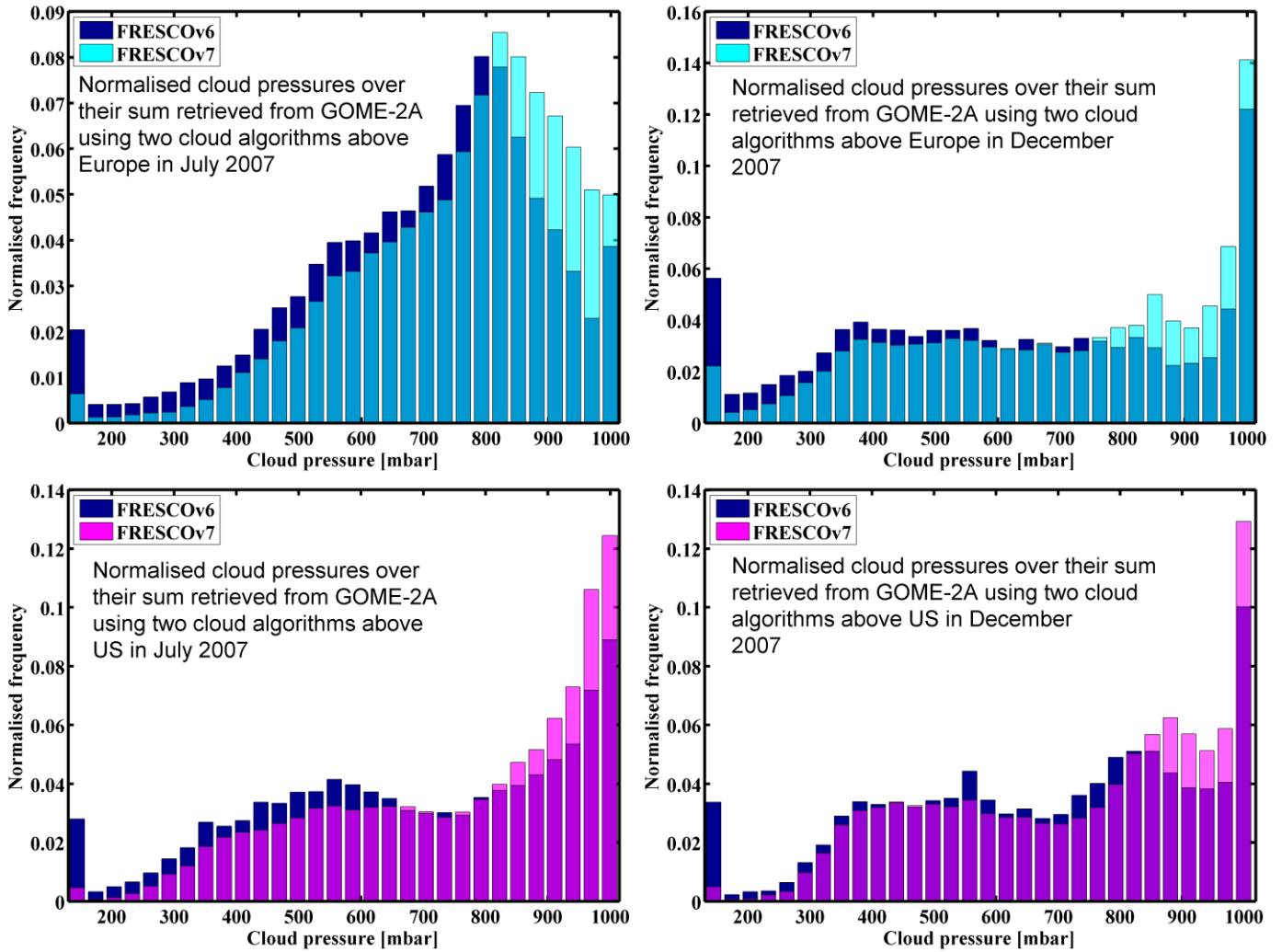


Figure 4.3: Cloud pressure differences between FRESKOv6 and v7 over Europe and the US in July and December 2007.

To investigate the accuracy of small cloud cover determination using both algorithms, Figure 4.4 demonstrates statistical comparisons between cloud parameters at cloud fraction smaller than 0.2 above the 6 regions. The average cloud pressure distributions between 750 and 800 mbar, varying slightly from region to region, at cloud fraction larger than 0.04 are consistent and reasonable. On the other hand, it is not realistic to have only very high clouds at very small cloud covers (<0.04). This means that cloud top heights from FRESKO+ should not be used at very small cloud fractions.

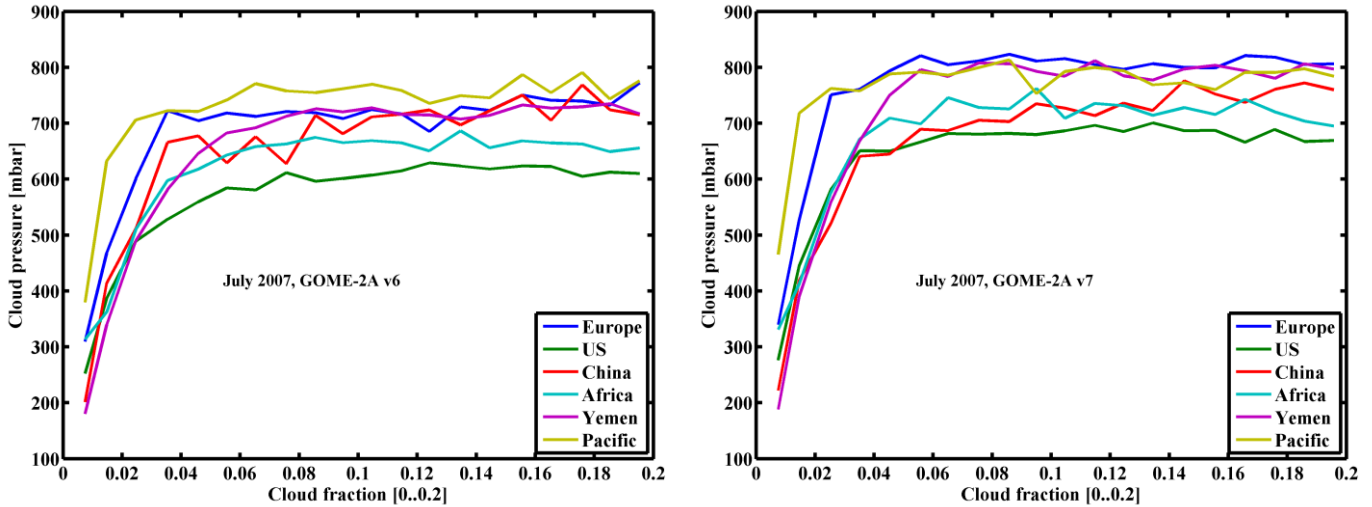


Figure 4.4: The contrast between FRESKOv6 and FRESKOv7 algorithms for cloud parameter at cloud fraction of <0.2 over six regions in July 2007.

4.3 Cloud impacts on tropospheric NO₂ SC

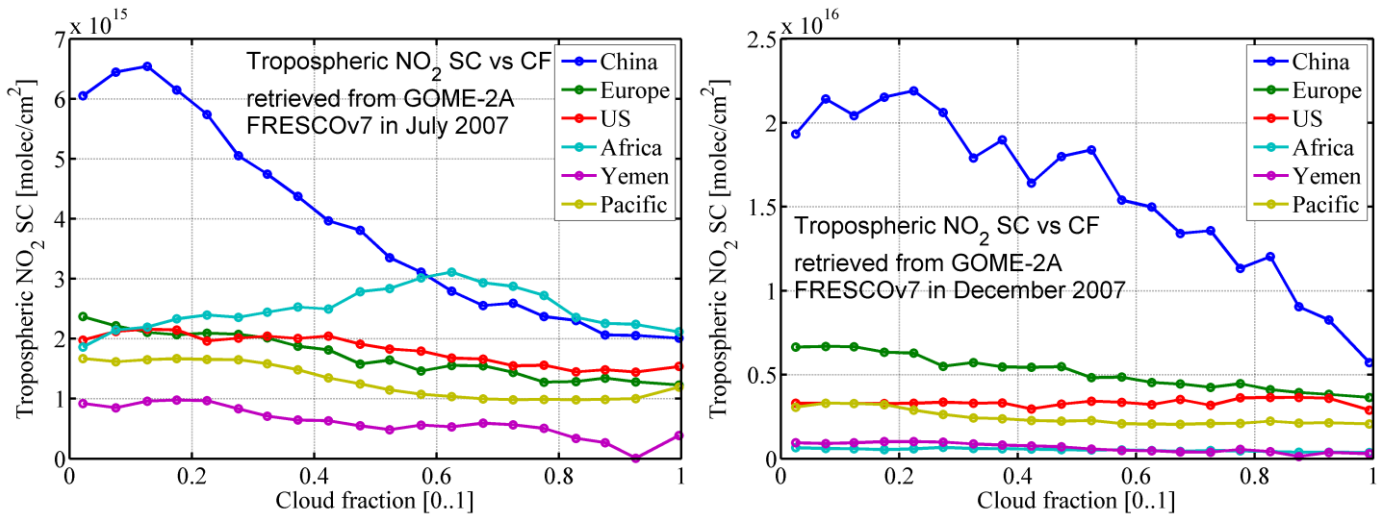


Figure 4.5: Cloud fraction effects on tropospheric NO₂ slant columns using GOME-2A FRESKOv7 in July (left) and December (right) 2007 over 6 regions

In most cloudy situations the bulk of tropospheric NO₂ is located below clouds while some NO₂ can be present above clouds, depending on cloud top height. For a cloudy pixel, the tropospheric NO₂ slant column which is beneath clouds is screened from the GOME-2A view and this effect increases with cloud fractions. It is therefore expected that over polluted regions, the NO₂ SC increases with increasing cloud fraction. Focusing more on the tropospheric slant column of NO₂ retrieval above Central Eastern China, clouds in July (summer) start gradually shielding NO₂ from

cloud fraction of 0.2 to be totally screened at cloud fraction of 1 as shown in Figure 4.5 (left). This behaviour is expected for relatively high clouds. The peak of NO₂ SC at cloud fractions between 0 and 0.2 can be interpreted as an enhancement of the NO₂ retrieval because of the signal sensitivity increase through multiple scattering, either by thin clouds or by aerosol layers. In addition to the shielding effect and the enhancement of NO₂ by multiple scattering, the probability of NO₂ being above clouds in December (winter) is larger, and the enhancement of NO₂ retrieval by the cloud albedo effect is more noticeable in Figure 4.5 (right). This behaviour is expected for lower clouds presenting winter. Because of the NO₂ seasonal variation, NO₂ columns in winter are larger than in summer especially over the polluted regions where the GOME-2A NO₂ signal is large even over cloudy scenes, as shown in Figure 4.5. The same behaviour is found for all regions with the exception of Africa in July.

In terms of the FRESCOv6 and FRESCOv7 cloud effects on the tropospheric NO₂ SC, both of algorithms result in similar impacts on the tropospheric NO₂ retrieval with very small statistical differences (Figure 4.6), which can be ignored when studying cloud impacts on NO₂ retrievals. Therefore, for the following analysis only FRESCO7 is used.

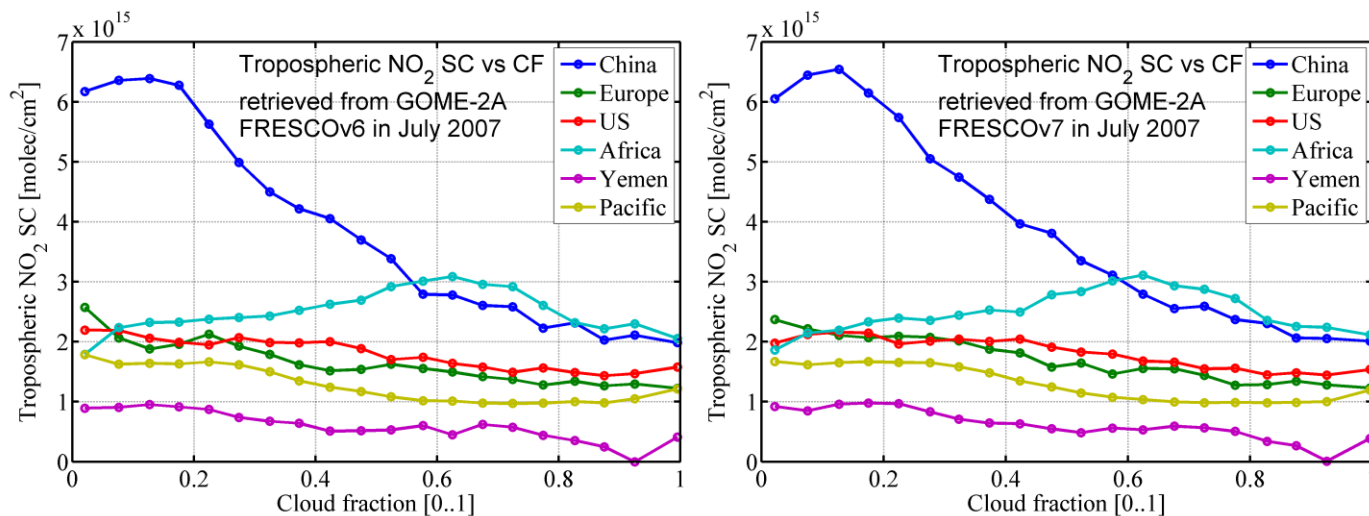


Figure 4.6: A comparison of FRESCOv6 (left) and FRESCOv7 (right) cloud fraction effects on tropospheric NO₂ SC in July 2007 above 6 regions.

4.4 Cloud top height effects on tropospheric NO₂ SC

In addition to cloud cover, cloud top height is an important parameter for the retrieval of tropospheric trace gases, including NO₂. The ability to account both possibilities, NO₂ being

screened beneath clouds in case of a high cloud scenario or to be partly or totally revealed for satellite observations in case of a low cloud scenario depends on the determination of cloud top height. Figure 4.7 shows how the tropospheric NO₂ SC is affected by cloud pressure in July (left) and in December (right) 2007 over the 6 regions. From the satellite perspective, the visibility of NO₂ increases as cloud tops decrease as more of the pollution NO₂ which is located close to the surface is revealed. It is therefore realistic that the retrieved NO₂ SC above Central Eastern China stepwise decreases from cloud pressure of 1000 to 550 mbar whether in July or in December as shown in Figure 4.7. However, NO₂ SC starts increasing again up to 130 mbar of cloud pressure. The latter behaviour does not agree with the expectations, but can be attributed to the impact of cloud fraction on cloud pressure determination. As shown in Figure 4.4, cloud top pressures for low cloud fractions tend to be very low, and therefore these scenes probably have small cloud fraction.

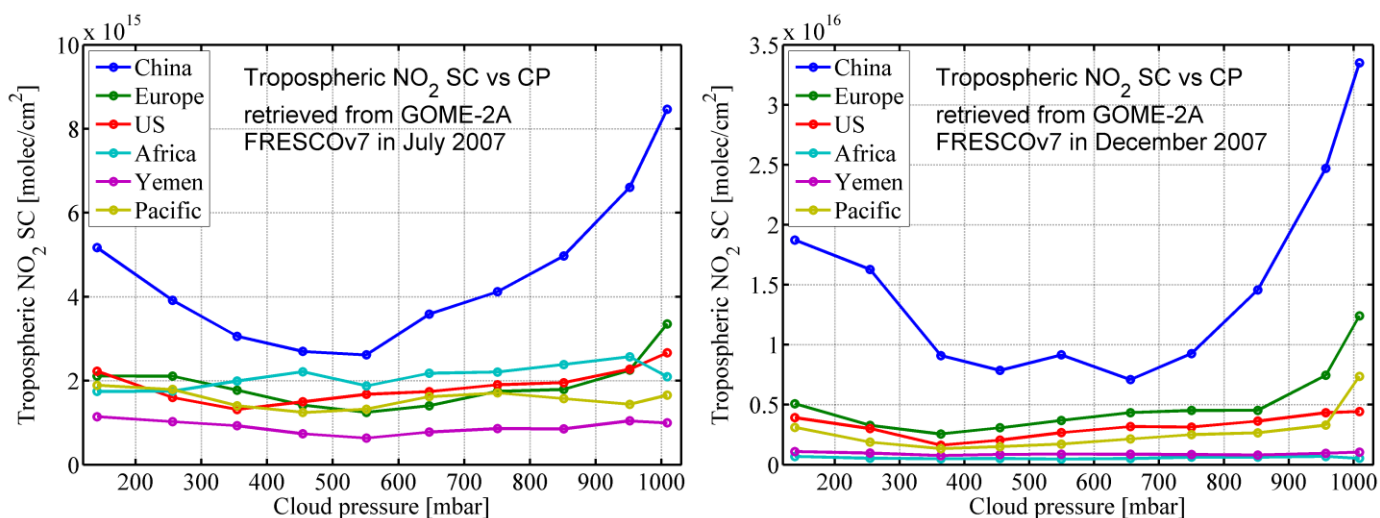


Figure 4.7: Cloud pressure impacts on tropospheric NO₂ SC from GOME-2A FRESCOv7 in July (left) and December (right) 2007 over 6 different regions

4.5 Cloud impacts on NO₂ VC

The NO₂ vertical column (VC) is calculated from the ratio of the SC to the AMF (SC/AMF). The NO₂ SC is directly measured from the satellite instruments while the NO₂ AMF is computed using a radiative transfer model and an atmospheric chemistry model providing the atmospheric NO₂ profiles. When clouds are present, the satellite observations cannot retrieve the NO₂ SC beneath clouds (ghost column). In this case, the prevented part of NO₂ has to be corrected by the AMFs including the cloud effect, as explained below. Ideally, the NO₂ VC should not be affected by

clouds and it is expected to be compromised only by a certain degree over all cloud fractions, otherwise the AMF is not well calculated.

Figure 4.8 (left) shows that the tropospheric NO₂ VCs in July 2007 are quite well corrected over cloud fractions up to 0.9 but they are overestimated at very large cloud fractions (>0.9), when focusing on NO₂ VC over China (blue line) where the largest amount of NO₂ is produced. On the other hand the overestimation of the NO₂ VCs is clearly observed over all cloud fractions in December (Figure 4.8, right), rising increasingly with increasing cloud fraction. It can be seen that the tropospheric NO₂ VC is quite correctly computed by AMF in July (summer) over high clouds, except over the largest cloud fractions because of the underestimation of AMF for high clouds. In terms of the overestimation of NO₂ VCs in December (winter), the AMF obviously seems to be underestimated at low clouds by expecting a large amount of NO₂ located below clouds while the realistic amount of NO₂ is lesser than such an expectation.

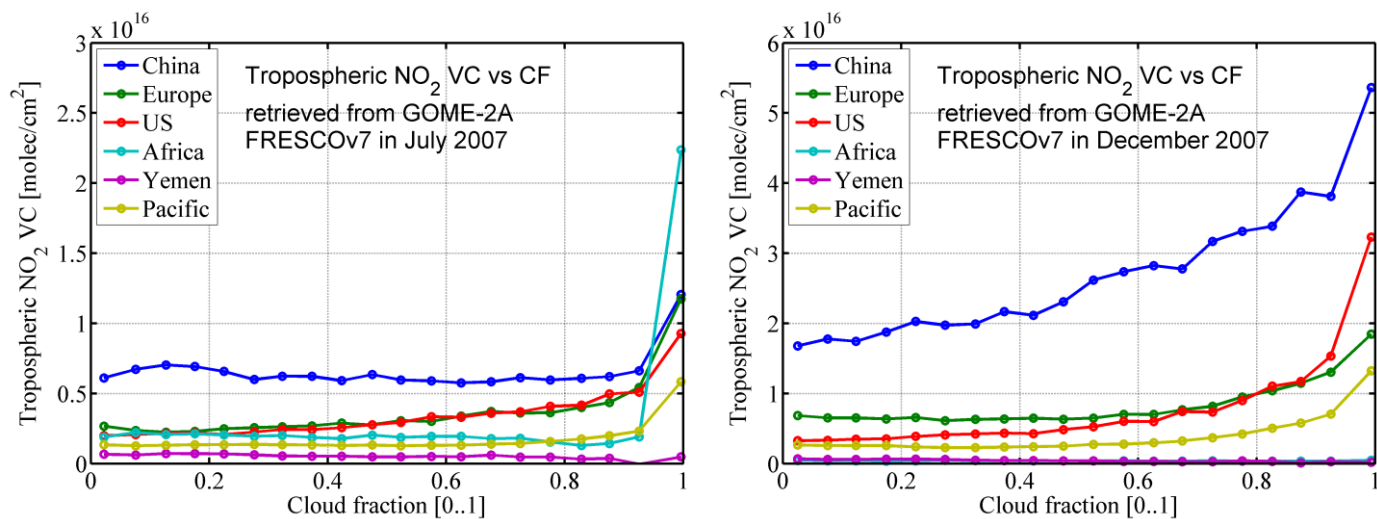


Figure 4.8: The tropospheric NO₂ VC from GOME-2A FRESCOv7 in July (left) and in December (right) 2007 over the mentioned regions

According to these results, some improvements on AMF determinations are urgently required, in particular, at low clouds and at very large cloud fractions in order to correct NO₂ VCs perfectly. Additionally, only observations at small cloud fractions should be used as was often done in other studies.

5 Cloud parameter effects on NO₂ AMF

5.1 An overview of AMF

The AMF is defined as the ratio of SC to VC of an atmospheric trace gas (here NO₂). The importance of AMF is to convert SC to VC in order to find a geophysical useful quantity of the abundance of an atmospheric absorber. The NO₂ AMF depends on the vertical distribution of NO₂, which is calculated using an atmospheric chemistry model, such as Global Earth Observing System-CHEM, and a radiative transfer model to evaluate the backscattered radiance (Palmer et al., 2001). Mathematically, It can be calculated employing the geometric AMF_G, the dimensionless shape factor $S(\sigma)$, and scattering weights $w(\sigma)$, as derived by (Palmer et al. 2001)

$$AMF = AMF_G \int_0^1 S(\sigma) w(\sigma) d\sigma \quad 5.1$$

In practice, a summation is used instead of the integral to calculate the AMF from Equation 5.1. Here, $S(\sigma)$ describes the normalised vertical distribution of NO₂. $w(\sigma)$ is the backscattered radiance which is computed from Rayleigh scattering and Mie scattering calculations in the UV/vis wavelengths. In the absence of these scattering mechanisms, the AMF is equal to the geometric AMF_G which depends only on viewing zenith angle and solar zenith angle. Since clouds influence the AMF determination, the backscattered radiance is decomposed into the contribution of clear sky and cloudy scenes to calculate the total AMF. The general formula to calculate the total NO₂ AMF is given by

$$AMF = \frac{AMF_a R_a (1 - f) + AMF_c R_c f}{R_a (1 - f) + R_c f} \quad 5.2$$

f indicates cloud fraction, which is evaluated for each pixel by determining the horizontal distribution of the cloud optical thickness using the Independent Pixel Approximation (IPA) (Marshak et al. 1998). R_a , R_c , AMF_a , and AMF_c denote the reflectivities and AMFs for clear sky and cloudy scenes, respectively. In case of a clear sky pixel, the AMF will be calculated only from the AMF_a term. On the other hand, for full cloudy pixels, the AMF is only calculated from the AMF_c term.

5.2 Evaluation of NO₂ AMFs in satellite data

5.2.1 Cloud cover impact on NO₂ AMF

The cloud impact on the NO₂ AMF is analysed using some global retrievals of NO₂ from the GOME-2A and OMI instruments on one day of 2007. The changes of the NO₂ AMF with respect to cloud fraction and cloud pressure parameters at solar zenith angles up to 70° were investigated. According to cloud fraction and cloud pressure, the NO₂ SC retrieval becomes smaller when cloud fraction is very large and when clouds are high. Therefore, the model, which is used to determine the AMF, predicts more NO₂ as ghost columns in the presence of clouds. Figure 5.1 (left) shows that the minimum values of the NO₂ AMF computed for GOME-2A (FRESCOv6 and FRESCOv7) are around 0.78 at fully cloudy pixels while the maximum AMF values are around 1.6 for the cloud free pixels. The fact that the AMF is not equal to 0 even for completely cloudy pixels can be explained by the presence of NO₂ above clouds.

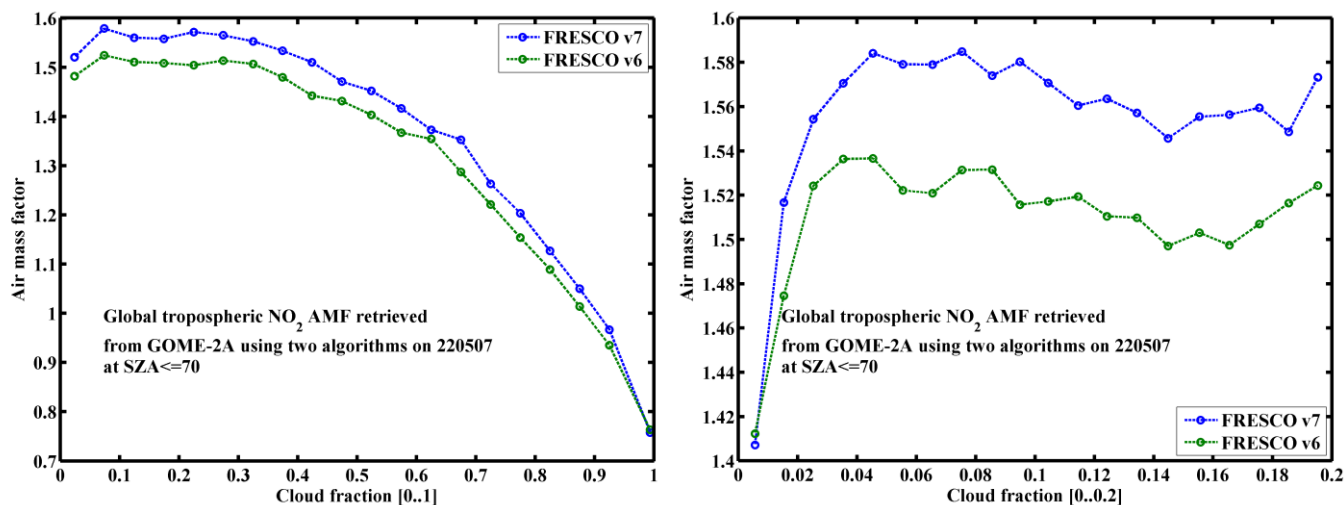


Figure 5.1: The difference of NO₂ AMFs with respect to cloud fraction using GOME-2A FRESCO7 and FRESCO6 algorithms on May 22, 2007 averaged over the global dataset.

The underestimation of the NO₂ AMF at very small cloud fraction (in between 0 and 0.04 cloud fraction, see Figure 5.1(right)) can again be traced to uncertainty of cloud parameters when evaluating very small cloud fractions as already discussed for Figure 4.4. As AMF is calculated based on many parameters (such as cloud albedo and the global surface albedo, NO₂ profile, SZA, VZA, cloud fraction, and cloud pressure), its values differ between FRESCOv6 and FRESCOv7 because of the difference of cloud parameter distributions. The FRESCOv7 algorithm, overall, results in larger values of NO₂ AMF than the FRESCOv6 algorithm over all cloud fractions by a few percent.

5.2.2 Cloud top height impact on NO₂ AMF

Figure 5.2 shows how NO₂ AMF is affected by cloud pressure at different slices of cloud covers, including the mean cloud fraction. The minimum values of NO₂ AMF are observed at very high clouds (around 200 mbar) and at large cloud fractions (between 0.8 and 1). In this case NO₂ is mostly blocked by clouds and recovered by AMF as a ghost column based on the priori profile of NO₂. On the other hand the maximum values of the NO₂ AMF are found at very low clouds (around 1000 mbar) and at the smallest cloud fractions (between 0 and 0.2). In this case, the NO₂ AMF is close to the clear sky AMF with taking into account the enhancement of NO₂ SC because of multiple scattering and high cloud albedo. In the average over all cloud fractions, the mean effect of global cloud cover on AMF is close to the AMF for small cloud fractions (0.2-0.6), which have the highest frequency of occurrence.

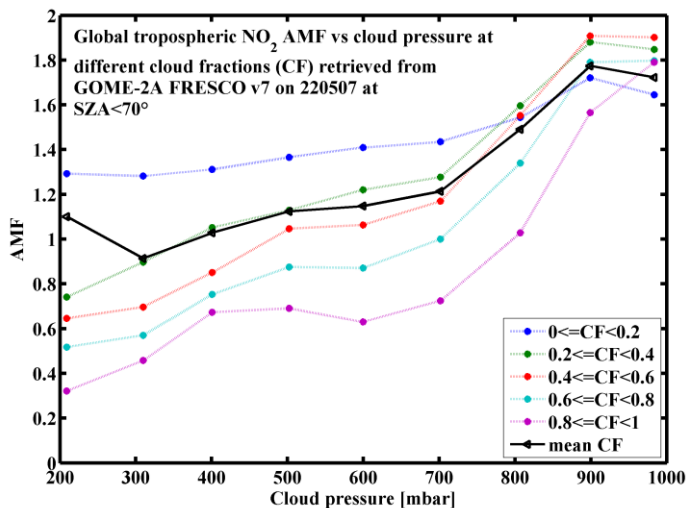


Figure 5.2: The difference of NO₂ AMF with respect to cloud pressure using GOME-2A FRESCO7 algorithm on May 22, 2007 averaged over global dataset.

5.2.3 Effects of cloud correction on NO₂ AMF at cloud fraction <20%

In several earlier studies (Richter et al. 2005, Hilboll et al. 2013) only data with small cloud fraction (<0.2) were used and no cloud correction was applied. Here the impact of cloud correction for these cases is evaluated following a similar analysis in Lorente et al. (2016).

In this section, cloud fractions of smaller than 20% are selected to investigate their effects on AMF calculations. The global NO₂ data used was retrieved on May 22th 2007 from the OMI and instrument using the new cloud algorithm. Small NO₂ VCs (<10¹⁵ molec/cm²) were excluded here from the datasets to focus on polluted regions.

In Figure 5.3, cloud fraction smaller than 20% are on the x-axis and cloud pressures are divided into different portions starting from the surface up to 200 mbar with an increment of 100 mbar. A statistical approach is used to compute the change of cloud corrected AMF relative to the clear sky AMF:

$$\text{corr_cloud} = \frac{\text{AMF}_{\text{cloud_corr}} - \text{AMF}_{\text{clear_sky}}}{\text{AMF}_{\text{cloud_corr}}} * 100 \quad 5.3$$

The observations from the results shown in Figure 5.3 can be summarized to the following three cases

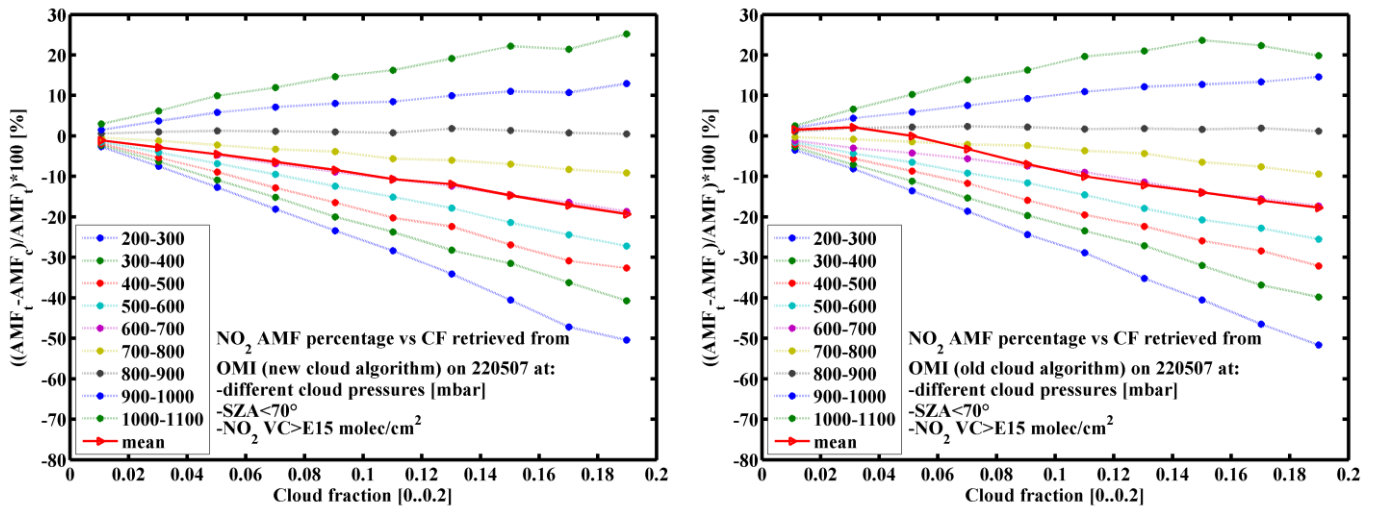


Figure 5.3: The effect of cloud correction on the tropospheric NO₂ AMF for cloud fraction <0.2 at different cloud pressures from OMI using new cloud algorithm (left) and old cloud algorithm (right) for a global retrieval on May 22, 2007.

First, the cloud correction is positive ($\text{AMF}_{\text{corr_cloud}} > \text{AMF}_{\text{clear_sky}}$) when clouds are very low (for cloud pressure > 900 mbar). This means that NO₂ is not only visible for the OMI view but its SC is enhanced relative to the clear sky measurement because of high cloud albedo.

Second, high clouds (for cloud pressure < 800 mbar) result in negative values of the cloud correction $\text{AMF}_{\text{corr_cloud}} < \text{AMF}_{\text{clear_sky}}$, the mean cloud pressures are in this case. This means, the retrieved NO₂ SC is smaller because of the shielding effect and it has to be substituted from the ghost column of NO₂, based on the used NO₂ model (Inness et al., 2013).

Third, cloud corrections can be negligible in case of $AMF_{corr_cloud}=AMF_{clear\ sky}$ for cloud pressures in between 800 mbar and 900 mbar. In this case the shielding and albedo effects cancel each other as there is NO_2 both below and above the clouds.

Similar results for the effect of cloud corrections on the tropospheric NO_2 AMF are obtained from the OMI instrument using the old cloud algorithm (Figure 5.3, right) with some notable differences originating from the statistical variations of cloud distributions for both OMI cloud algorithms, which will be discussed in section 6.

In addition to the analysis on OMI data, the same investigation was performed on data from the GOME-2A instrument using the FRESCOv7 (Figure 5.4, left) and FRESCOv6 (Figure 5.4, right) algorithms.

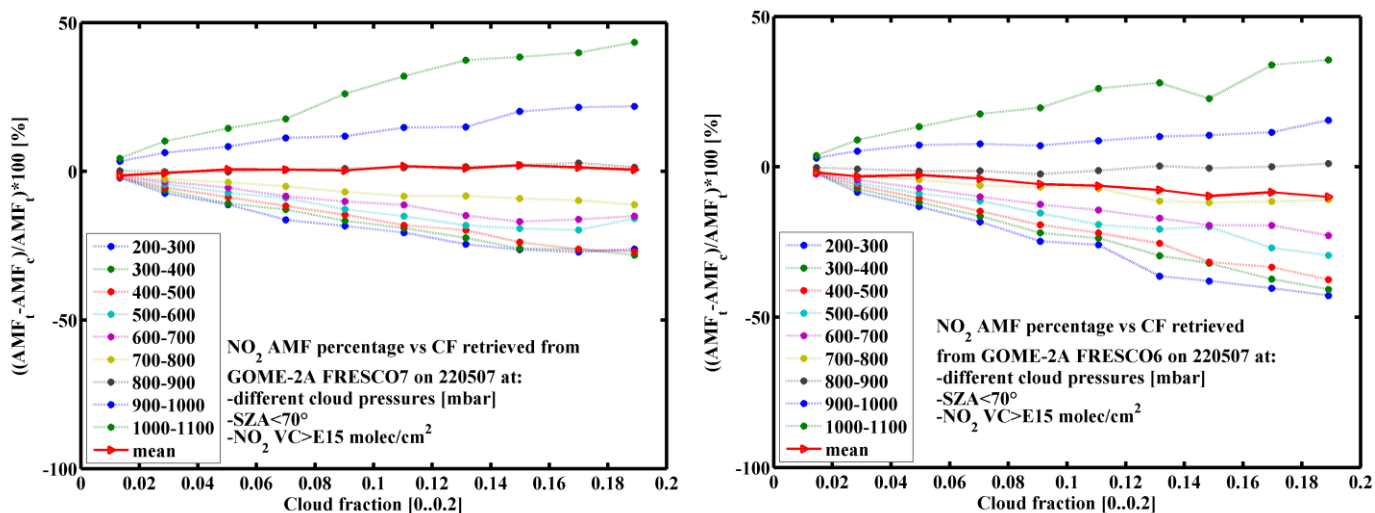


Figure 5.4: The effect of cloud correction on the tropospheric NO_2 AMF for cloud fraction <0.2 at different cloud pressures from GOME-2A using FRESCOv7 (left) FRESCOv6 (right) for a global retrieval on May 22, 2007.

Comparison between OMI and GOME-2A shows more differences with overall smaller cloud effects and nearly no effect on average for FRESCOv7 (Figure 5.4). This surprising result is linked to differences in the cloud statistics and the better spatial resolution of OMI.

Although cloud correction is more pronounced for large cloud fractions it can be important for small cloud fractions as well (<0.2). Overall, without such cloud corrections, the NO_2 AMF will be underestimated for very low clouds and overestimated for high clouds.

6 Cloud impacts on NO₂ retrieval observed from the OMI instrument

The evaluation of cloud effects on GOME-2A data represented in chapter 6 have been performed on OMI data. Again, measurements were used over the 6 targeted regions (given in Table 4.1) in July and December 2007. For these measurements, cloud fractions and cloud pressure were processed using either the so-called new cloud algorithm or the old cloud algorithm, which represent the last version and the previous version of the OMI O₂-O₂ cloud products, respectively. In this section, cloud distributions over the 6 regions will be provided within a comparison between the two OMI algorithms.

6.1 Cloud distributions using the old and the new cloud algorithm

As clouds vary from season to season and from region to region according to meteorology of clouds, variability of clouds in the following analyses is expected to be present both between regions and among seasons. The effective cloud fraction (f_{eff}) is expected to be evaluated better from the OMI instrument than from GOME-2A because of the good spatial resolution of the OMI footprint (13×24 km²). The assumption of the ground and cloud surfaces to be Lambertian reflectors has an important effect on the computation of f_{eff} . For instance, the cloud albedo is assumed to be 0.8 and the ground albedo is interpolated from a LUT using the surface albedo climatology of the OMI data base. Hence, an increase of the assumed cloud albedo will diminish the retrieved cloud fraction and vice versa. Likewise, an increase of the calculated surface albedo will result in more cloud free pixels. Therefore, the uncertainty of cloud pixels increases at very small cloud fractions (i.e. <0.2) when the measured reflectance from the ground surface is dominant, excluding the reflectance from the snow and ice surfaces. In terms of cloud pressure determination, the GOME-2A O₂ A-band cloud products are more reliable than the OMI O₂-O₂ cloud products because the O₂ A-band absorption is stronger than the O₂ dimer band absorption, according to the optical thicknesses of oxygen molecules and oxygen dimer.

6.1.1 Cloud distributions over Central Eastern China

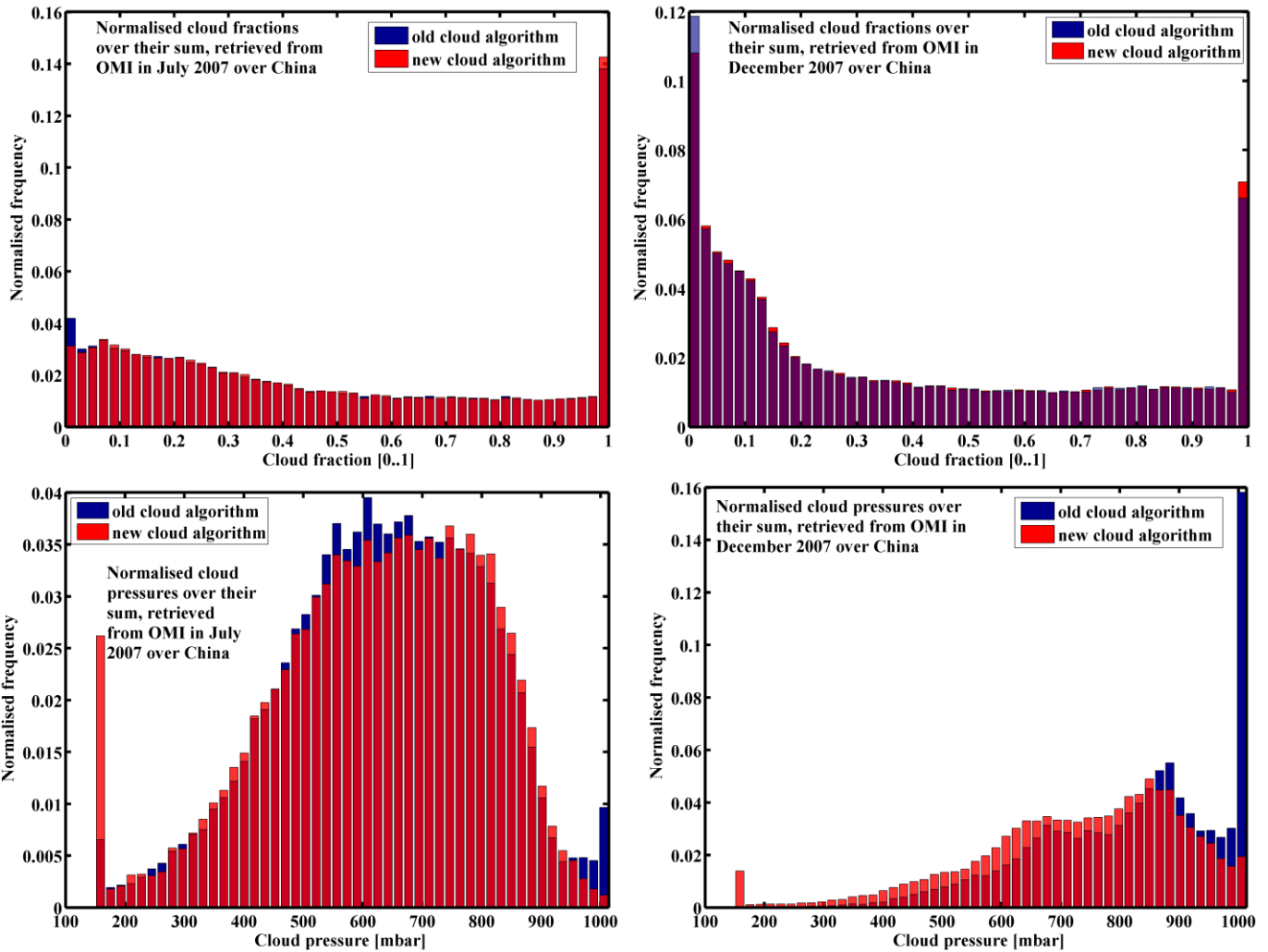


Figure 6.1: OMI cloud property frequency distributions over Central Eastern China in July (left column) and in December (right column) 2007, CFs (upper row) and CPs (lower row).

Figure 6.1 shows the cloud fraction (upper row) and cloud pressure (lower row) statistics over Central Eastern China in July (left column) and December (right column) 2007. It can be seen that many pixels have a cloud fraction of 1 and that most measurements have cloud pressure of 650 mbar in July while most pixels have very small cloud fractions and high cloud pressure (around 700 mbar and 900 mbar) in December. Because of that, clouds are dominant and higher in summer compared to winter. This indicates that it is possible for some tropospheric NO₂ SCs to be above clouds in December. On the other hand summer clouds, in this case, shield NO₂ below clouds from OMI view.

In contrast to the GOME-2A cloud algorithms, The OMI cloud algorithms (the old version and the new version are shown in blue and red colors, respectively) seem consistent in determining cloud fraction with a small difference around very small cloud fractions. The old cloud algorithm results in more cloud free pixels while the new algorithm has more cloudy pixels. The reason behind this difference is many parameters used for the LUTs have been updated for the new version such as the cloud albedo and surface albedo (Veefkind et al. 2016). A dramatic change of cloud pressure calculation between the old and new algorithms can be clearly noticed from Figure 4.1 (lower row), particularly in December, because of the consideration of the temperature effect in the new algorithm. The new algorithm was a maximum at low cloud pressure while most pixels of the old algorithm are observed at high cloud pressure, especially in December when temperature is quite varied. The difference of cloud pressure pixel distributions between these algorithms varies between the 6 regions, depending on geographical site and season, which can be realized as follows. Both of these algorithms show crests of accumulated pixels at the boundary values of cloud fraction and cloud pressure (the maximum and minimum limits) because of the clipping of unrealistic values by the two algorithms.

6.1.2 Cloud distributions over Central Western Europe

Cloudy scenes are generally dominant over Central Western Europe whether in July or in December. In July (Figure 6.2, left upper column) Most cloudy pixels have small cloud fractions (<0.5) while in December (Figure 6.2, right upper column) the number of cloudy pixels at large cloud fractions (>0.5) is greater than at small cloud fractions. The distribution of cloud pressure pixels is different for the old and the new algorithms but their maxima agree at cloud pressures of around 750 mbar in July (Figure 6.2, left lower row) and around 850 mbar in December (Figure 6.2, right lower row). This implies that more clouds are present in winter compared to summer and that they are lower in winter than in summer, as expected. In terms of the cloud algorithm differences, the differences, which have been explained for the previous region, are repeated here, but in different degree. According to these distributions of clouds, the probability of some NO_2 being above clouds is larger in December than in summer.

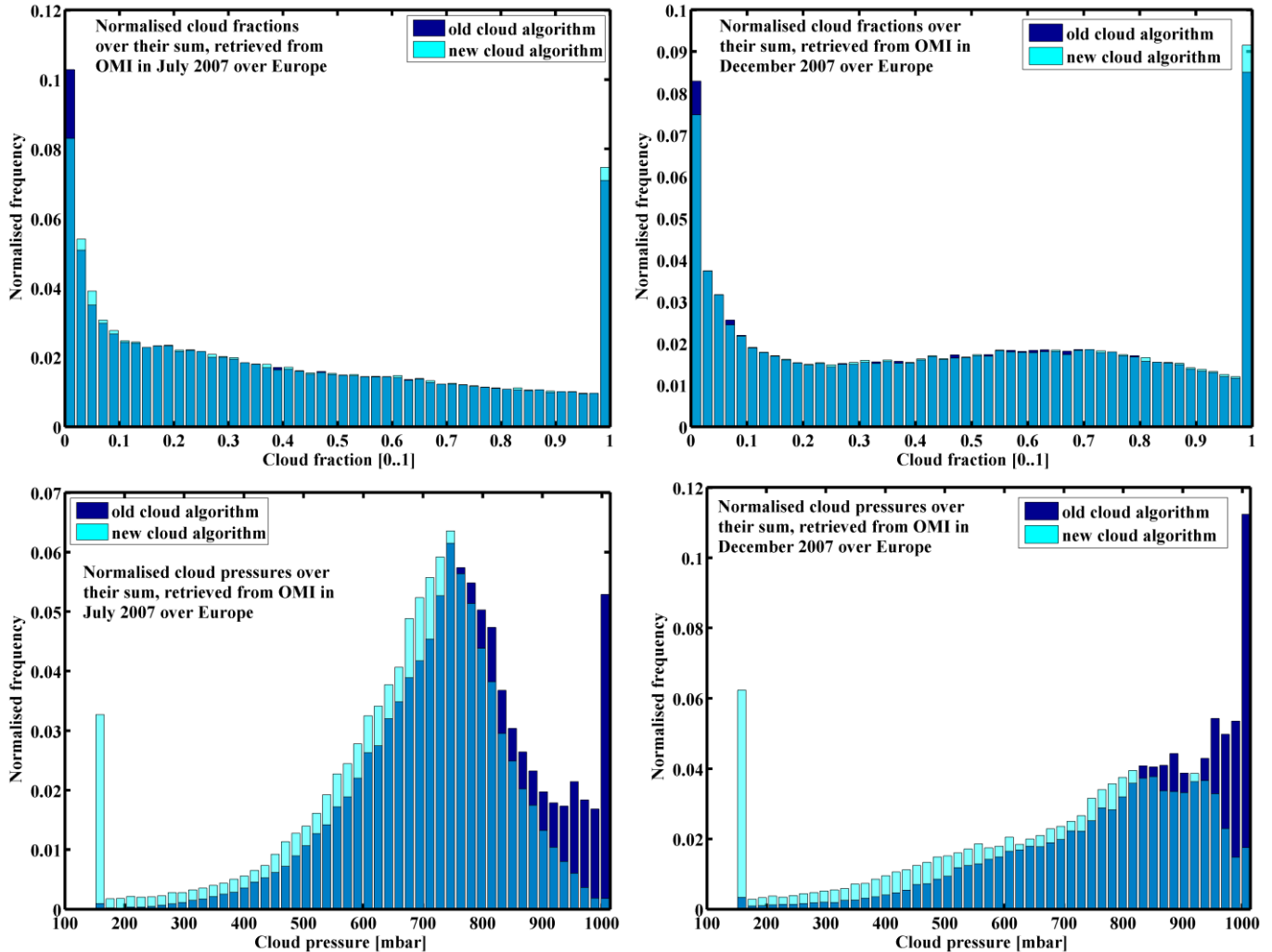


Figure 6.2: The OMI cloud distribution over Central Western Europe in July (left column) and in December (right column) 2007, CFs (upper row) and CPs (lower row).

6.1.3 Cloud distributions over Eastern US

The OMI cloud statistics for the Eastern US is shown in Figure 6.3. It can be seen that more pixels are found at cloud fractions less than 0.3 in July (left upper column). On the other hand, numerous pixels are found at very large cloud fractions, with the exception of flagged pixels at cloud fraction of 0, in December (right upper column) above Eastern US. Despite the cloud algorithm differences, the peaks of the pixel frequencies are similar at around 700 mbar and 900 mbar of cloud pressure in July (left lower row) and in December (right lower row), respectively. This distribution of clouds indicates that the OMI monitoring has observed fewer and higher clouds in summer than in winter. The tropospheric NO₂ is, therefore, expected to be shielded in July more than in December, based on its vertical distribution.

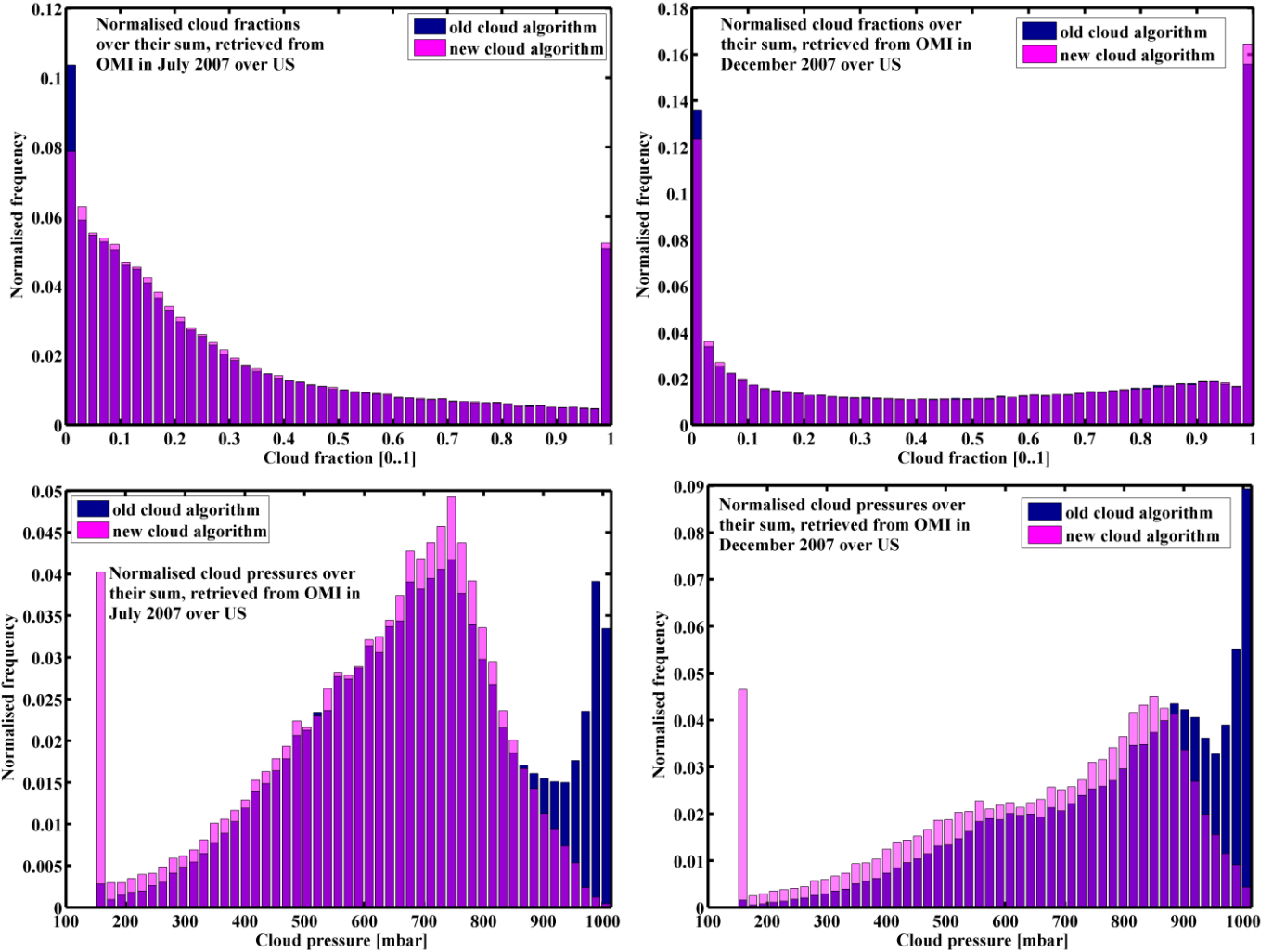


Figure 6.3: The OMI cloud distribution over Eastern US in July (left column) and in December (right column) 2007, CFs (upper row) and CPs (lower row).

6.1.4 Cloud distribution over Central Africa

To compare between summer and winter clouds above Central Africa, it has to be mentioned that different scales are applied the y-axis of histograms (Figure 6.4), specifically a large scale for the histograms of cloud fraction and cloud pressure in July and a small scale for the histograms in December. Figure 6.4 (upper row) shows the cloud free scenes are dominant over this region through looking at the cloud fraction statistics in July (left upper column) and in December (right upper column). It is also clear that there are pixels recorded at very high cloud fractions in December but not in July. Most pixels have cloud pressure of 550 mbar in December (right lower row) and both cloud algorithms are quite in agreement. However, they are distributed vertically in a wide range of cloud pressure (from 850 mbar up to 200 mbar) in July (left lower row) using the new

algorithm whereas the old algorithm results in more pixels at cloud pressure of 860 mbar. This indicates that the measurements in winter are cloudier and the clouds higher than in summer. Even though fewer clouds are observed in this region, compared to the previous regions, their impacts on NO₂ retrievals are significant because of their high altitudes, which affect NO₂ retrieval by preventing the OMI signal from including the lower atmosphere. The larger difference in cloud pressure is probably explained by the small cloud fraction which results in large CP uncertainties.

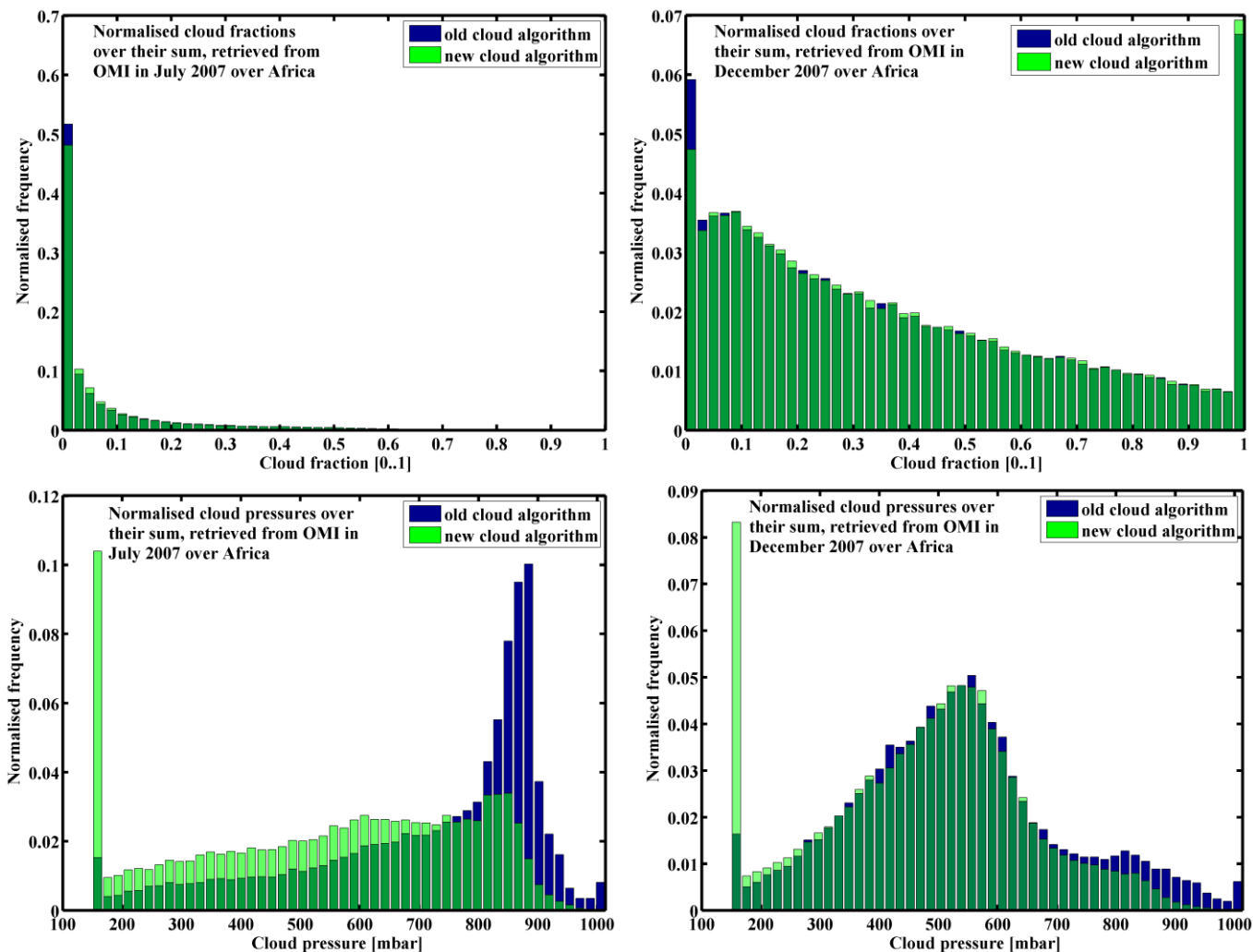


Figure 6.4: The OMI cloud distribution over Central Africa in July (left column) and in December (right column) 2007, CFs (upper row) and CPs (lower row).

6.1.5 Cloud distribution over Yemen

Being located at a subtropical region, clouds above Yemen are very rare as shown in Figure 6.5 (upper row). The measurements over Yemen have mostly very small cloud fractions (around <0.2) whether in July (left upper column) or in December (right upper column). In more detail, much

more pixels are peaked at cloud fraction of 0 but neither in summer nor in winter, pixels are recorded at very large cloud fractions.

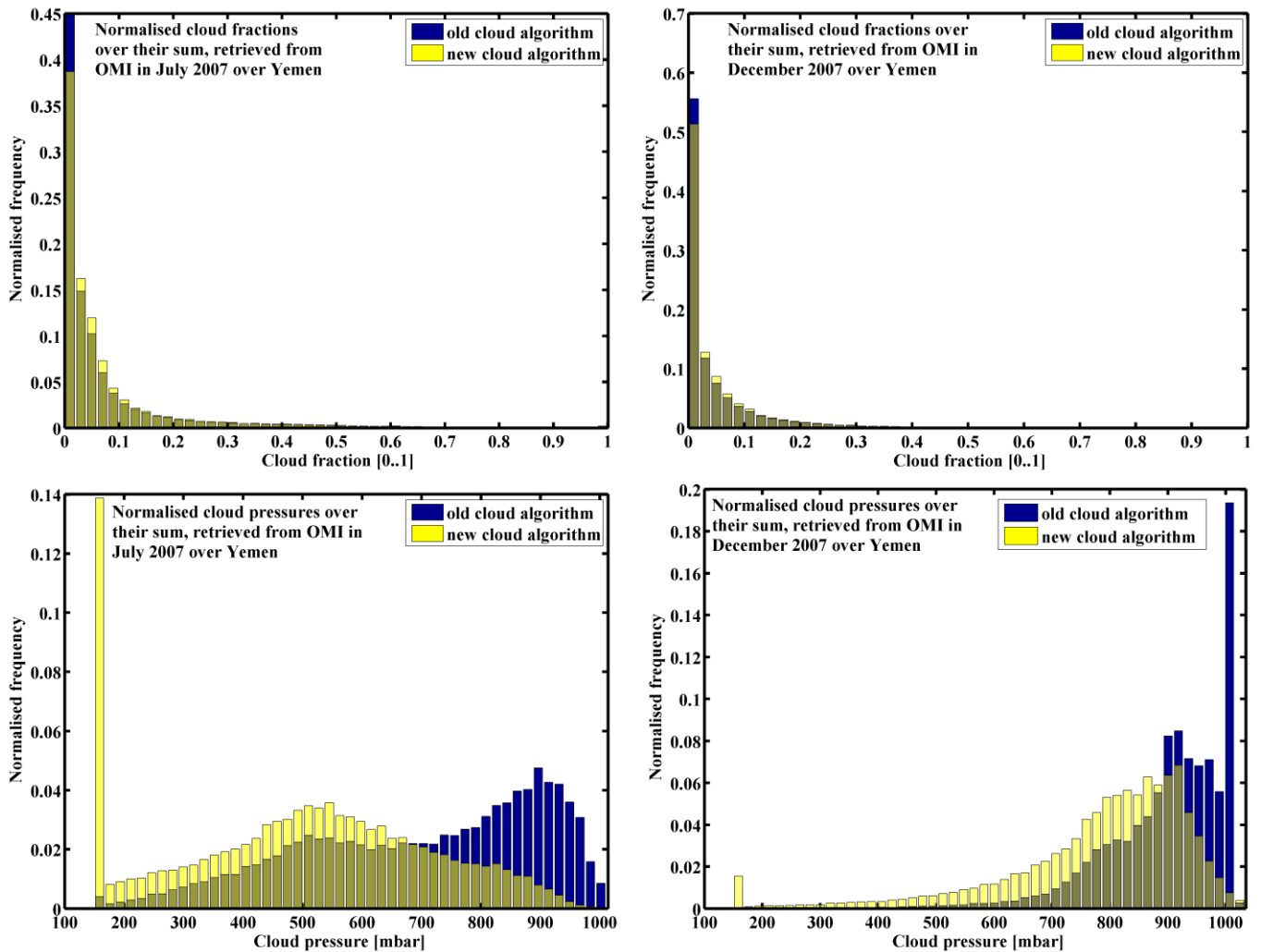


Figure 6.5: OMI cloud distribution over Yemen in July (left column) and in December (right column) 2007, CFs (upper row) and CPs (lower row).

In terms of cloud top height in July (left lower row), the pixel frequency peaks at low cloud pressure (around 500 mbar) using the new cloud algorithm while it is peaked at high cloud pressure (around 900 mbar) when using the old cloud algorithm. Since temperature in July is quite different from mid-latitude (which was used globally in the old algorithm) to the current region (new algorithm approximation), the difference of cloud pressure determinations between the old and the new cloud algorithm is large. It is realistic that summer clouds above Yemen are very high as reported by the new cloud algorithm. Cloud pressure distributions from both algorithms are more consistent in December (right lower row) around 900 mbar, where most pixels are found when ignoring the

single crest of the old algorithm pixels at highest cloud pressure. These cloud observations indicate that the few clouds present are distributed at high altitudes in summer and at low altitudes in winter over Yemen. These clouds do not have a major effect in shielding the tropospheric NO₂ columns even if Yemen were a hotspot region for NO₂.

6.1.6 Cloud distributions over Northern Pacific Ocean

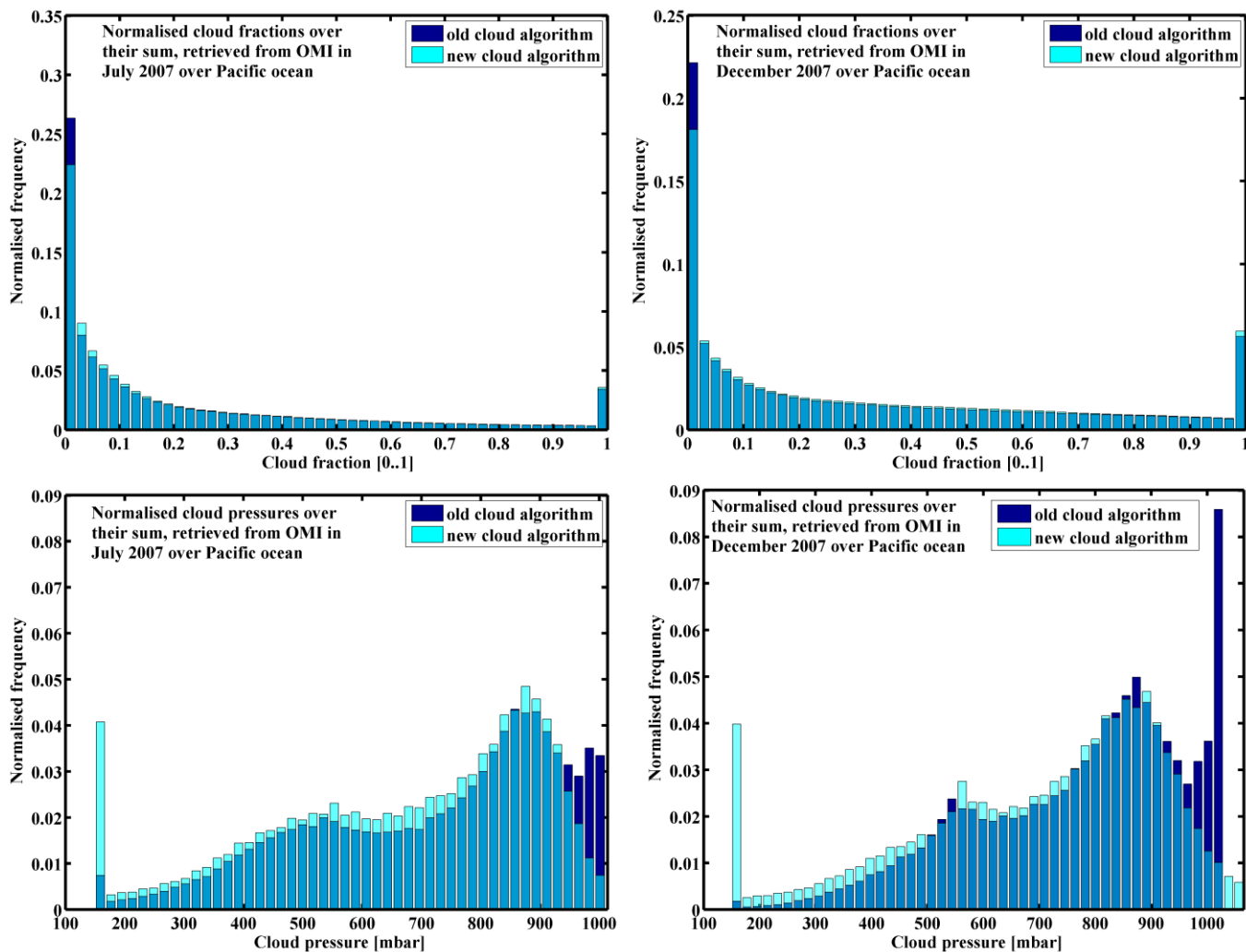


Figure 6.6: OMI cloud distribution over the Northern Pacific Ocean in July (left column) and in December (right column) 2007, CFs (upper row) and CPs (lower row).

Figure 6.6 shows cloud statistics over the Northern Pacific Ocean in July (left column) and in December (right column). These scenes are typically dominated by cloud free scenes with most pixels found at small cloud fractions (<0.2) whether in July (left upper column) or in December (right upper column). However, more cloudy pixels are observed in December at larger cloud

fractions (>0.4). Similar cloud pressure distributions are present in July (left lower row) and in December (right lower row) regardless of which of the two cloud algorithms is used.

The maximum in the cloud pressure distribution is noticed at cloud pressure around 880 mbar in July and in December and a smaller peak is repeated at cloud pressures around 500 mbar for July and around 550 mbar for December. According to this distribution of clouds, the seasonal variation of clouds above Northern Pacific Ocean is small for both cloud fractions and cloud pressure. As a result, it is expected that the tropospheric NO_2 retrievals will be impacted similarly by such clouds in July and in December. In summary, the two OMI cloud versions are quite consistent for cloud fractions but they change in cloud pressure, in particular for small cloud fractions.

6.2 Cloud impacts on NO_2 SC from OMI

The cloud impacts discussed for the GOME-2A measurements above 6 regions are similarly analyzed and repeated using the OMI instrument but the results are not similar because of the instrumental differences. The good spatial resolution of the OMI footprint does not only allow small cloud covers to be detected but also enables measurements to statistically be improved by providing numerous pixels over a certain region. The results are obtained using the two cloud algorithms and are compared for different months (July and December 2007) as well as to the GOME-2A results. To simplify the relationship between cloud impacts and NO_2 retrievals, the tropospheric NO_2 SC is averaged over a certain interval of cloud fraction (here, 0.02 is used above all regions). It is more reliable to focus on a region that is strongly polluted by NO_2 (such as China) to study cloud effects on NO_2 retrievals as follows. These effects are shown in Figure 6.7, distinguished by different color lines for each region.

Figure 6.7 (left upper row) shows that the tropospheric NO_2 SC in July above Central Eastern China (blue curve) retrieved using the new OMI cloud algorithm is clearly shielded at cloud fractions larger than 0.3, decreasing with increasing cloud cover. Because the algorithms do not discriminate between clouds and aerosol, thick aerosol layers and thin clouds are both accounted for as small fractions of clouds (Veeffkind et al. 2016). Hence, to explain the peak of NO_2 SC in between cloud fractions of 0 and 0.3, two scenarios can be considered to interpret cloud effects on NO_2 .

First, a thin cloud or an aerosol layer can enhance NO₂ retrieval through strengthening the sensitivity of OMI signal by multiple scattering, especially when NO₂ is mixed with such a cloud. If so, the NO₂ SCs are increasingly enhanced starting from very small cloud fraction reaching to the maximum retrieval (5×10^{15} mole cm⁻²) around cloud fraction of 0.2, and then it continuously starts to decrease (screened) with increasing cloud fraction. In the alternative scenario of a decreasing fraction of relatively high clouds, the NO₂ SC would have dropped starting from very small cloud fractions and continuously decreasing with increasing cloud cover as a result of shielding effect.

Second, an absorbing aerosol layer could also decrease NO₂ SCs, particularly over polluted regions such as China. In this scenario, the NO₂ SC at cloud fractions smaller than 0.2 starts to be decreasing from the maximum value (5×10^{15} mole cm⁻²) around cloud fraction of 0.2 to (3.6×10^{15} mole cm⁻²) reaching the smallest cloud fraction. In the absent of this effect, the NO₂ SCs would have been increasing from cloud fraction of 0.2 to peak (maximum retrieval) at very small cloud fraction. Since both scenarios are equally probable, more studies are needed to investigate under which conditions each scenario could have occurred.

The largest NO₂ SCs are observed above China produced from anthropogenic emissions, followed by Africa (in July) originating from wildfires, and then Europe and the US. On the other hand the smallest amount of NO₂ is measured over the Northern Pacific Ocean and Yemen, both clean regions where NO₂ is formed by natural phenomena such as lightning and chemical interactions of nitrogen with free radical HOx. The latter regions were interesting to compare between cloud distributions over regional variations but they are not useful for evaluation of the significance of cloud impacts on NO₂ retrievals. It can be seen that largest difference of the tropospheric NO₂ SC between all regions is found at small cloud fractions while the difference is shrinking towards large cloud covers. This implies that the regional variation of NO₂ loading cannot be retrieved over different regions at fully cloudy scenes but it can be well recognized at small cloud covers. Although NO₂ SC at cloud fraction of 1 could be expected to be fully screened (retrieval=0) there is some NO₂ detected also above clouds, which would not have been detected without cloud albedo effect. In this case, the possibility of NO₂ to be produced from lightning has to be taken into account, in particular with high clouds.

Additionally, cloud impacts on NO₂ retrieval are not exactly similar above all regions because of regional variation and different types of clouds as well as different vertical distribution of NO₂ over

the regions. In addition to that, the tropospheric portions above urban regions that are polluted by NO_2 (such as China, Europe, and US) contain different types of aerosol because of the different anthropogenic and natural emissions.

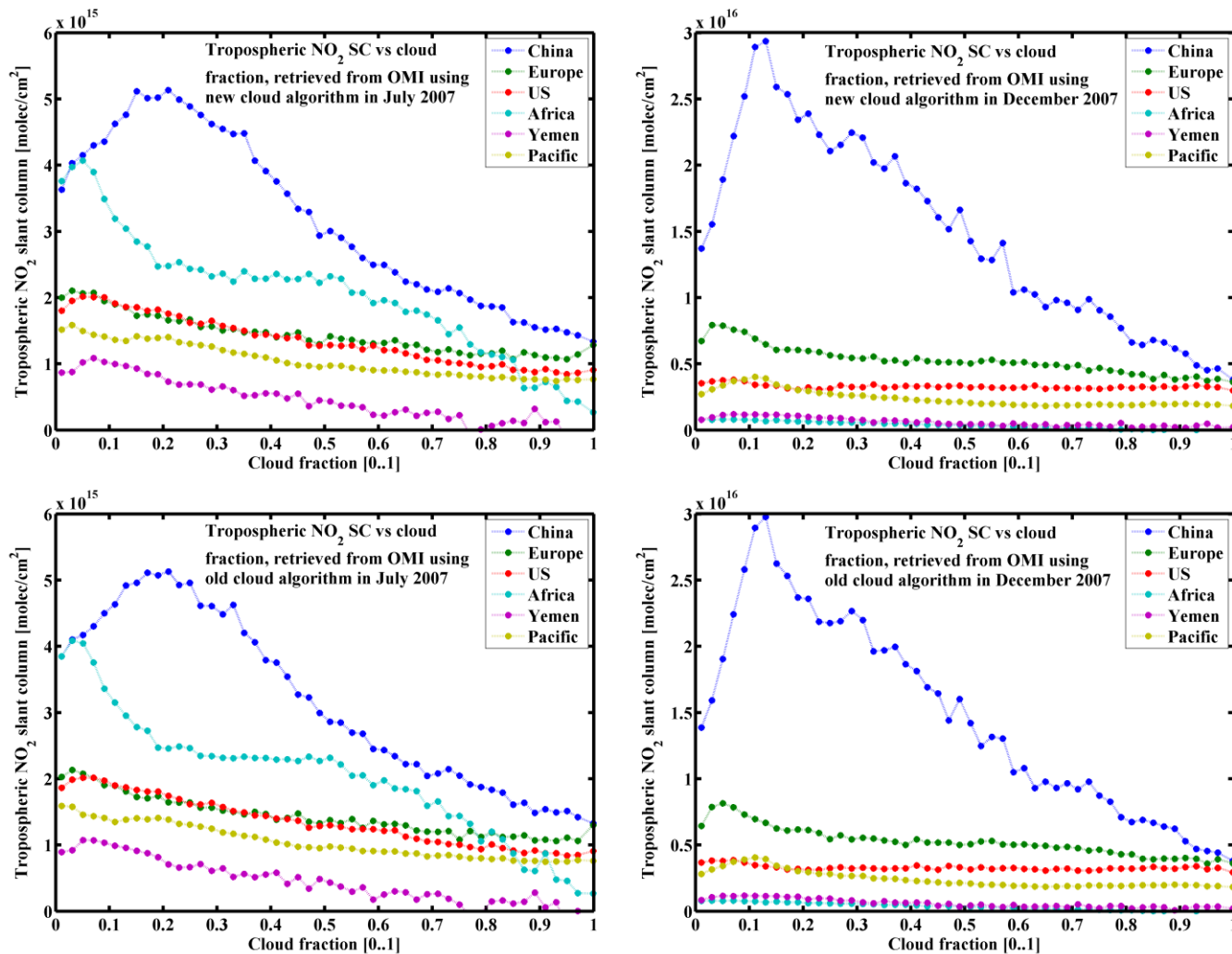


Figure 6.7: Cloud impacts on tropospheric NO_2 SC in July (left column) and December (right column) 2007 over 6 regions, from OMI using new algorithm (upper row) and old algorithm (lower row).

Because lower clouds are present in December, their effects on NO_2 retrievals vary depending on where exactly the NO_2 is located (below clouds, above clouds or in between clouds). In addition to the seasonal variation of clouds, the seasonal variation of NO_2 is obviously noticed above the 6 regions in Figure 6.7 (right upper row). The amount of NO_2 in December is higher than in July because of household combustions (as a source of NO_2 , e.g. heating systems), less photolysis interactions of NO_x and lower OH levels in December. It should be mentioned that the overpass

time of the OMI instrument (around local noon) has an important effect on NO₂ retrieval because of the diurnal variation of NO₂ (lowest retrieval of NO₂ at noon), which has an additional significance for instrumental variation (here it can be comparable to the GOME-2A NO₂). For instance, the maximum NO₂ SC retrieval above China is about (3×10^{16} mole cm⁻²) retrieved at cloud fraction of around 0.1 compared to (5×10^{15} mole cm⁻²) of maximum NO₂ SC retrieval at cloud fraction of around 0.2 in July. The shift of NO₂ SC peak at very small cloud fraction by step of 0.1 from summer to winter can be interpreted as an effect of seasonal variations of clouds and NO₂.

Comparing between NO₂ SCs retrieved using the old cloud algorithm (Figure 6.7, upper row) and the new cloud algorithm (Figure 6.7, lower row), the tow show no notable difference for NO₂ SC retrievals, except very small statistical differences as a result of the change of cloud algorithm approximations to calculate cloud fraction and cloud pressure, as explained previously. As mentioned for the GOME-2A cloud algorithms (FRESCOv6 and FRESCOv7), the differences of the OMI cloud algorithms should be taken into consideration when determining cloud parameters but they have little impact on the NO₂ retrievals.

In terms of cloud pressure impacts on the tropospheric NO₂ SC retrievals, Figure 6.8 shows that NO₂ is concentrated in the troposphere in between the surface (approximately 1000 mbar) and cloud pressure of 700 mbar, specifically above China in December 2007. The lower the cloud, the larger the retrieved NO₂ SC.

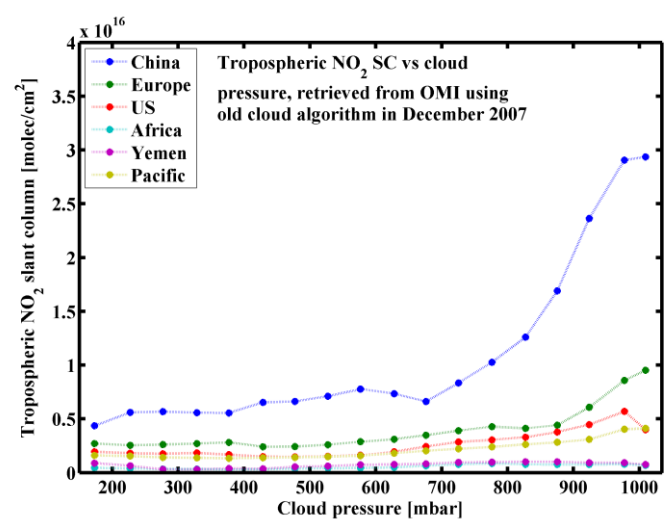


Figure 6.8: Cloud pressure impacts on tropospheric NO₂ SC retrieved from OMI old algorithm in December 2007 over 6 regions

It is reasonable that small amounts of NO₂ are observed even at very high clouds (from cloud pressure of 700 mbar up to 200 mbar) as the figure includes all cloud fractions. High clouds completely screen NO₂ but NO₂ retrievals above clouds (at very low clouds, around 900-1000 mbar of cloud pressure) are enhanced because of high cloud albedo. Cloud pressure can clearly show both the shielding effect and the enhancement of NO₂ retrieval by cloud albedo.

6.3 Impacts of clouds on tropospheric NO₂ VC

NO₂ vertical columns including cloud correction should have the same NO₂ values over all cloud fractions as discussed with the GOME-2A NO₂ VCs. It is important for the cloud fraction and cloud pressure parameters to be well evaluated so that NO₂ VC can be determined in the presence of clouds. Otherwise, the error of NO₂ VC evaluation will be very large as a result of the combination of SC and AMF uncertainties.

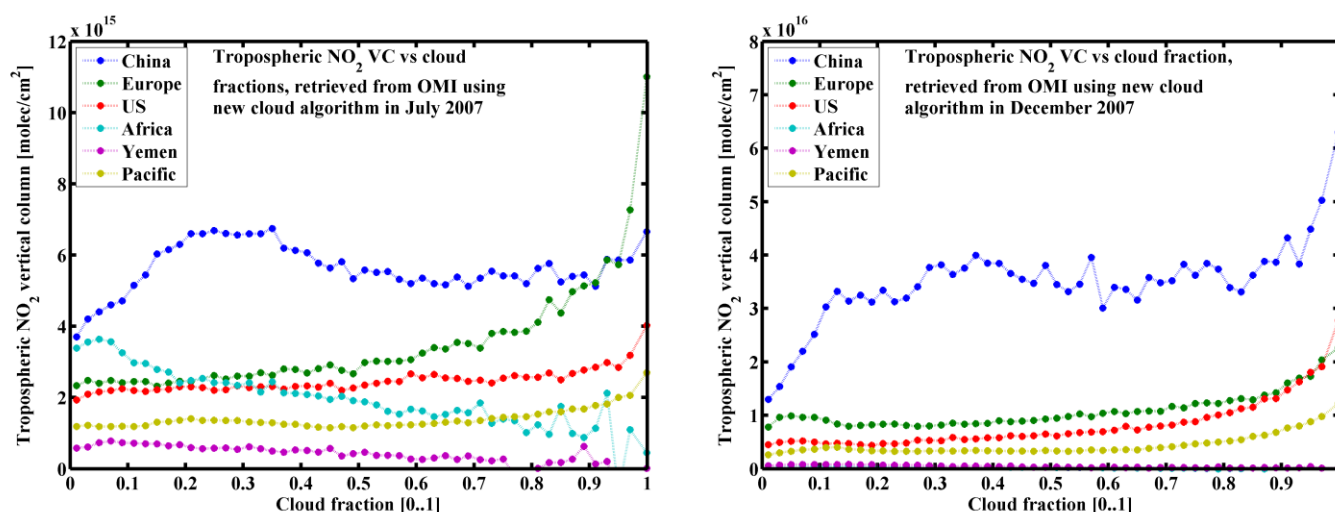


Figure 6.9: Cloud impacts on tropospheric NO₂ VC from OMI new cloud algorithm in July (left) and December 2007 (right) over 6 regions

As can be noticed from Figure 6.9 (left), the tropospheric NO₂ VC above China (blue line) is quite constant at cloud fractions between 0.4 and 1. This means, NO₂ VC is reliable at large and high clouds (in summer) based on NO₂ profile over the selected region whereas it is overestimated in between 0.4 and 0.2 of cloud fractions, exactly at the part of NO₂ SC enhanced by multiple scattering. This probably explained by the fact, that the AMF takes clouds into account but not aerosols. The AMF also does not expect the reduction of NO₂ SC at cloud fractions between 0 and 0.2 which results in underestimation of NO₂ VC at small cloud fractions. In the comparison with

Europe, the result of NO₂ VC above US and Pacific Ocean can be more acceptable. According to different cloud distributions, the OMI NO₂ VC seems to be more reliable than the GOME-2A NO₂ VC, especially, in December where low clouds are present, as shown in Figure 6.9 (right). In more detail, it can be seen that an overestimation of AMF results in underestimation for NO₂ VC, which has been noticed from Figure 6.9 (right) over China at very small cloud fractions, and vice versa for very large cloud fractions. Results from the same evaluation using the old cloud algorithm are shown in the appendix.

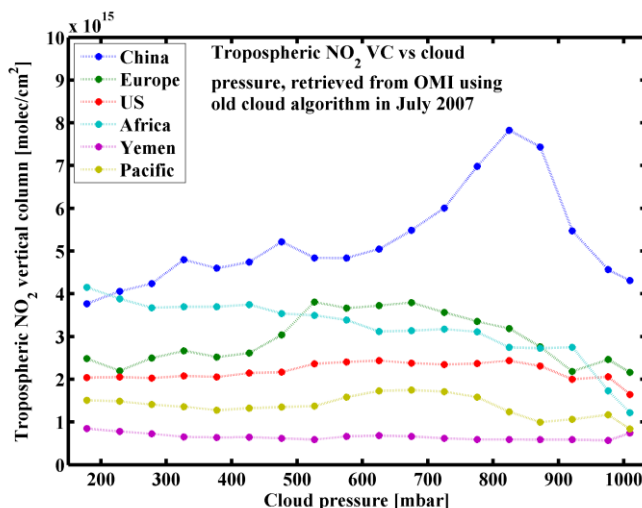


Figure 6.10: Cloud pressure effect on tropospheric NO₂ VC from OMI old cloud algorithm in July 2007 over 6 regions

Although cloud fraction impacts on NO₂ VC include the impact of cloud pressure, some unexpected results of cloud pressure impacts on NO₂ VC are evident in Figure 6.10. Instead of having the same values for all cloud pressure, the NO₂ VCs over China in July (blue line) peak around 820 mbar cloud pressure, where most clouds are present. This can mean that the NO₂ SCs are larger above clouds resulting in an overestimation of the NO₂ AMF. The most probable reason for this unexpected effect is that the AMFs are not correctly evaluated over low clouds because of the used NO₂ profile. For the NO₂ VCs above Europe, US, Africa, Yemen, and Pacific Ocean (Figure 6.10, different color lines), the AMFs are quite correctly evaluated, specifically at cloud pressures smaller than 900 mbar. Similar results are obtained using different cloud algorithms and instruments in different times. Results are provided in the Appendix.

7 Cloud impacts on NO₂ columns: The global view

In this section, global cloud and tropospheric NO₂ retrievals are evaluated on May 22nd in 2007 and 2012 from the OMI instrument using the old cloud algorithm. Because clouds and NO₂ vary over time, it should be mentioned that the OMI instrument obtains its retrievals close to local noontime due to its equatorial crossing time (13:45). NO₂ SCs and VCs were averaged over intervals of cloud fraction and cloud pressure, 0.05 and 50 mbar respectively. Since the tropospheric NO₂ slant column density is mainly concentrated above urban regions, the mean NO₂ columns will be very small because of the global average over wide unpolluted areas. NO₂ amounts over some of these areas do not exceed the atmospheric NO₂ background resulting in negative retrievals. In this case, the negative values of NO₂ SCs and VCs were excluded from the calculations.

7.1 Global cloud distributions

As shown in Figure 7.1, the distribution of cloud pixels is quite similar on the two days selected in 2007 and 2012 whether for cloud fraction (left) or for cloud pressure (right). It is realistic that the frequency of occurrence of cloud fractions decreases with increasing cloud fraction because at the scale of OMI measurements, pixels are rarely completely cloud covered. There are two maxima in the cloud fraction distribution (at cloud fraction of 0 and 1) because of flagged pixels at boundaries. Statistically, cloud free scenes represent roughly 68% of the global cloud distribution while 32% remains for cloudy scenes. These percentages are calculated using the average of pixel frequencies for over a cloud fraction increment of 5%. Similar global cloud statistics were obtained using the GOME-2A instrument, provided in the Appendix. Cloud pressure is consistent for the two days in 2007 and 2012, the number of cloud pixels (clouds) decreasing with increasing the cloud top altitude. This distribution of cloud pressure is in agreement with the vertical distribution of water vapour mixing ratio in the troposphere (Palchetti et al., 2008). As has already been discussed, clouds influence NO₂ retrieval depending on the cloud fraction and their altitude. Moreover, cloud optical thickness (COT) is a determinative factor to evaluate cloud fraction which implicitly affects NO₂ retrieval (i.e. thin cloud and thick cloud have different effects). The COT effect is not explicitly taken into consideration in this study, but considered through cloud fraction effects. In both

FRESCO+ and the O₂-O₂ algorithm, clouds are assumed to have a large COT and albedo of 0.8. clouds having similar COT (and thus lower albedo) result in reduced cloud fraction.

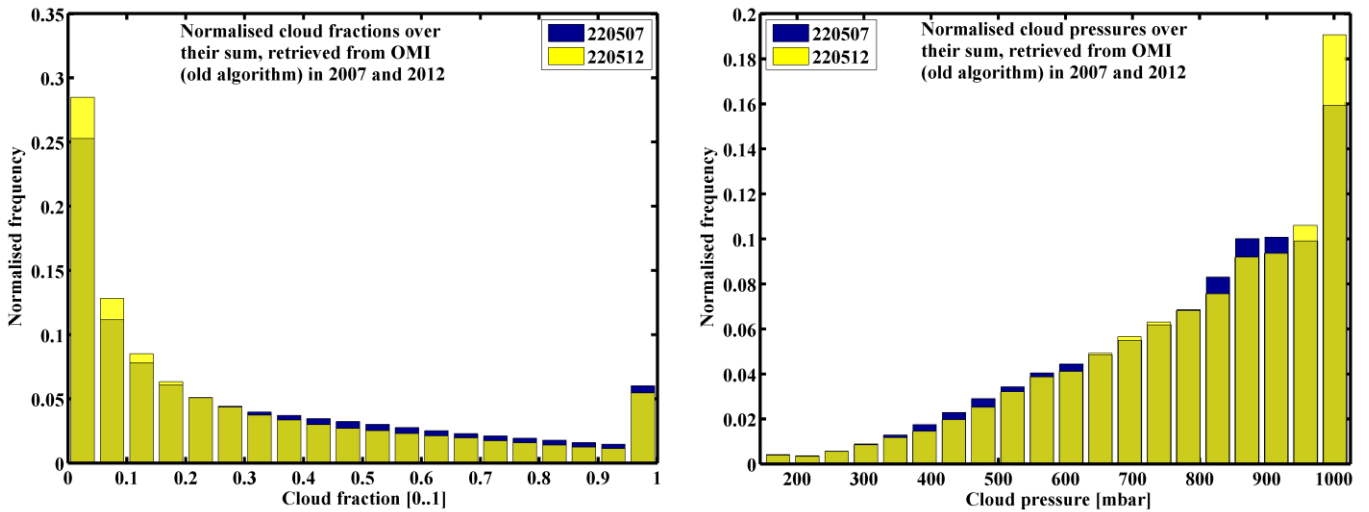


Figure 7.1: OMI global cloud statistics for May 22 in 2007 and 2012, cloud fraction (left) and cloud pressure (right).

According to the cloud statistics, most clouds are located at cloud pressure around 700 mbar, especially, those having cloud fractions between 0.1 and 1 as shown in Figure 7.2. On the other hand, very small cloud fractions are located around cloud pressure of 900 mbar for both years.

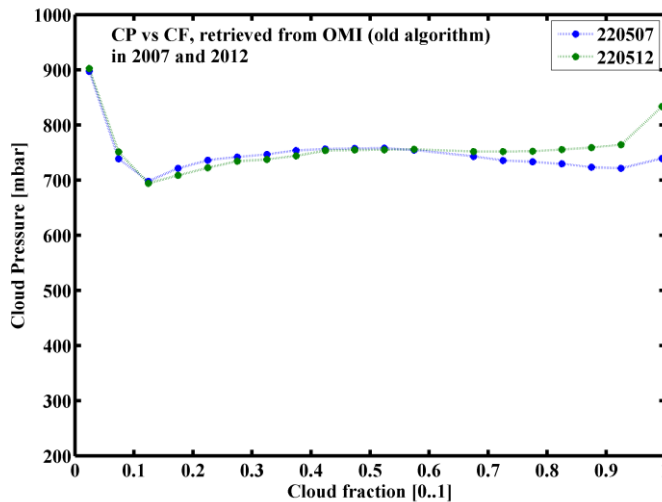


Figure 7.2: Global statistics of cloud fraction and cloud pressure from OMI on one day of 2007 and 2012

More histograms and plots were created using about global retrievals over consecutive days (one week of 2007), showing similar cloud statistics, included in the Appendix.

7.2 Global cloud impacts on Tropospheric NO₂ SC in 2007 and 2012

Figure 7.3 (left) shows that the cloud effects on the tropospheric NO₂ SCs are reasonable over cloud fractions in 2007 (blue line) by shielding NO₂ while it is unexpected for 2012 at cloud fraction larger than 0.8. The enhancement of NO₂ retrieval is not noticed at small cloud fractions because of the average of NO₂ distribution over global clouds. Furthermore, the enhancement of NO₂ retrievals is restricted to the polluted regions, where aerosol impacts can also be taken into account. The polluted regions also represent very small areas compared to the total Earth's atmosphere. In terms of cloud pressure effects (Figure 7.3 right), the NO₂ SC values are realistic at cloud pressure from 400 mbar to 1000 mbar but it cannot at all be reliable for 2007 because NO₂ SCs become affected by the statistical distribution more than by clouds.

Overall, global cloud impacts are weaker and more complicated than regional cloud impacts over polluted regions. In addition to that, datasets over one day are not enough to find out such global effects, which require more observations over longer times.

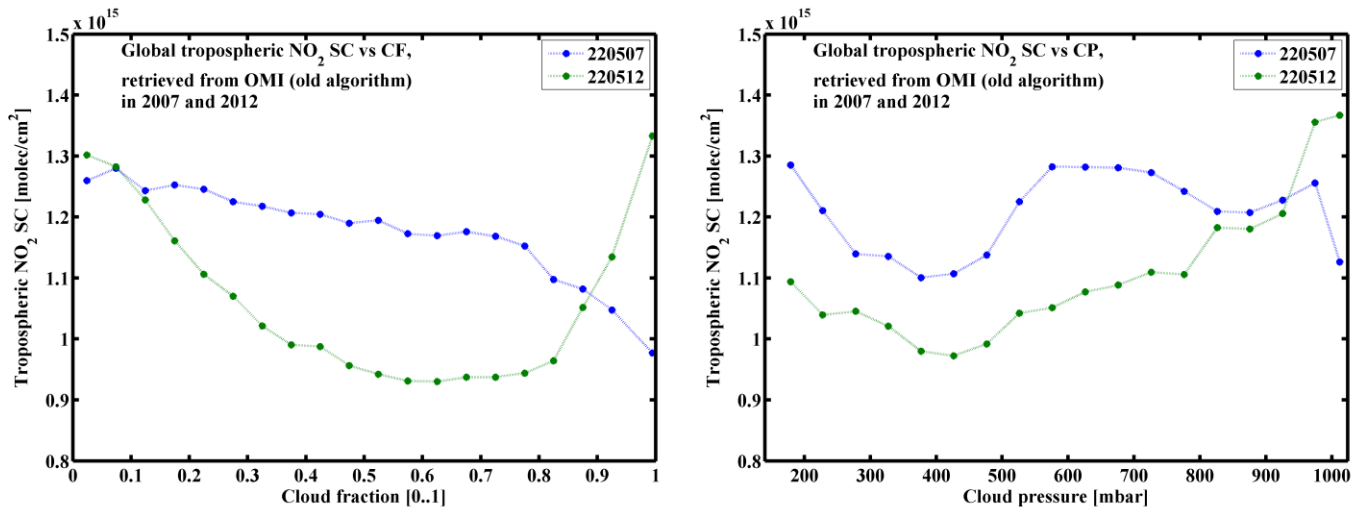


Figure 7.3: Global cloud impacts on tropospheric NO₂ SC retrieved from OMI old algorithm on one day of 2007 and 2012, with CF (left) and CP (right).

In the Appendix, some results are provided to compare global cloud impacts over weekdays to the current results in this section. The NO₂ SCs are consistent under cloud cover impacts over weekdays but they show similar effects for cloud pressure, which are shown here.

7.3 Effects on Tropospheric NO₂ AMF and VC

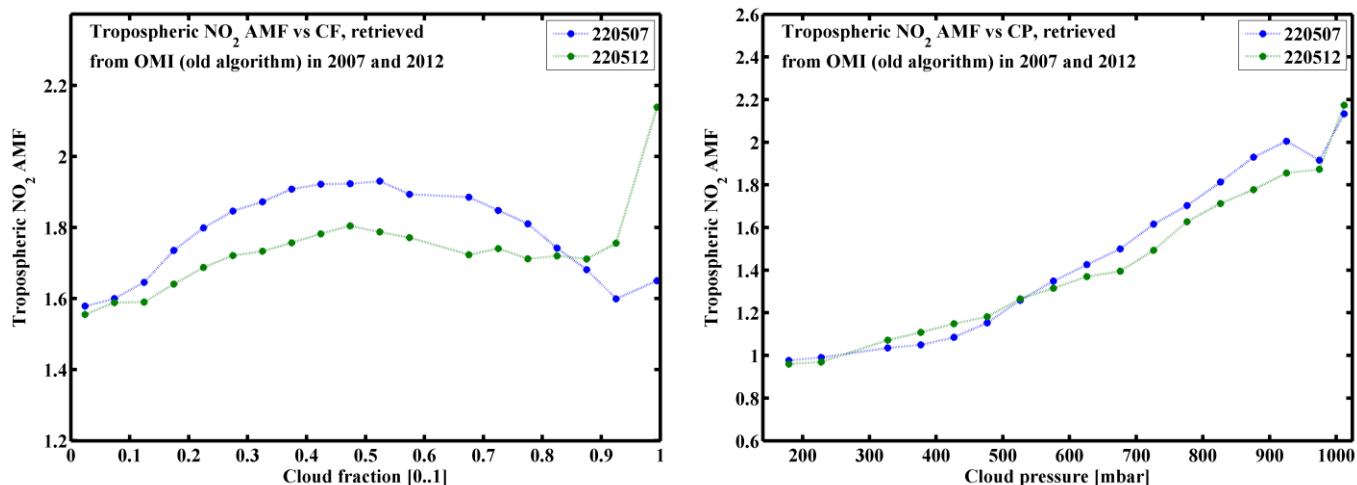


Figure 7.4: Global tropospheric NO₂ AMF versus CF (left) and CP (right) over one day of 2007 and 2012

Cloud fraction impacts on the NO₂ AMF cannot be expected (Figure 7.4, left) compared to the AMF of NO₂ on one day in 2007 (Figure 5.1), which can be attributed to the uncertainty of NO₂ profile evaluation. On the other hand, the NO₂ AMF affected by cloud pressure is reasonable as shown in Figure 7.4 (right). Additionally, the SC data are dominated by background NO₂ which is higher in the atmosphere. Therefore, the AMF is always larger than for polluted scenes, increases in the presence of clouds and in particular if the clouds are low.

The NO₂ VC is overestimated at small and large cloud fractions while an underestimation of NO₂ VC is observed at cloud fraction around 0.5 for both years (Figure 7.5, left). Cloud pressure effects on the global NO₂ VC (Figure 7.5, right) show decreasing VCs with increasing cloud pressure. This indicates that the increase of AMF (Figure 7.4, right) is too large, probably because the CTM used has too much NO₂ above clouds. Such results imply that global retrievals are not recommended to be used for studying cloud impacts on NO₂ retrieval but they can be interesting to compare global cloud distributions over different time apart from their impacts on tropospheric trace gases.

In the Appendix, the analysis of global measurements for cloud and NO₂ is repeated over one week of 2007, showing an overestimation of tropospheric NO₂ VCs at large cloud fractions (between 0.5 and 1) and quite realistic NO₂ VCs for cloud fractions smaller than 0.5 over weekdays. On the other hand, they are in agreement with the current results of this section in terms of cloud pressure effect.

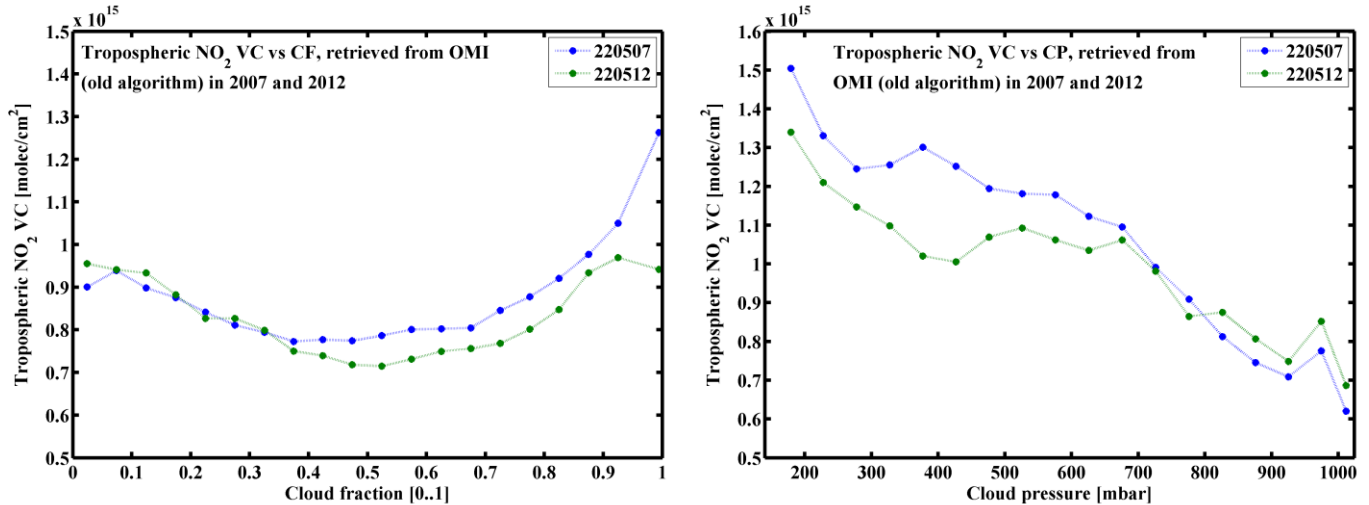


Figure 7.5: Global tropospheric NO₂ VC versus CF (left) and CP (right) over one day of 2007 and 2012.

In summary, all kind of NO₂ scenarios are mixed and the background situations dominant in global data. Therefore, the results are difficult to interpret.

8 Conclusion

Clouds are distributed throughout the atmosphere, mostly in the troposphere over tropics and mid-latitudes, varying regionally and seasonally depending on the dynamical conditions during their formation. The atmospheric NO₂ is a production of natural sources (e.g. lightning and soil emissions) and anthropogenic emissions (e.g. combustion engines and biomass burning), mostly found in the atmosphere close to its sources, in particular above urban and industrialised regions. The amount of NO₂ changes with time through diurnal and seasonal variations because of its photolysis interactions and its short life time in the atmosphere. Cloud retrievals are performed from space based observations employing the O₂ A-band and O₂-O₂ band for GOME-2A FRESCO+ and OMI cloud algorithms, respectively, to determine cloud parameters while NO₂ retrievals are obtained from DOAS fitting between 400 nm and 500 nm.

The last two versions of cloud algorithms for GOME-2A and OMI (namely, FRESCOv6; FRESCOv7 and old; new O₂-O₂ algorithms, respectively) are utilized for retrieving cloud fraction and cloud pressure. In spite of the significant differences of cloud distributions retrieved when using different algorithms, the cloud impacts on NO₂ retrievals were similar, especially for the same instrument. Practically, it was observed that NO₂ below clouds is screened from the satellite

observations as the result of the shielding effect while NO₂ slant columns above clouds were enhanced by high cloud albedo. Over China, NO₂ SCs reduce at small cloud fractions (<0.2) which can be interpreted as a twofold effect, either to increase NO₂ signal by multiple scattering through thin clouds and aerosol particles or to decrease the sensitivity of NO₂ signal by absorbing aerosol, which are not recognized by cloud algorithms. Cloud correction has to be taken into consideration for NO₂ AMF calculation even for small cloud fractions (smaller than 20%) as otherwise NO₂ columns are systematically underestimated. The NO₂ VC was evaluated for high clouds better than for low clouds depending on cloud determination, as has been noticed above polluted regions in July and December 2007 whether from GOME-2A measurements or from OMI measurements. The good spatial resolution of OMI footprint results in more pixels, improving the statistical determination when processing cloud effects on NO₂ retrievals, compared to the GOME-2A footprint. By comparison with regional retrievals, the global retrievals were interesting for studying cloud distributions but they showed weak cloud impacts on NO₂ slant and vertical columns because of the statistical effect of global NO₂ distributions where background scenarios are dominant.

9 Outlook

Because of the limited time available, not all points could be covered in this Master thesis. Possible future topics are summarized in the following:

- Extending the study to cloud effects not only on NO₂ retrievals but also on other atmospheric trace gases will be significant to evaluate satellite retrievals in the presence of clouds.
- More investigations about aerosol and small cloud cover impacts are needed to discover the origin of unexpected behavior of the NO₂ SCs over China.
- Finding (and resolving) the reason behind systematic overestimations of ghost columns at large cloud fractions, in particular over background regions, will result in more reliable evaluations for VCs.

10 References

- Acarreta, J., De Haan, J., and Stammes, P.: Cloud pressure retrieval using O₂-O₂ absorption band at 477 nm, *Geoph. Res.*, 109, 2004.
- Boersma, K., Eskes, H., and Brinksma, E.: Error analysis for tropospheric NO₂ retrieval from space, *J. Geophys. Res.*, 109, D04311, doi: 10.1029/2003JD003962, 2004.
- Bovensmann, H., Burrows, J., Buchwitz, M., Frerick, J., Noel, S., Rozanov, V., Chance, K., and Goede, A.: SCIAMACHY: Mission objectives and measurement modes, *J. Atmos. Sci.*, 56, 127–150, 1999.
- Burrows, J., Platt, U., and Borrell, P.: Tropospheric remote sensing from space, *Springer Verlag*, Heidelberg, ISBN 978-3-642-14790-3, 2011.
- Burrows, J., Weber, M., Buchwitz, M., Rozanov, V., Weissenmayer, A., Richter, A., Debeek, R., Hoogen, R., Bramstedt, K., Eichmann, K., Eisinger, M., and Perner, D.: The Global Ozone Monitoring Experiment (GOME): Mission Concept and First Scientific Results, *J. Atmos. Sci.*, 56, 151-175, 1999.
- Crutzen, P.: The role of NO and NO₂ in the chemistry of the troposphere and stratosphere, *Ann. Rev. Earth Planet Sci.*, 7,443-472,1979.
- Gottwald, M., Bovensman, H., Lichtenberg, G., Noel, S., Bargaen, A., Slijkhuis, S., Piters, A., Hoogeveen, R., Savigny, C., Buchwitz, M., Kokhanovsky, A., Richter, A., Rozanov, A., Holzer-Popp, T., Bramstedt, K., Lambert, J., Skupin, J., Wittrock, F., Schrijver, H., Burrows, J.: SCIAMACHY, Monitoring the Changing Earth's Atmosphere, *DLR*, 2006.
- Hao, N., Koukouli, M., Inness, A., Valks, P., Loyola, D., Zimmer, W., Balis, D., Zyrichidou, I., Roozendael, M., Lerot, C., and Spurr, R.: GOME-2 total ozone columns from MetOp-A/MetOp-B and assimilation in the MACC system, *Atmos. Meas. Tech.*, 7, 2937-2951, 2014.
- Hilboll, A., Richter, A., and Burrows, J.: Supplementary material to “Long-term changes of tropospheric NO₂ over megacities derived from multiple satellite instruments”, *Atmos. Chem. Phys.*, 13, 1–3, 2013.

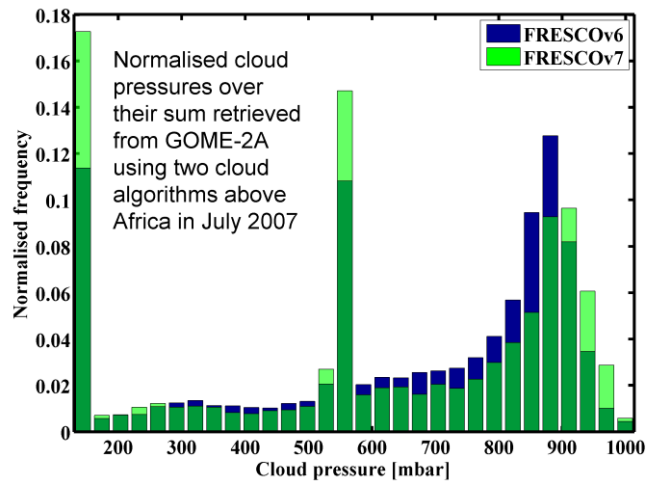
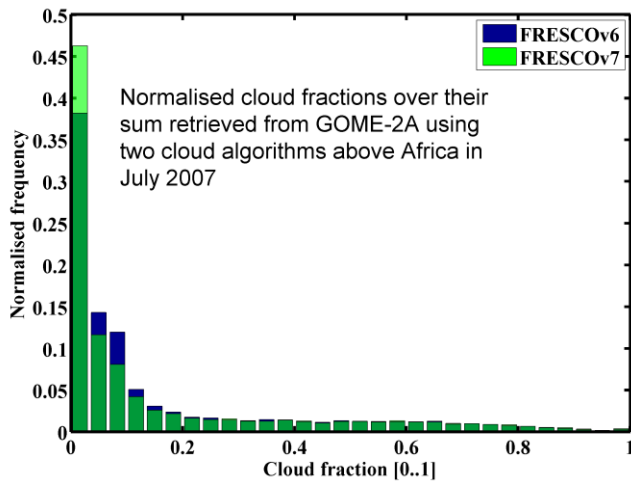
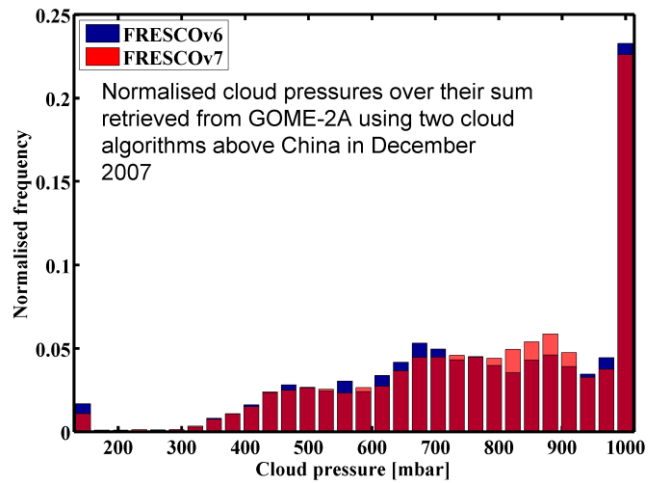
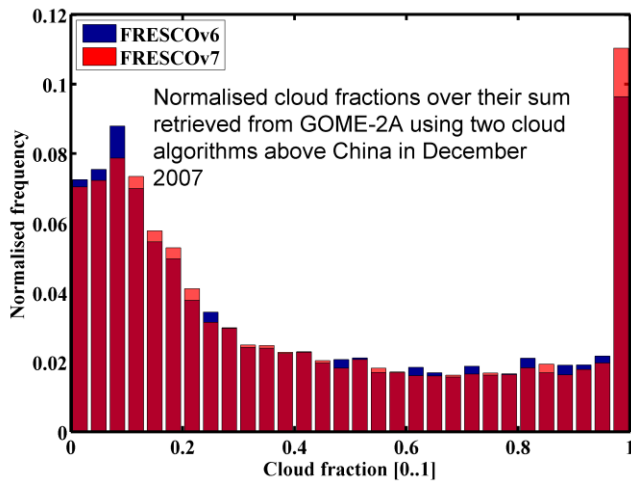
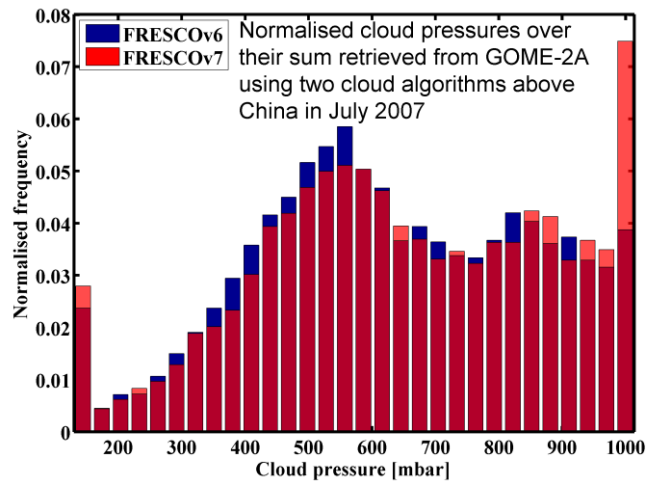
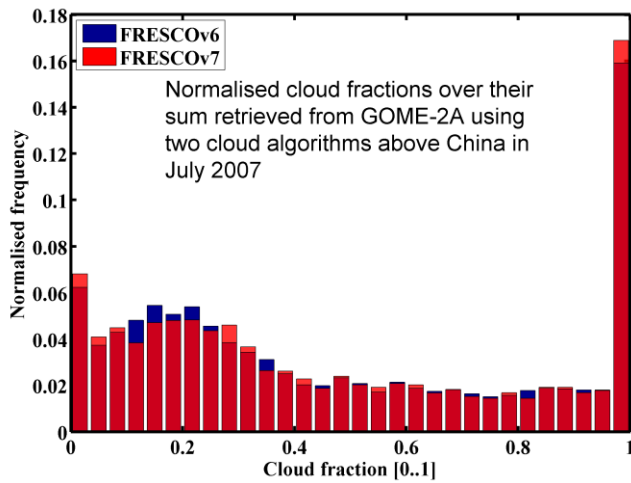
- Hoeningner, G., Friedeburg, C., and Platt, U.: Multi axis differential optical absorption spectroscopy (MAX-DOAS), *Atmos. Chem. Phys.*, 4, 231-254, 2004.
- Inness, A., Baier, F., Benedetti, A., Bouarar, I., Chabrillat, S., Clark, H., Clerbaux, C., Coheur, P., Engelen, R., Errera, Q., Flemming, J., George, M., Granier, C., Hadji-Lazaro, J., Huijnen, V., Hurtmans, D., Jones, L., Kaiser, W., Kapsomenakis, K., Lefever, K., Leitao, J., Razinger, M., Richter, A., Schultz, M., Simmons, A., Suttie, M., Stein, O., Thepaut, J., Thouret, V., Vrekoussis, M., Zerefos, C., and the MACC team: The MACC reanalysis: an 8 yr data set of atmospheric composition, *Atmos. Chem. Phys.*, 13, 4073-4109, 2013.
- Koelemeijer, R., Stammes, P., Hovenier, J., and de Haan, J.: A fast method for retrieval of cloud parameters using oxygen A band measurements from the Global Ozone Monitoring Experiment, *Geoph. Res.*, 106, 3475-3490, 2001.
- Levelt, P., Van den Oord, G., Dobber, M., Malkki, A., Visser, H., de Vries, J., Stammes, P., Lundell, J., and Saari, H.: The ozone monitoring instrument. *Geosci. Remote Sens. IEEE Trans.*, 44, 1093-1101, 2006.
- Lorente, A., Boersma, K., Yu, H., Dörner, S., Hilboll, A., Richter, A., Liu, M., Lamsal, L., Barkley, M., Smedt, I., Roozendael, M., Wang, Y., Wagner, T., Beirle, S., Lin, J., Krotkov, N., Stammes, P., Wang, P., Eskes, H., and Krol, M.: Structural uncertainty in air mass factor calculation for NO₂ and HCHO satellite retrievals, *Atmos. Meas. Tech. Discuss.*, doi:10.5194/amt-2016-306, 2016.
- Marshak, A., Davis, A., Cahalan, R., and Wiscombe, W.: Nonlocal Independent Pixel Approximation: Direct and Inverse Problems, *IEEE Trans. Geosc. Remot. Sens.*, 36, 1998.
- Marshak, A., Davis, A., Wiscombe, W., and Titov, G.: The Verisimilitude of the Independent Pixel Approximation Used in Cloud Remote Sensing, *Remote Sens. Environ.*, 52, 72-78, 1995.
- Martin, R., Chance, K., Jacob, D., Kurosu, T., Spurr, R., Bucseles, P., Gleason, J., Palmer, P., Bey, I., Fiore, A., Li, Q., Yantosca, R., and Koelemeijer, R.: an improved retrieval of tropospheric nitrogen dioxide from GOME, *Geoph. Res.*, 107, 2002.
- Newnham, D., and Ballard, J.: Visible absorption cross section and integrated absorption intensities of molecular oxygen (O₂ and O₄), *Geoph. Res.*, 103, 28,801-28,816, 1998.

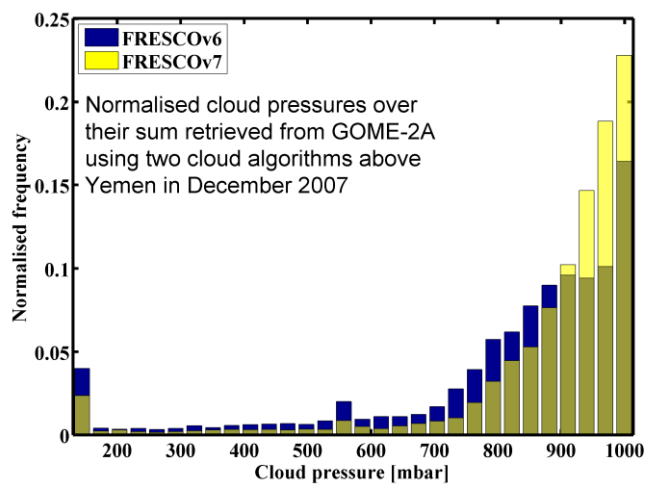
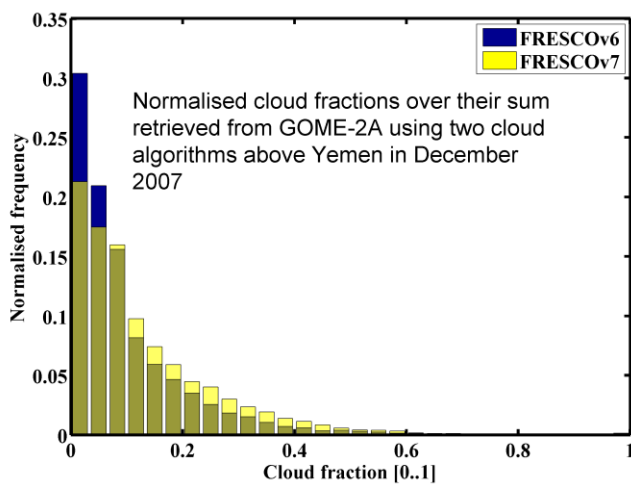
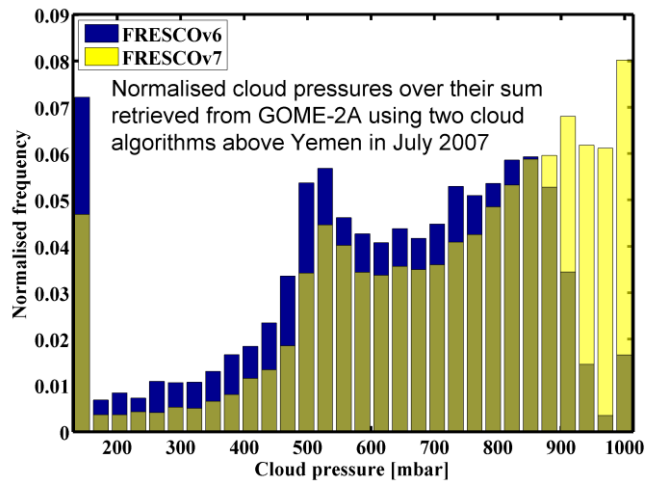
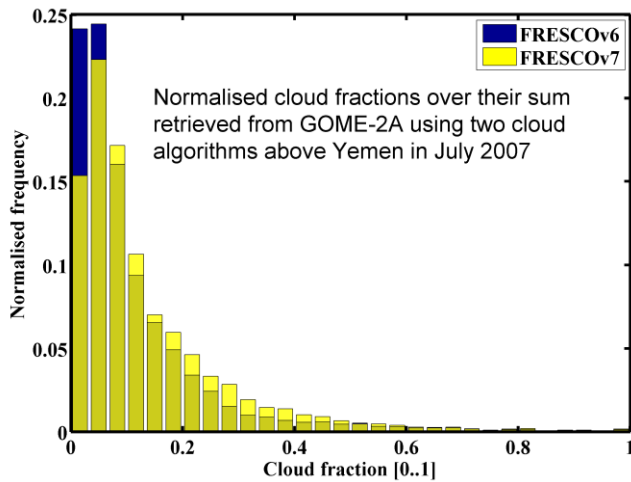
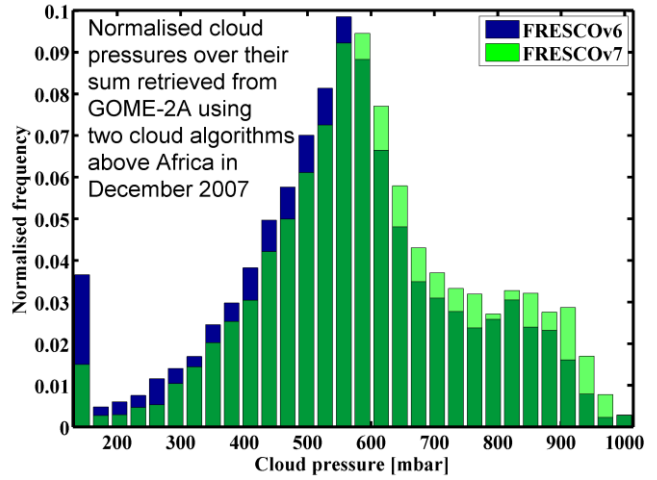
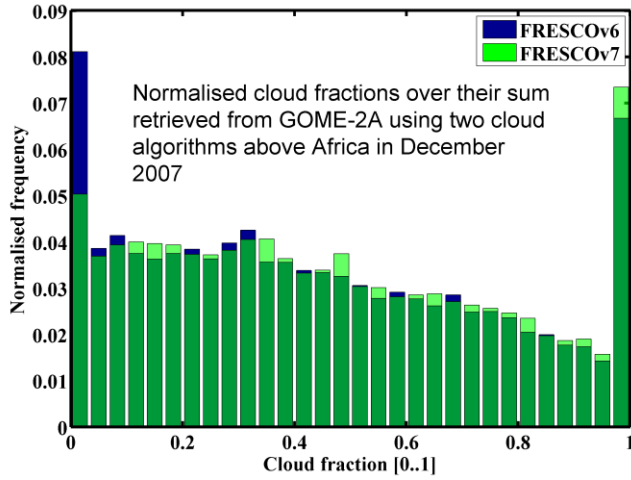
- Palchetti, L., Bianchini, G., Carli, B., Cortesi, U., and Bianco, S.: Measurement of water vapour vertical profile and of the Earth's outgoing far infrared flux, *Atmos. Chem. Phys.*, 8, 2885-2894, 2008.
- Richter, A. and Burrows, J.: Tropospheric NO₂ from GOME measurements, *Adv. Space Res.*, 29, 1673-1683, 2002.
- Richter, A., Burrows, J., Nüß, H., Granier, C., and Niemeier, U.: Increase in tropospheric nitrogen dioxide over China observed from space, *Nature*, 437, 129-132, 2005.
- Richter, A.: Satellite remote sensing of tropospheric composition- principle, results, and challenges, *EPJ Web of Conference*, 9, 181-189, doi: 10.1051/epjconf/201009014, 2010.
- Stammes, P., Sneep, M., Haan, J., Veefkind, J., Wang, P., and Levelt, P.: Effective cloud fractions from the Ozone Monitoring Instrument: Theoretical framework and validation, *J. Geophys. Res.*, 113, D16S38, doi: 10.1029/2007JD008820, 2008.
- Tuinder, O., de Winter-Sorkina, R., and Builtjes, P.: Retrieval methods of effective cloud cover from the GOME instrument: an intercomparison, *Atmos. Chem. Phys.*, 4, 255-273, 2004.
- Veefkind, J., de Haan, J., Sneep, and M., Levelt, P.: Improvements of the OMI O2-O2 Operational Cloud Algorithm and Comparisons with Ground-Based Radar-Lidar Observations, *Atmos. Meas. Tech. Discuss.*, 2016.
- Venter, D., Vakkari, V., Beukes, J., Zyl, P., Laakso, H., Mabaso, D., Tiitta, P., Josipovic, M., Kulmala, M., Pienaar, J., Laakso, L.: An air quality assessment in the industrialised western Bushveld Igneous Complex, South Africa, *S. Afr. J. Sci.*, 108(9/10), 2012.
- Vountas, M., Rozanov, V., and Burrows, J.: Ring effect: Impact of Rotational Raman Scattering on Radiative Transfer in Earth's Atmosphere, *J. Quant. Spectrosc. Radiat. Transfer*, 60, 943-961, 1998.
- Wallace, J., and Hobbs, P.: Atmospheric science, Second addition, *Elsevier*, Canada, United State, ISBN 13: 978-0-12-732951-2, 2006.
- Wang, P., Richter, A., Bruns, M., Rozanov, V., Burrows, J., Heue, K., Wagner, T., Pundt, I., and Platt, U.: Measurements of tropospheric NO₂ with an airborne multi-axis DOAS instrument, *Atmos. Chem. Phys.*, 5, 337-343, 2005.

Wang, P., Stammes, P., van der A, R., Pinardi, G., and van Roozendael, M.: FRESCO+: an improved O₂ A-band cloud retrieval algorithm for tropospheric trace gas retrievals, *Atmos. Chem. Phys.*, 8, 6565-6576,2007.

Wayne, R., Barnes, I., Biggs, P., Burrows, J., Canosa-Mas, C., Hjorth, J., Le Bras, G., Moortgat, G., Perner, D., Poulet, G., Restelli, G. and Sidebottom, H.: The nitrate radical: Physics, chemistry, and the atmosphere, *Atmos. Environ. Part A, Gen. Top.*, 25(1), 1–203, doi:10.1016/0960-1686(91)90192-A, 1991.

11 Appendix





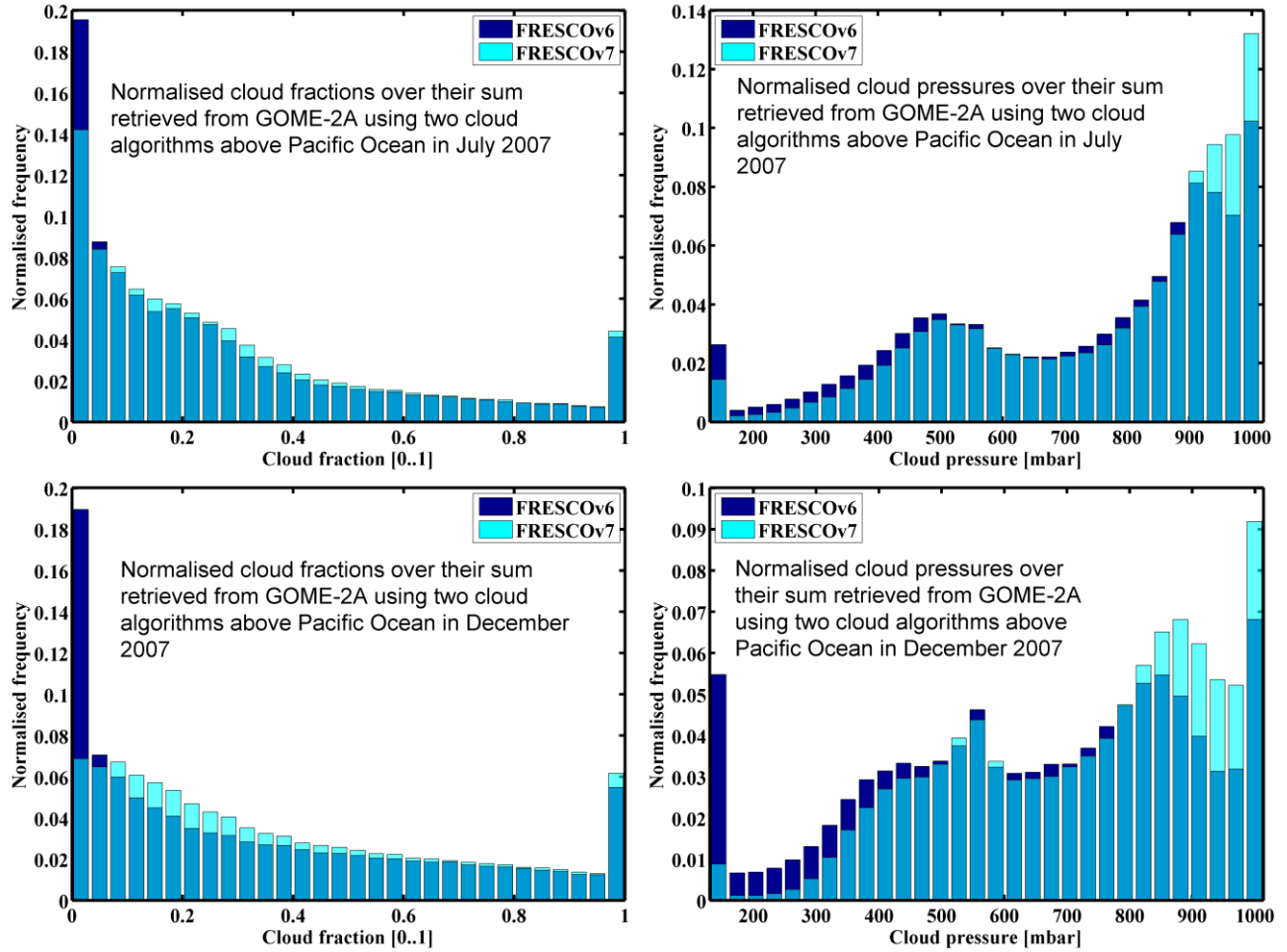


Figure 11.1: Cloud distribution retrieved from GOME-2A using FRESCOv6 and FRESCOv7 over 4 regions, cloud fraction (left column) and cloud pressure (right column).

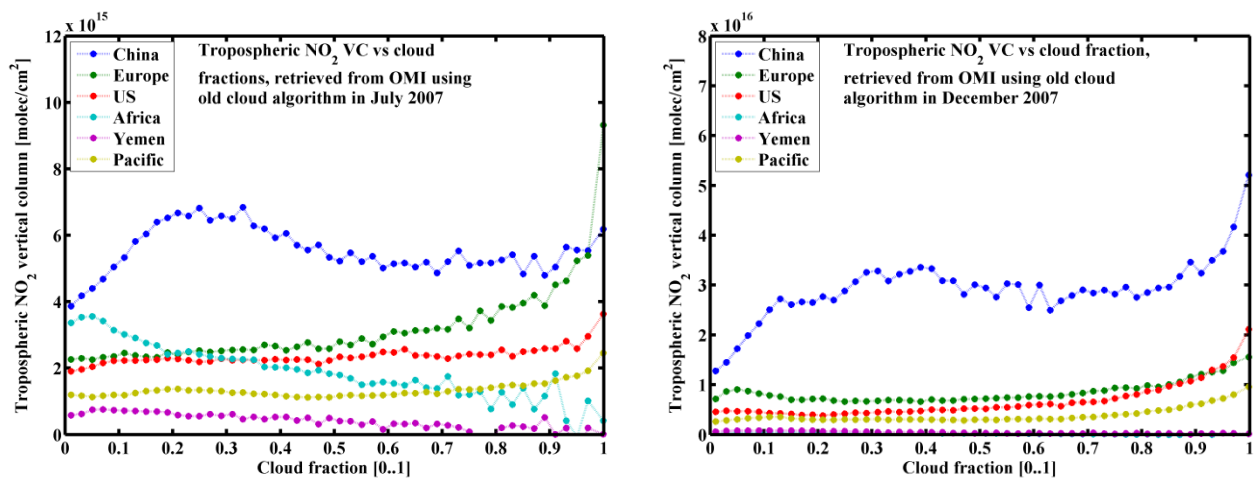


Figure 11.2: Cloud effects on tropospheric NO₂ VC retrieved from OMI in July (left) and December (right) 2007 over 6 regions.

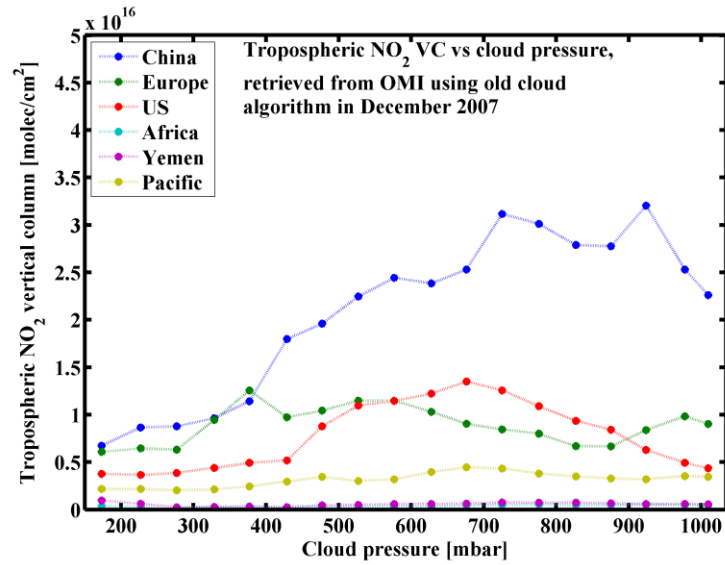
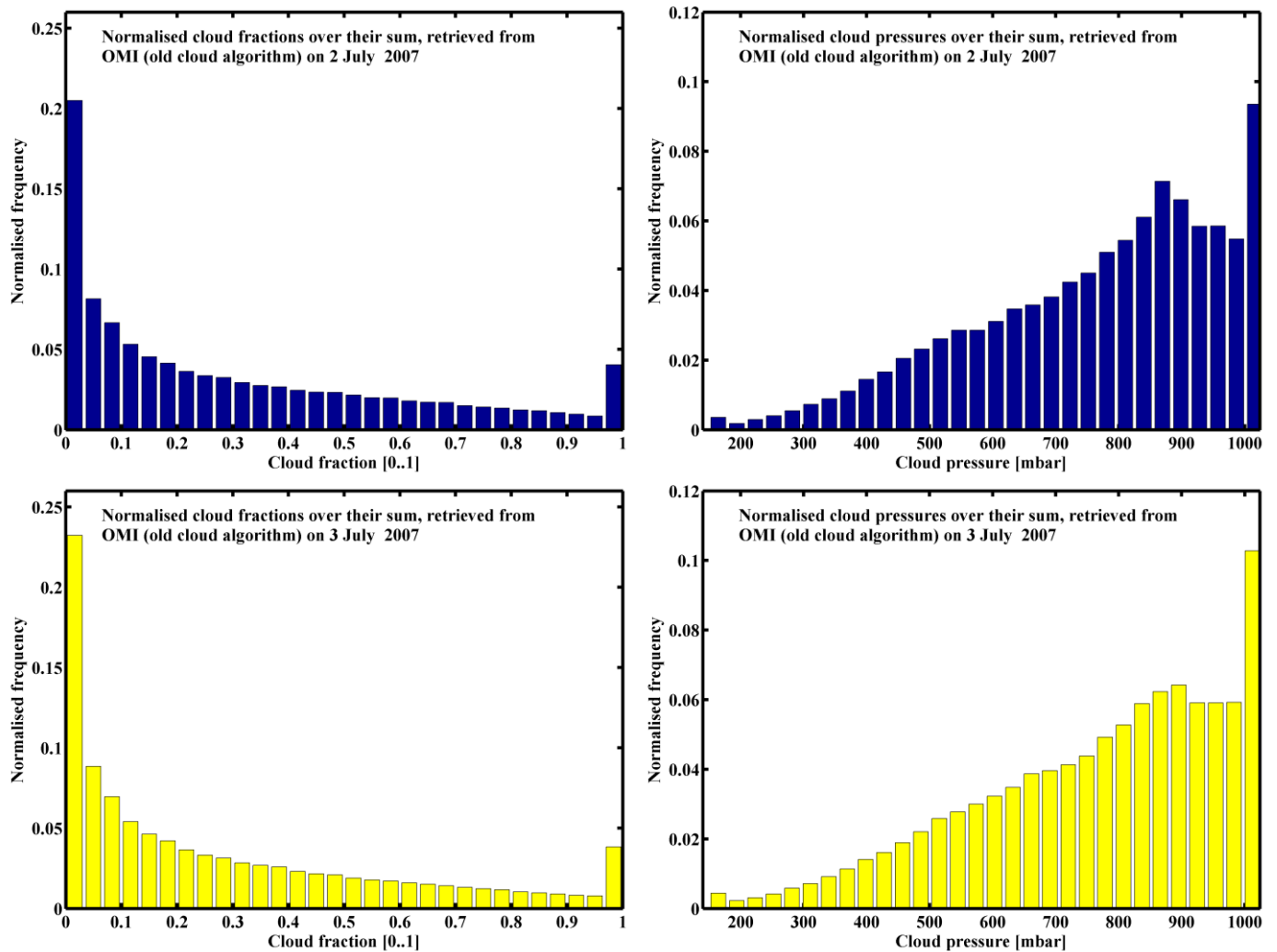
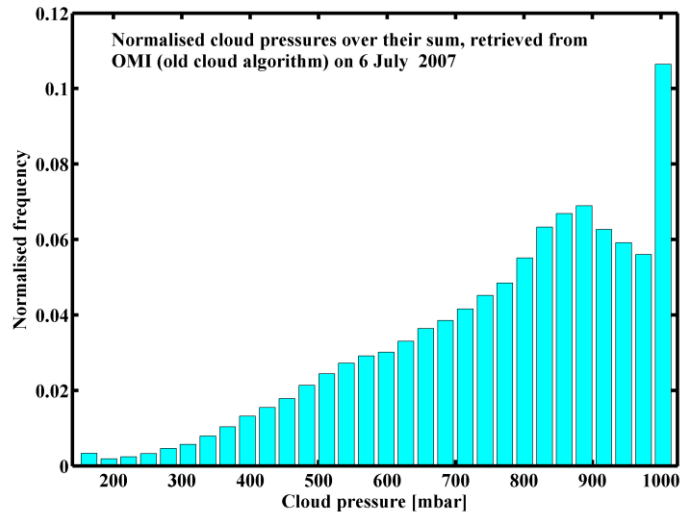
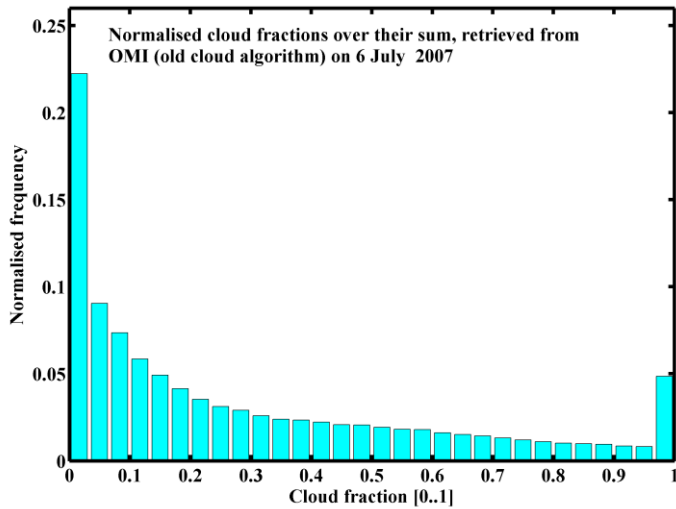
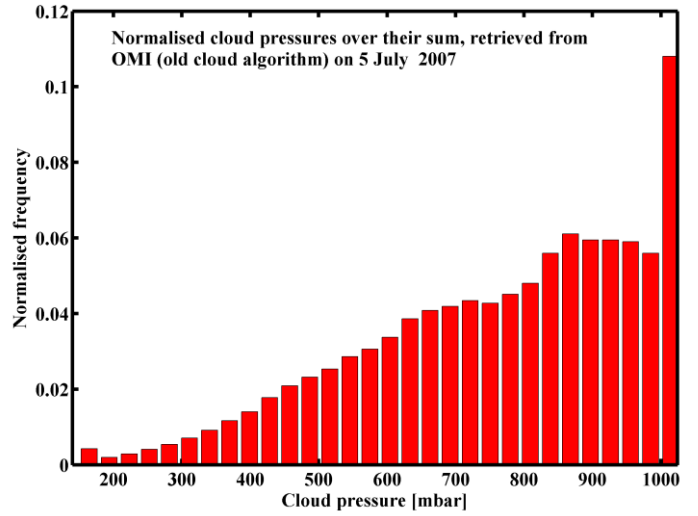
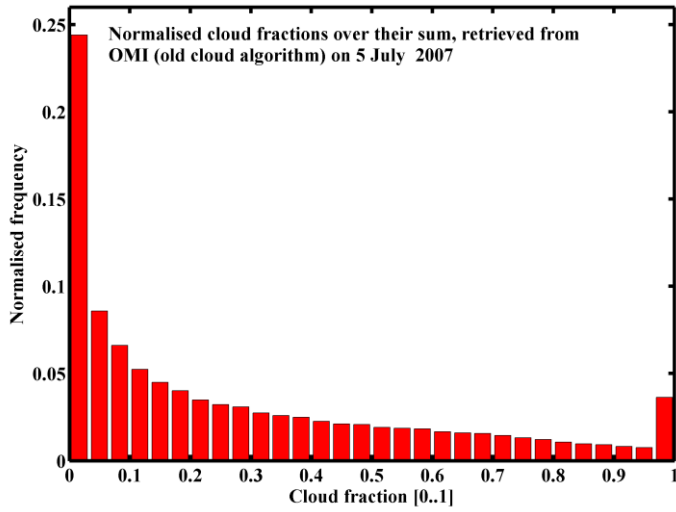
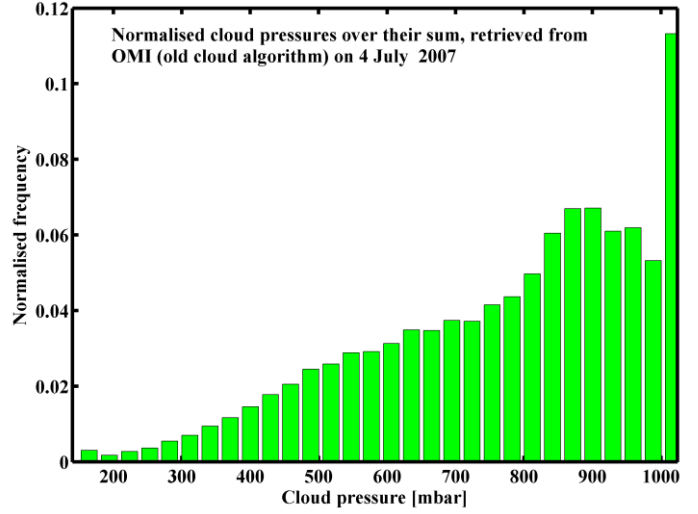
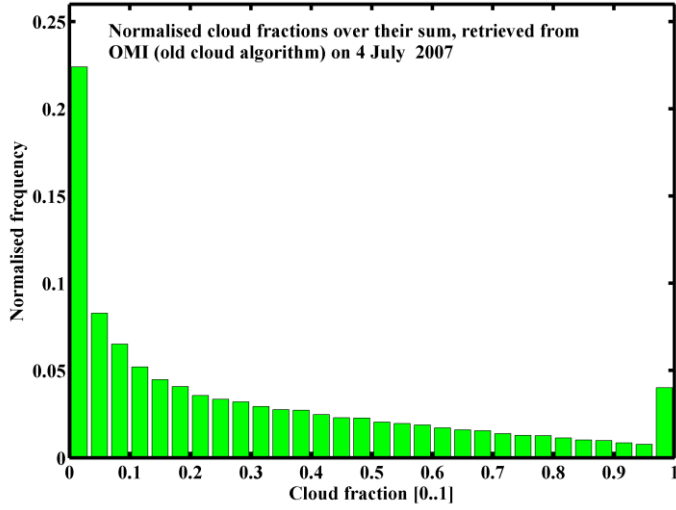


Figure 11.3: Cloud pressure effects on tropospheric NO₂ VC in December 2007 over 6 regions.





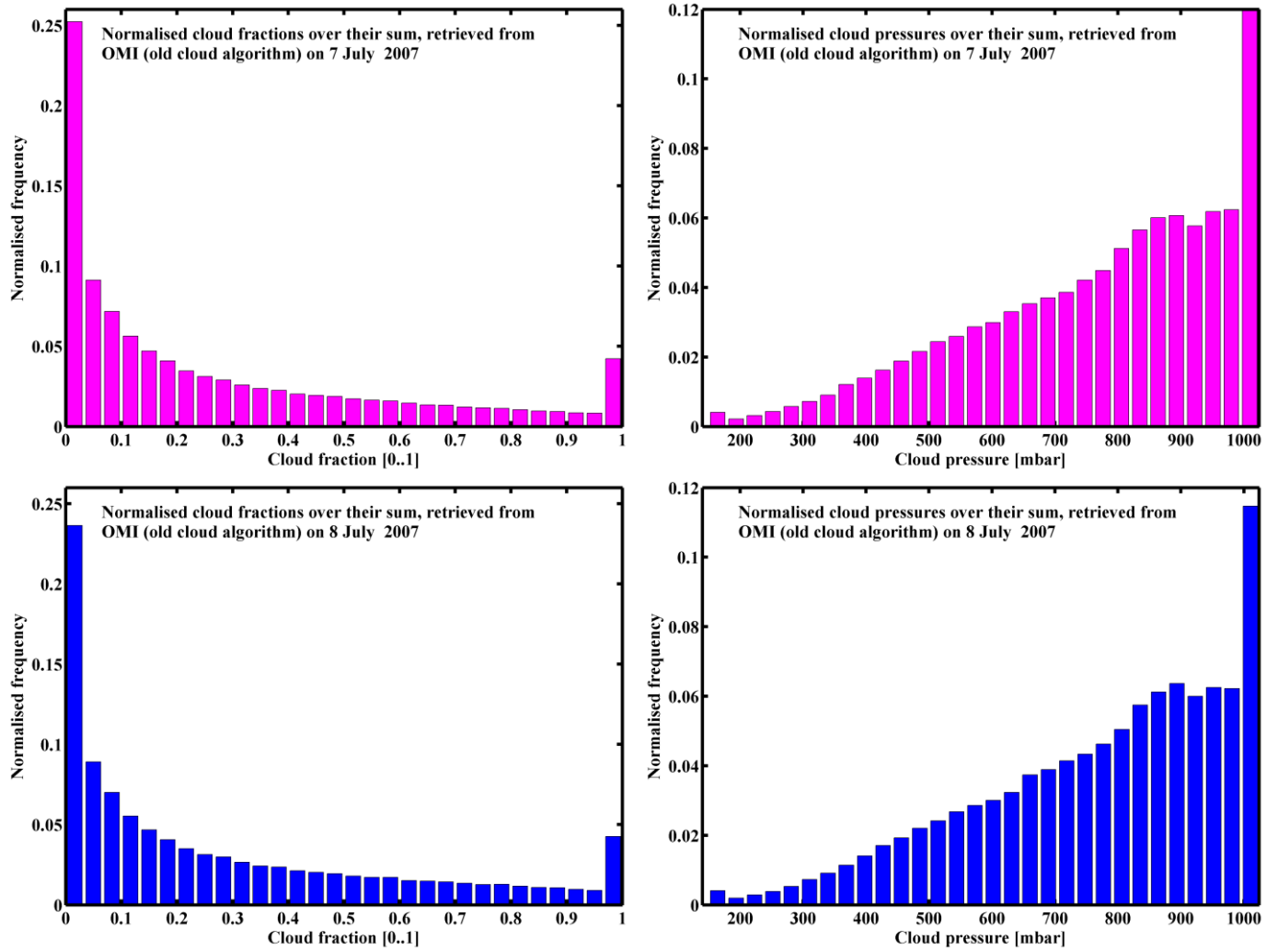


Figure 11.4: Global cloud distributions from OMI over one week in 2007, cloud fraction (left column) and cloud pressure (right column).

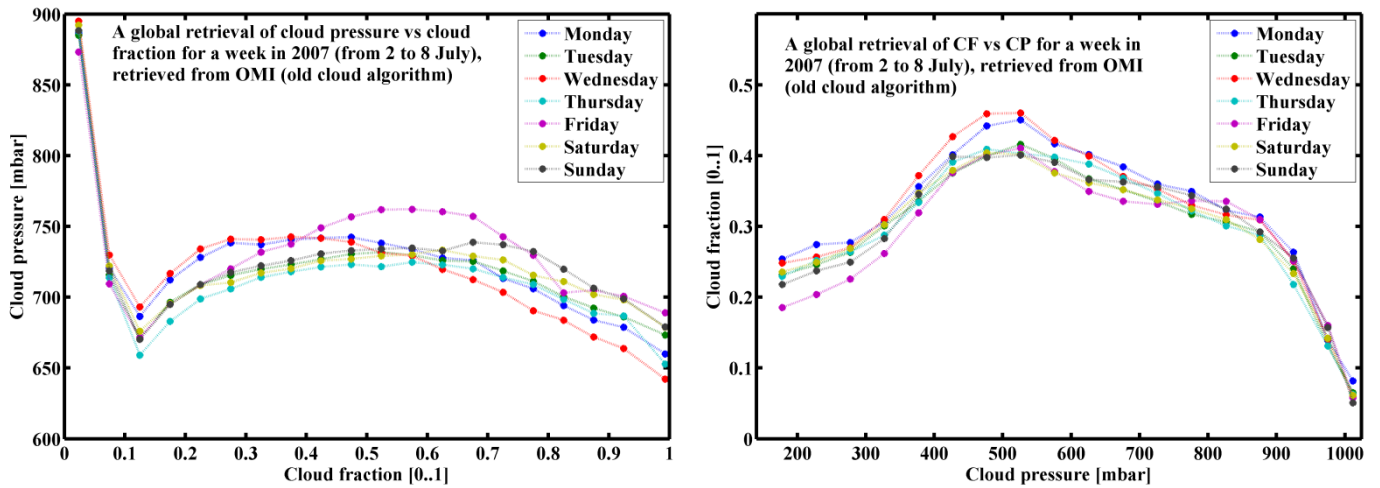


Figure 11.5: Global cloud statistics retrieved from OMI over one week in 2007, cloud fraction vs cloud pressure

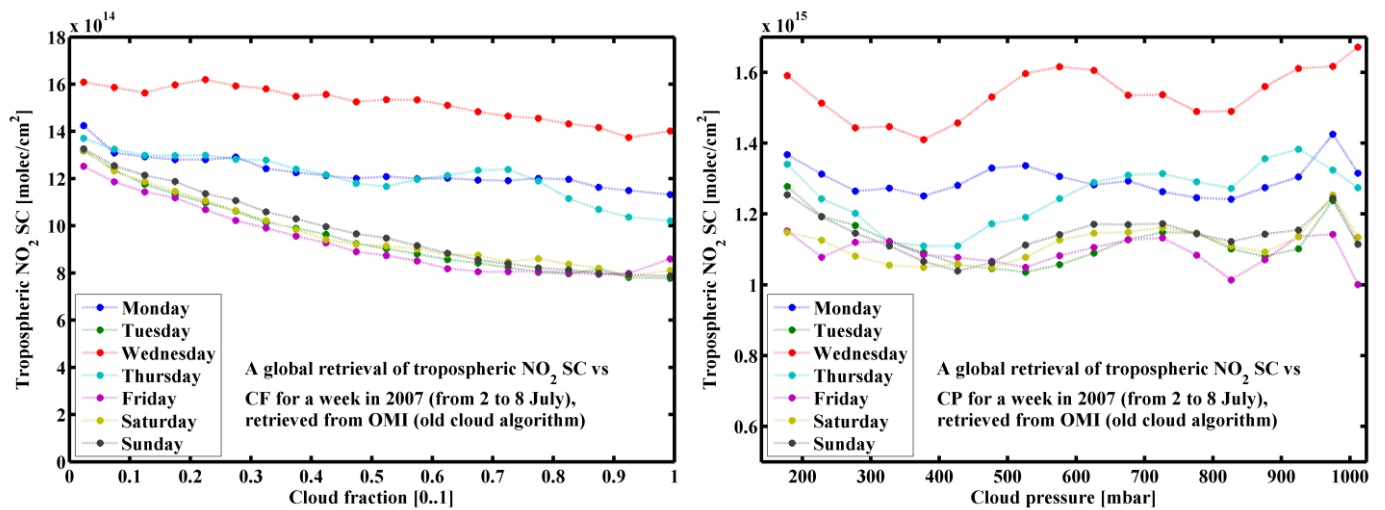


Figure 11.6: Global cloud fraction (left) and cloud pressure (right) impacts on tropospheric NO₂ SC retrieved from OMI over one week in 2007.

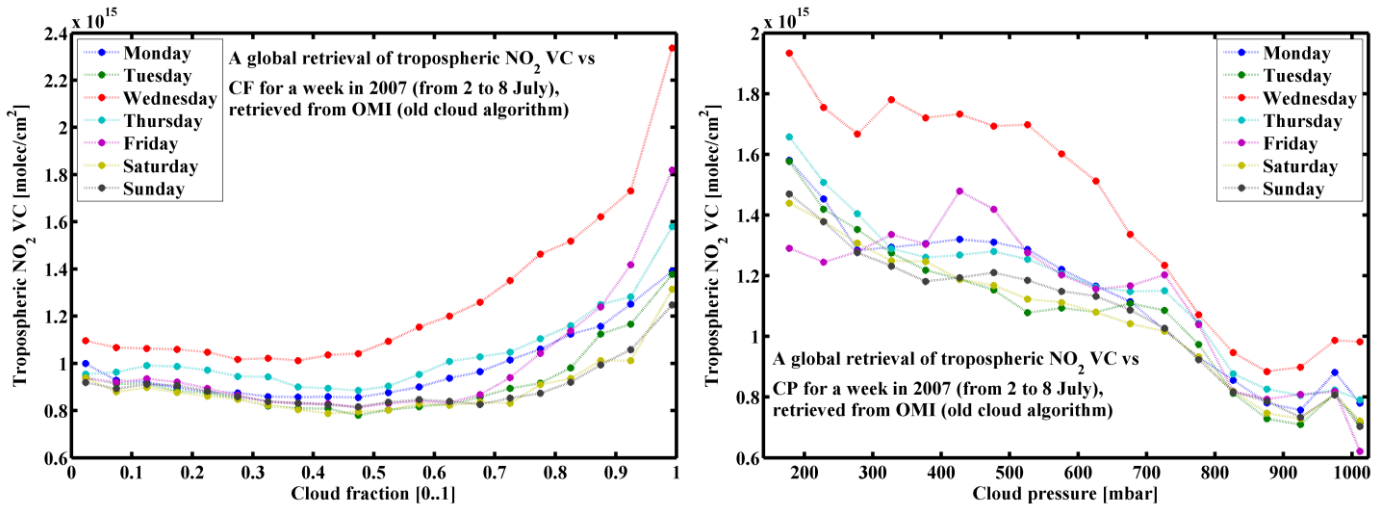


Figure 11.7: Global cloud fraction (left) and cloud pressure (right) impacts on tropospheric NO₂ VC retrieved from OMI over one week in 2007.

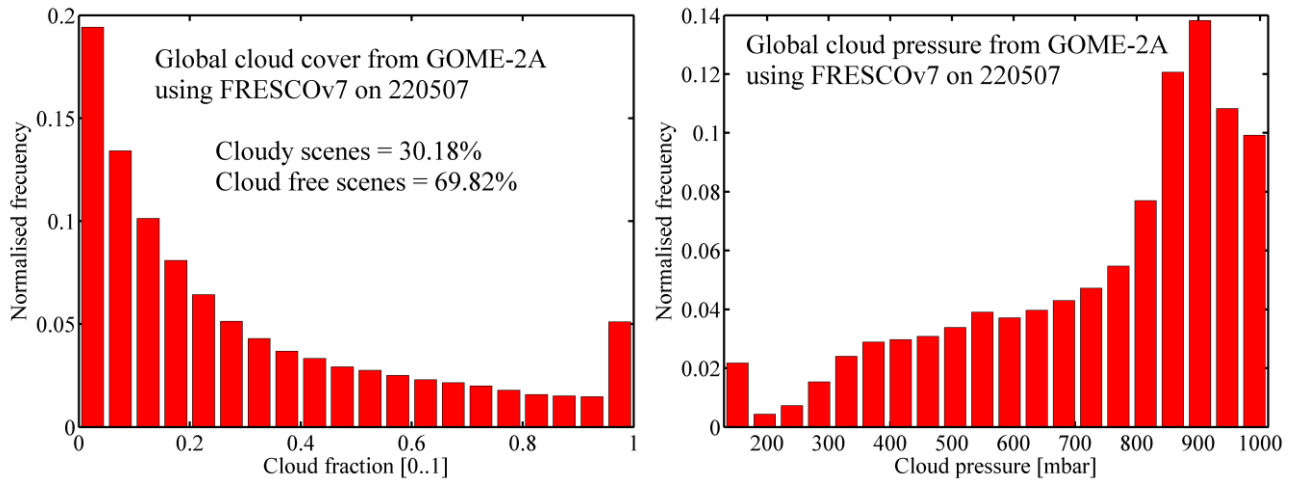


Figure 11.8: Global cloud statistics from GOME-2A on 220507, cloud fraction (left) and cloud pressure (right).